# PREPARATION OF NANO-MATERIALS AND THEIR RECYCLABLE APPLICATION IN THE REMOVAL OF ORGANIC DYES FROM AQUEOUS SOLUTION

BY

**MD. BIN YEAMIN**

SUBMITTED IN PARTIAL FULFILMENT OF THE REQUIREMENT FOR THE DEGREE OF M.PHIL. IN CHEMISTRY

**DEPARTMENT OF CHEMISTRY**

BANGLADESH UNIVERSITY OF ENGINEERING AND TECHNOLOGY

(BUET)

DHAKA 1000, BANGLADESH

JUNE, 2012

# Declaration

This thesis work has been done by the candidate himself and does not contain any material extracted from elsewhere or from a work published by anybody else. It is hereby declared that this thesis or any part of it has not been submitted elsewhere for the award of any degree or diploma.

**Md. Bin Yeamin**
**(Candidate)**

# CERTIFICATE

This is to certify that the research work embodying in this thesis has been carried out under my supervision. The work presented herein is original. This thesis has not been submitted elsewhere for the award of any other degree or diploma in any University or institution.

Dr. Al-Nakib Chowdhury
(Supervisor)
Professor
Department of Chemistry
BUET, Dhaka
Bangladesh

# Dedicated to

All Martyred Brave Hearts

&

To My Father’s Memory

Bangladesh University of Engineering and Technology, Dhaka

Department of Chemistry

Certification of Thesis

A thesis on

**"PREPARATION OF NANO-MATERIALS AND THEIR RECYCLABLE APPLICATION IN THE REMOVAL OF ORGANIC DYES FROM AQUEOUS SOLUTION"**

BY

**MD. BIN YEAMIN**

Roll No: 1009033201F, Session: October, 2009 has been accepted as satisfactory in partial fulfillment of the requirements for the degree of Master of Philosophy (M. Phil.) in Chemistry on June 30, 2012.

BOARD OF EXAMINERS

1. **Dr. Al-Nakib Chowdhury**
   Professor
   Department of Chemistry
   BUET, Dhaka
   _____
   Supervisor & Chairman

2. **Dr. Shakila Rahman**
   Professor and Head
   Department of Chemistry
   BUET, Dhaka
   _____
   Member (Ex-officio)

3. **Dr. Md. Monimul Huque**
   Professor
   Department of Chemistry
   BUET, Dhaka
   _____
   Member

4. **Dr. A. I. Mustafa**
   Professor
   Chairman, BCSIR, Dhaka
   _____
   Member (External)

# ABTRACT

In this study, different starch-based natural polymeric materials especially wheat powder (WP) and turmeric powder (TP) were collected from local market. Then the glutinous substances of these powder samples were removed by continuous washing with water and filtering followed by fornication to prepare their functional forms for the efficient adsorption of dyes from aqueous solution. Starch nanoparticles (SN) was synthesized from wheat powder by nanoprecipitation method. Furthermore, nanocomposites of polyaniline (PANI) and starch were prepared *in situ* and *ex-situ* polymerization of aniline using starch as a filler material in order to improve the mechanical and physical properties of the starch. Moreover, dispersion of the starch into PANI matrix makes the prepared composites biodegradable. Both kinds of nanomaterials were characterized with infra-red spectroscopic (IR), thermal analysis (DTA), scanning electron microscopic (SEM) and x-ray diffraction techniques (XRD).

The average size of SN estimated from Debye-Scherrer formula is 9 nm. Besides, the average particle size of PANI/starch Composite is about 18 nm which is smaller than that of PANI (20 nm). Comparison of thermal properties of the composites with the pure starch and PANI ensured the presence of both the starch and PANI in the composites. A good match was found also in the IR spectrum of the materials.

Adsorption behavior of the raw biosorbents (WP, TP and Starch) and synthetic adsorbents i.e., PANI, PANI/starch composite-1 and PANI/starch composite-2 were compared for the two typical ionic dyes, specifically, cationic methylene blue (MB) and anionic orange green (OG) based on the removal of the dyes as a result of adsorption from their neutral aqueous solution at room temperature. In the case of MB dye adsorption, the adsorption efficiencies of TP, PANI, Composite-1 and Composite-2 were found to be maximum and comparable. The adsorption efficiencies of WP, pure starch and SN were reasonably low, but the efficiency of SN was higher than that of pure starch. High adsorption efficiency of SN was revealed by SEM and XRD analysis to be due to the smaller particle size.

The OG dye was not adsorbed onto TP and other starch-based biosorbents i.e., WP, Starch and SN and showed very little adsorption capacities compared to the synthetic adsorbents PANI, Composite-1 and Composite-2.

Pure starch and starch-based WP and TP undergo biodegradation. Even though the SN has a higher efficacy than the pure starch, it has no experience of biodegradation. We estimated a rough calculation of the expenses of the biosorbents comparing with that of the synthetic conducting polymer adsorbents. Indeed WP and TP are too cheaper adsorbents. Moreover these adsorbents are biodegradable. Thus, we were interested in the detail adsorption study of these low-cost, biodegradable adsorbents which could also be recycled to produce alcohol and to recover the dyes for reuse.

In case of WP, the adsorption of MB is more favorable at low temperature. Conversely, for TP, the adsorption process of MB is more favorable at higher temperatures. Moreover, the adsorption of MB onto WP and TP follow the pseudo-second order adsorption mechanism and the adsorption is of Langmuir type.

With increasing the concentration of the electrolytes from 0 to 6 mM, the adsorption of MB dye onto TP was not decreased mostly but the adsorption was declined drastically onto WP. MB dye desorption from WP adsorbent was higher (80 %) in presence of divalent cation calcium ion rather in the presence of monovalent cation sodium (55 %). These ions might block the active sites of the adsorbents surface thus quite deactivating TP and WP towards MB dye.

It is very interesting to observe that OG dye didn't undergo any adsorption onto TP and showed a small adsorption onto WP in aqueous solution of pH 6.86. But in presence of $FeCl_3.6H_2O$, the adsorption of OG both onto WP and TP rapidly increases in the same pH. It is because the [Fe (III)] coagulant forms complex with the starch content of WP and TP.

The recovery (desorption) of MB adsorbed onto WP was carried out by changing temperature from 29 ºC to 37 ºC. Percent recovery of MB was found 70 % at 29 ºC but 81 % at 37 ºC. The higher rate of desorption at higher temperature would be due to the increasing of thermal energy of the adsorbed species.

**ACKNOWLEDGEMENT**

I would like to express my sincere appreciation to my respectable teacher and research supervisor Dr. Al-Nakib Chowdhury, Professor, Department of Chemistry, Bangladesh University of Engineering & Technology (BUET), Dhaka, Bangladesh for his consent to achieve my present research work and for his nonstop guidance, prompting idea, laborious efforts and dynamic encouragement throughout the progress of my research work. His acute interest, wise advices and worthy suggestion inspired me to face all sorts of problems confidently regarding my work.

I am grateful to Dr. Md. Monimul Huque, Professor, Department of Chemistry, BUET; Dr. Md. Manwarul Islam, Professor, Department of Chemistry, BUET; Dr. Md. Wahab Khan, Professor, Department of Chemistry, BUET; Dr. Md. Nazrul Islam, Associate Professor, Department of Chemistry, BUET; Mrs. Danisa Tabassum, Assistant Professor, Department of Chemistry, BUET; Dr. Abu Bin Imran, Assistant Professor, Department of Chemistry, BUET; Dr. Sakawat Hossain, Assistant Professor, Department of Chemistry, BUET and Dr. Shakila Rahman, Professor and Head, Department of Chemistry, BUET for their cordial advices and suggestions in my research. I am also grateful to other teachers and staff of Department of Chemistry, BUET.

I opt to convey my special thanks to Dr. Md. Mominul Islam, Assistant Professor, Department of Chemistry, Dhaka University (DU) for his constant cooperation and valuable discussion throughout the hole of my work. I am also pleased to Dr. A. Gafur, BCSIR, Dhaka for his kind assistance in taking XRD and Dr. Saleh Ahmed, Scientific Officer, Center of Advanced Research in Science, DU for his tireless cooperation in taking SEM of my samples.

I am grateful to the authority of BUET for providing financial assistance for my research work.

I would like to extend my thanks to Mr. Syed Abdul Monim, Mrs. Samira Saimoma, Mr. Arup Kumar Roy and Mrs. Maria Rahman who shared their view with me in solving different problems related to the research. Thanks to Mr. Kabir Hossain, Department of Chemistry, BUET, Dhaka for his cooperation in taking IR spectra of my research work. Above all, all thanks and gratitude is due to my almighty Allah whose blessings and sympathetic directions had been with me throughout the execution of my entire research.

**MD. BIN YEAMIN**
Author

# CONTENTS

## Chapter 2: Experimental



## Chapter 3: Results and Discussion

## LIST OF FIGURES

## LIST OF TABLES

## LIST OF SCHEMES

## 1.1 Background

Over the past decade, nanomaterials have been the subject of enormous interest. These materials, notable for their extremely small feature size, have the potential for wide-ranging industrial, biomedical, and electronic applications. As a result of recent improvement in technologies to see and manipulate these materials, the nanomaterials field has seen a huge increase in funding from private enterprises and government, and academic researchers within the field have formed many partnerships.

Nanomaterials can be metals, ceramics, polymeric materials, or composite materials. Their defining characteristic is a very small feature size in the range of 1-100 nanometer (nm) in at least one dimension. The unit of nanometer derives its prefix nano from a Greek word meaning dwarf or extremely small. One nanometer spans 3-5 atoms lined up in a row. By comparison, the diameter of a human hair is about 5 orders of magnitude larger than a nanoscale particle. Nanomaterials are not simply another step in miniaturization, but a different arena entirely; the nanoworld lies midway between the scale of atomic and quantum phenomena, and the scale of bulk materials. At the nanomaterial level, some material properties are affected by the laws of atomic physics, rather than behaving as traditional bulk materials do.

Although widespread interest in nanomaterials is recent, the concept was raised over 40 years ago. Physicist Richard Feynman delivered a talk in 1959 entitled "There's Plenty of Room at the Bottom", in which he commented that there were no fundamental physical reasons that materials could not be fabricated by maneuvering individual atoms. Nanomaterials have actually been produced and used by humans for hundreds of years - the beautiful ruby red color of some glass is due to gold nanoparticles trapped in the glass matrix. The decorative glaze known as luster, found on some medieval pottery, contains metallic spherical nanoparticles dispersed in a complex way in the glaze, which give rise to its special optical properties. The techniques used to produce these materials were considered trade secrets at the time, and are not wholly understood even now.

Development of nanotechnology has been spurred by refinement of tools to see the nanoworld, such as more sophisticated electron microscopy and scanning tunneling microscopy. By 1990, scientists at IBM had managed to position individual xenon atoms on a nickel surface to spell out the company logo, using scanning tunneling microscopy probes, as a demonstration of the extraordinary new technology being developed. In the mid-1980s a new class of material - hollow carbon spheres - was discovered. These spheres were called buckyballs or fullerenes, in honor of architect and futurist Buckminster Fuller, who designed a geodesic dome with geometry similar to that found on the molecular level in fullerenes. The $C_{60}$ (60 carbon atoms chemically bonded together in a ball-shaped molecule) buckyballs inspired research that led to fabrication of carbon nanofibers, with diameters under 100 nm. In 1991 S. Iijima of NEC in Japan reported the first observation of carbon nanotubes [1], which are now produced by a number of companies in commercial quantities. The world market for nanocomposites (one of many types of nanomaterials) grew to millions of pounds by 1999 and is still growing fast.

The variety of nanomaterials is great, and their range of properties and possible applications appear to be enormous, from extraordinarily tiny electronic devices, including miniature batteries, to biomedical uses, and as packaging films, superabsorbants, components of armor, and parts of automobiles. General Motors claims to have the first vehicle to use the materials for exterior automotive applications, in running boards on its mid-size vans. Editors of the journal *Science* profiled work that resulted in molecular-sized electronic circuits as the most important scientific development in 2001 [2]. It is clear that researchers are merely on the threshold of understanding and development, and that a great deal of fundamental work remains to be done.

Their extremely small feature size is of the same scale as the critical size for physical phenomena - for example, the radius of the tip of a crack in a material may be in the range 1-100 nm. The way a crack grows in a larger-scale, bulk material is likely to be different from crack propagation in a nanomaterial where crack and particle size are comparable. Fundamental electronic, magnetic, optical, chemical, and biological processes are also different at this level. Where proteins are 10-1000 nm in size, and

cell walls 1-100 nm thick, their behavior on encountering a nanomaterial may be quite different from that seen in relation to larger-scale materials. Nanocapsules and nanodevices may present new possibilities for drug delivery, gene therapy, and medical diagnostics.

Surfaces and interfaces are also important in explaining nanomaterial behavior. In bulk materials, only a relatively small percentage of atoms will be at or near a surface or interface (like a crystal grain boundary). In nanomaterials, the small feature size ensures that many atoms, perhaps half or more in some cases, will be near interfaces. Surface properties such as energy levels, electronic structure, and reactivity can be quite different from interior states, and give rise to quite different material properties.

Polymeric materials based nanocomposites are in one small division of nanomaterials. There are several varieties of polymeric nanocomposites, but the most commercially advanced are those that involve dispersion of small amounts of nanoparticles in a polymer matrix. Those most humble of materials, clays, have been found to impart amazing properties. For example, adding such small amounts as 2 % by volume of silicate nanoparticles to a polyimide resin increases the strength by 100 %. One should keep in mind, of course, that 2 % by volume of very small particles is a great many reinforcing particles. Addition of nanoparticles not only improves the mechanical properties, but also has been shown to improve thermal stability, in some cases allowing use of polymer-matrix nanocomposites an additional 100 degrees Centigrade above the normal service conditions. Decrease in material flammability has also been studied, an especially important property for transportation applications where choice of material is influenced by safety concerns. Clay/polymer nanocomposites have been considered as matrix materials for fiber-based composites destined for aerospace components. Aircraft and spacecraft components require lightweight materials with high strength and stiffness, among other qualities. Nanocomposites, with their superior thermal resistance, are also attractive for such applications as housings for electronics.

Others have examined the electrical properties of nanocomposites, with an eye to developing new conductive materials. The use of polymer-based nanocomposites has been expanded to anti-corrosion coatings on metals, and thin-film sensors. Their photoluminescence and other optical properties are being explored. Polymer-matrix nanocomposites can also be used to package films, an application which exploits their superior barrier properties and low permeability.

Although some nanomaterials require rather exotic approaches to synthesis and processing, many polymer-matrix nanocomposites can be prepared quite readily. Clay/polymer nanocomposites have been made by subjecting a clay such as montmorillonite to ion exchange or other pretreatment, then mixing the particles with polymer melts. There are also a number of other ways to fabricate the materials, including reactive processes involving in situ polymerization. The low volume fraction of reinforcement particles allows the use of well-established and well-understood processing methods, such as extrusion and injection molding. Ease of processing and forming may be one explanation for the rapidly expanding applications of the materials. Automotive companies, in particular, have quickly adopted nanocomposites in large scale applications, including structural parts of vehicles.

The most energetic research probably concerns carbon nanotubes. Nanoparticles of carbon - rods, fibers, tubes with single walls or double walls, open or closed ends, and straight or spiral forms - have been synthesized in the past 10 years. There is good reason to devote so much effort to them: carbon nanotubes have been shown to have unique properties, stiffness and strength higher than any other material, for example, as well as extraordinary electronic properties. Carbon nanotubes are reported to be thermally stable in vacuum up to 2800 degrees Centigrade, to have a capacity to carry an electric current a thousand times better than copper wires, and to have twice the thermal conductivity of diamond (which is also a form of carbon). Carbon nanotubes are used as reinforcing particles in nanocomposites, but also have many other potential applications. They could be the basis for a new era of electronic devices smaller and more powerful than any previously envisioned. Nanocomputers based on carbon nanotubes have already been demonstrated.

It is not so amazing, then, that government bodies, companies, and university researchers are joining forces or competing to synthesize, investigate, produce, and apply these amazing nanomaterials.

## 1.2 Nanomaterials

Nanomaterials is a field that takes a materials science-based approach to nanotechnology. It studies materials with morphological features on the nanoscale, and especially those that have special properties stemming from their nanoscale dimensions. Nanoscale is usually defined as smaller than a one tenth of a micrometer in at least one dimension, though this term is sometimes also used for materials smaller than one micrometer.

Nanotechnology [3] refers broadly to manipulating matter at the atomic or molecular scale and using materials and structures with nanosized dimension, usually ranging from 1 to 100 nanometers. Nanometer-sized particles have been developed to improve the mechanical properties of tires, initiate photographic film development, and serve as vital catalysts in the petrochemical industry.

Nanomaterials have offered great promise for delivering novel and improved environmental technology products by exhibiting their enhanced reactivity towards targeted contaminants and better mobility in the environmental media. For example, natural weathering of minerals and microorganisms produce nanosized colloids, which include dispersions of nanosized particles with special properties that can be important in the transport, transformation, and bioavailability of environmentally harmful substances [4]. Nanomaterials also offer applications to pollution prevention through improved catalytic processes that produce less waste, better sensors for process controls, enhanced separations, and increased understanding of the nano-sized natural processes that are involved in industrial processes [5].

### 1.2.1 Classification

Nanomaterials can be defined as materials which have structured components with at least one dimension less than 100 nm. Materials that have one dimension in the nanoscale are layers, such as a thin films or surface coatings. The classes of nanomaterials listed below are all very general and multi-functional.

*Fullerenes: Buckyballs and Carbon tubes*

Buckminsterfullerene $C_{60}$, also known as the buckyball, is a representative member of the carbon structures known as fullerenes. Members of the fullerene family are a major subject of research falling under the nanotechnology umbrella.

Carbon nanotubes (CNTs) were discovered by Sumio Iijima in 1991. Carbon nanotubes are fullerene-related structures which consist of rolled graphene sheets. There are two types of CNT: single-walled (one tube) or multi-walled (more tubes). Both of these are typically a few nanometres in diameter and several micrometres to centimetres long. Both members of the fullerene structural class, buckyballs and carbon tubes are carbon based, lattice-like, potentially porous molecules.

*Liquid Crystals:* Liquid crystal pharmaceuticals are composed of organic liquid crystal materials that mimic naturally-occuring biomolecules like proteins or lipids. They are considered a very safe method for drug delivery and can target specific areas of the body where tissues are inflammed, or where tumors are found.

*Liposomes:* Liposomes are lipid-based liquid crystals, used extensively in the pharmaceutical and cosmetic industries because of their capacity for breaking down inside cells once their delivery function has been met. Liposomes were the first engineered nanoparticles used for drug delivery but problems such as their propensity to fuse together in aqueous environments and release their payload, have lead to replacement, or stabilization using newer alternative nanoparticles.

*Nanoshell:* Also referred to as core-shells, nanoshells are spherical cores of a particular compound surrounded by a shell or outer coating of another, which is a few nanometers thick.

*Quantum dots:* Also known as nanocrystals, quantum dots are nanosized semiconductors that, depending on their size, can emit light in all colours of the rainbow. These nanostructures confine conduction band electrons, valence band holes, or excitons in all three spacial directions. Examples of quantum dots are semiconductor nanocrystals and core-shell nanocrystals, where there is an interface between different semiconductor materials. They have been applied in biotechnology for cell labelling and imaging, particularly in cancer imaging studies.

*Superparamagnetic nanoparticles:* Superparamagnetic molecules are those that are attracted to a magnetic field but do not retain residual magnetism after the field is removed. Nanoparticles of iron oxide with diameters in the 5-100 nm range, have been used for selective magnetic bioseparations. Typical techniques involve coating the particles with antibodies to cell-specific antigens, for separation from the surrounding matrix.

*Dendrimers:* Dendrimers are highly branched structures gaining wide use in nanomedicine because of the multiple molecular "hooks" on their surfaces that can be used to attach cell-identification tags, fluorescent dyes, enzymes and other molecules. The first dendritic molecules were produced around 1980, but interest in them has blossomed more recently as biotechnological uses are discovered.

*Nanorods:* Typically 1-100 nm in length, nanorods are most often made from semiconducting materials and used in nanomedicine as imaging and contrast agents. Nanorods can be made by generating small cylinders of silicon, gold or inorganic phosphate, among other materials.

*Nanowires:* Nanowires are ultrafine wires or linear arrays of dots, made from a wide range of materials

### 1.2.2 Properties of Nanomaterials

Two principal factors cause the properties [6-8] of nanomaterials to differ significantly from other materials: increased relative surface area, and quantum effects. The vastly increased ratio of surface area to volume present in many nanoscale materials, which makes possible new quantum mechanical effects. One example is the "quantum size effect" where the electronic properties of solids are altered with great reductions in particle size. This effect does not come into play by going from macro to micro dimensions. However, it becomes pronounced when the nanometer size range is reached. A certain number of physical properties also alter with the change from macroscopic systems. Novel mechanical properties of nanomaterials is a subject of nanomechanics research. Catalytic activities also reveal new behaviour in the interaction with biomaterials.

The general properties of nanomaterials are listed below:

**a) Electrical properties**

The electrical properties of nanomaterials vary between metallic to semiconducting materials. It depends on the diameter of the nanomaterials. The very high electrical conductivity of nanomaterial is due to minimum defects in the structure.

**b) Thermal conductivity**

The thermal conductivity of nanomaterials are very high, is due to the vibration of covalent bonds. Its thermal conductivity is 10 times greater than the metal. The very high thermal conductivity of nanomaterial is also due to minimum defects in the structure.

**c) Mechanical properties**

Nanomaterials are very strong and withstand extreme strain. Most of the materials fracture on bending because of the presence of more defects, but nanomaterials possesss only few defects in the structure.

### 1.2.3 Nanomaterials' Characterization

Nanomaterial characterization is necessary to establish understanding and control of nanoparticle synthesis and applications. Characterization is done by using a variety of different techniques, mainly drawn from materials science.

There are traditional techniques developed during 20th century in interface and colloid science for characterizing nanomaterials. These methods include several different techniques for characterizing particle size distribution. This characterization is imperative because many materials that are expected to be nano-sized are actually aggregated in solutions. Some of methods are based on light scattering. Others apply ultrasound, such as ultrasound attenuation spectroscopy for testing concentrated nano-dispersions and microemulsions [9].

There is also a group of traditional techniques for characterizing surface charge or zeta potential of nano-particles in solutions. This information is required for proper system stabilzation, preventing its aggregation or flocculation. These methods include microelectrophoresis, electrophoretic light scattering and electroacoustics. The last one, for instance colloid vibration current method is suitable for characterizing concentrated systems.

Most frequently used modern techniques are electron microscopy (TEM, SEM), atomic force microscopy (AFM), dynamic light scattering (DLS), X-ray photoelectron spectroscopy (XPS), powder X-ray diffraction (XRD), Fourier transform infrared spectroscopy (FTIR), matrix-assisted laser desorption/ionization time-of-flight mass spectrometry (MALDI-TOF), ultraviolet-visible spectroscopy, dual polarisation interferometry and nuclear magnetic resonance (NMR).

### 1.2.4 Applications of Nanomaterials

Since nanomaterials possess unique, beneficial chemical, physical, and mechanical properties, they can be used for a wide variety of applications. These applications include, but are not limited to, the following:

#### A. Next-Generation Computer Chips

The microelectronics industry has been emphasising miniaturisation, whereby the circuits, such as transistors, resistors, and capacitors, are reduced in size. By achieving a significant reduction in their size, the microprocessors, which contain these components, can run much faster, thereby enabling computations at far greater speeds. However, there are several technological impediments to these advancements, including lack of the ultrafine precursors to manufacture these components; poor dissipation of tremendous amount of heat generated by these microprocessors due to faster speeds; short mean time to failures (poor reliability) etc. Nanomaterials help the industry break these barriers down by providing the manufacturers with nanocrystalline starting materials, ultra-high purity materials, materials with better thermal conductivity, and longer-lasting, durable interconnections (connections between various components in the microprocessors).

#### B. Kinetic Energy (KE) Penetrators with Enhanced Lethality

The Department of Defense (DoD) is currently using depleted-uranium (DU) projectiles (penetrators) for its lethality against hardened targets and enemy armoured vehicles. However, DU has residual radioactivity, and hence, it is toxic (carcinogenic), explosive, and lethal to the personnel who use them. However, some of the important reasons for the continued use of DU penetrators are that they possess a unique self-sharpening mechanism on impact with a target, and the lack of suitable non-explosive, non-hazardous replacement for DU. Nanocrystalline tungsten heavy alloys lend themselves to such a self-sharpening mechanisms because of their unique deformation characteristics, such as grain-boundary sliding. Hence, nanocrystalline tungsten heavy alloys and composites are being evaluated as potential candidates to replace DU penetrators.

**C. Better Insulation Materials**

Nanocrystalline materials synthesised by the sol-gel technique result in foam like structures called "aerogels." These aerogels are porous and extremely lightweight; yet, they can loads equivalent to 100 times their weight. Aerogels are composed of three-dimensional, continuous networks of particles with air (or any other fluid, such as a gas) trapped at their interstices. Since they are porous and air is trapped at the interstices, aerogels are currently being used for insulation in offices, homes, etc. By using aerogels for insulation, heating and cooling bills are drastically reduced, thereby saving power and reducing the attendant environmental pollution. They are also being used as materials for "smart" windows, which darken when the sun is too bright (just as in changeable lenses in prescription spectacles and sunglasses) and they lighten themselves, when the sun is not shining too brightly.

**D. Phosphors for High-Definition TV**

The resolution of a television, or a monitor, depends greatly on the size of the pixel. These pixels are essentially made of materials called "phosphors," which glow when struck by a stream of electrons inside the cathode ray tube (CRT). The resolution improves with a reduction in the size of the pixel, or the phosphors. Nanocrystalline zinc selenide, zinc sulfide, cadmium sulfide, and lead telluride synthesised by the sol-gel techniques are candidates for improving the resolution of monitors. The use of nanophosphors is envisioned to reduce the cost of these displays so as to render high-definition televisions (HDTVs) and personal computers affordable to be purchased by an average household in the U. S.

**E. Low-Cost Flat-Panel Displays**

Flat-panel displays represent a huge market in the laptop (portable) computers industry. However, Japan is leading this market, primarily because of its research and development efforts on the materials for such displays. By synthesising nanocrystalline phosphors, the resolution of these display devices can be greatly enhanced, and the manufacturing costs can be significantly reduced. Also, the flat-panel displays constructed out of nanomaterials possess much higher brightness and

contrast than the conventional ones owing to their enhanced electrical and magnetic properties.

**F. Tougher and Harder Cutting Tools**

Cutting tools made of nanocrystalline materials, such as tungsten carbide, tantalum carbide, and titanium carbide, are much harder, much more wear-resistant, erosion-resistant, and last longer than their conventional (large-grained) counterparts. They also enable the manufacturer to machine various materials much faster, thereby increasing productivity and significantly reducing manufacturing costs. Also, for the miniaturisation of microelectronic circuits, the industry needs microdrills (drill bits with diameter less than the thickness of an average human hair or 100 μm) with enhanced edge retention and far better wear resistance. Since nanocrystalline carbides are much stronger, harder, and wear-resistant, they are currently being used in these microdrills.

**G. Elimination of Pollutants**

Nanocrystalline materials possess extremely large grain boundaries relative to their grain size. Hence, nanomaterials are very active in terms of chemical, physical, and mechanical properties. Due to their enhanced chemical activity, nanomaterials can be used as catalysts to react with such noxious and toxic gases as carbon monoxide and nitrogen oxide in automobile catalytic converters and power generation equipment to prevent environmental pollution arising from burning gasoline and coal.

**H. High Energy Density Batteries**

Conventional and rechargeable batteries are used in almost all applications that require electric power. These applications include automobiles, laptop computers, electric vehicles, next-generation electric vehicles (NGEV) to reduce environmental pollution, personal stereos, cellular phones, cordless phones, toys, and watches. The energy density (storage capacity) of these batteries is quite low requiring frequent recharging. The life of conventional and rechargeable batteries is also low. Nanocrystalline materials synthesised by sol-gel techniques are candidates for

separator plates in batteries because of their foam-like (aerogel) structure, which can hold considerably more energy than their conventional counterparts. Furthermore, nickel-metal hydride (Ni-MH) batteries made of nanocrystalline nickel and metal hydrides are envisioned to require far less frequent recharging and to last much longer because of their large grain boundary (surface) area and enhanced physical, chemical, and mechanical properties.

**I. High-Power Magnets**

The strength of a magnet is measured in terms of coercivity and saturation magnetisation values. These values increase with a decrease in the grain size and an increase in the specific surface area (surface area per unit volume of the grains) of the grains. It has been shown that magnets made of nanocrystalline yttrium-samarium-cobalt grains possess very unusual magnetic properties due to their extremely large surface area. Typical applications for these high-power rare-earth magnets include quieter submarines, automobile alternators, land-based power generators, motors for ships, ultra-sensitive analytical instruments, and magnetic resonance imaging (MRI) in medical diagnostics.

**J. High-Sensitivity Sensors**

Sensors employ their sensitivity to the changes in various parameters they are designed to measure. The measured parameters include electrical resistivity, chemical activity, magnetic permeability, thermal conductivity, and capacitance. All of these parameters depend greatly on the microstructure (grain size) of the materials employed in the sensors. A change in the sensor's environment is manifested by the sensor material's chemical, physical, or mechanical characteristics, which is exploited for detection. For instance, a carbon monoxide sensor made of zirconium oxide (zirconia) uses its chemical stability to detect the presence of carbon monoxide. In the event of carbon monoxide's presence, the oxygen atoms in zirconium oxide react with the carbon in carbon monoxide to partially reduce zirconium oxide. This reaction triggers a change in the sensor's characteristics, such as conductivity (or resistivity) and capacitance. The rate and the extent of this reaction are greatly increased by a

decrease in the grain size. Hence, sensors made nanocrystalline materials are extremely sensitive to the change in their environment. Typical applications for sensors made out of nanocrystalline materials are smoke detectors, ice detectors on aircraft wings, automobile engine performance sensor, etc.

**K. Automobiles with Greater Fuel Efficiency**

Currently, automobile engines waste considerable amounts of gasoline, thereby contributing to environmental pollution by not completely combusting the fuel. A conventional spark plug is not designed to burn the gasoline completely and efficiently. This problem is compounded by defective, or worn-out, spark plug electrodes. Since nanomaterials are stronger, harder, and much more wear-resistant and erosion-resistant, they are presently being envisioned to be used as spark plugs. These electrodes render the spark plugs longer-lasting and combust fuel far more efficiently and completely. A radically new spark plug design called the "railplug" is also in the prototype stages. This railplug uses the technology derived from the "railgun," which is a spin-off of the popular Star Wars defense program. However, these railplugs generate much more powerful sparks (with an energy density of approximately 1 $kJ/mm^2$). Hence, conventional materials erode and corrode too soon and quite frequently to be of any practical use in automobiles. Nevertheless, railplugs made of nanomaterials last much longer even the conventional spark plugs. Also, automobiles waste significant amounts of energy by losing the thermal energy generated by the engine. This is especially true in the case of diesel engines. Hence, the engine cylinders (liners) are currently being envisioned to be coated with nanocrystalline ceramics, such as zirconia and alumina, so that they retain heat much more efficiently and result in complete and efficient combustion of the fuel.

**M. Aerospace Components with Enhanced Performance Characteristics**

Due to the risks involved in flying, aircraft manufacturers strive to make the aerospace components stronger, tougher, and last longer. One of the key properties required of the aircraft components is the fatigue strength, which decreases with the component’s age. By making the components out of stronger materials, the life of the

aircraft is greatly increased. The fatigue strength increases with a reduction in the grain size of the material. Nanomaterials provide such a significant reduction in the grain size over conventional materials that the fatigue life is increased by an average of 200-300 %. Furthermore, components made of nanomaterials are stronger and can operate at higher temperatures, aircrafts can fly faster and more efficiently (for the same amount of aviation fuel). In spacecrafts, elevated-temperature strength of the material is crucial because the components (such as rocket engines, thrusters, and vectoring nozzles) operate at much higher temperatures than aircrafts and higher speeds. Nanomaterials are perfect candidates for spacecraft applications, as well.

**N. Better and Future Weapons Platforms**

Conventional guns, such as cannons, 155 mm howitzers, and multiple-launch rocket system (MLRS), utilise the chemical energy derived by igniting a charge of chemicals (gun powder). The maximum velocity at which the penetrator can be propelled is approximately 1.5-2.0 km/sec. On the other hand, electromagnetic launchers (EML guns), or railguns, use the electrical energy, and the concomitant magnetic field (energy), to propel the penetrators/projectiles at velocities up to 10 km/sec. This increase in velocity results in greater kinetic energy for the same penetrator mass. The greater the energy, the greater is the damage inflicted on the target. For this and other reasons, the DoD (especially, the U. S. Army) has conducted extensive research into the railguns. Since a railgun operates on electrical energy, the rails need to be very good conductors of electricity. Also, they need to be so strong and rigid that the railgun does not sag while firing and buckle under its own weight. The obvious choice for high electrical conductivity is copper. However, the railguns made out of copper wear out much too quickly due to the erosion of the rails by the hypervelocity projectiles and they lack high-temperature strength. The wear and erosion of copper rails necessitate inordinately frequent barrel replacements. In order to satisfy these requirements, a nanocrystalline composite material made of tungsten, copper, and titanium diboride is being evaluated as a potential candidate. This nanocomposite possesses the requisite electrical conductivity, adequate thermal conductivity, excellent high strength, high rigidity, hardness, and wear/erosion resistance. This

results in longer-lasting, wear-resistant, and erosion-resistant railguns, which can be fired more frequently and often than their conventional counterparts.

**O. Longer-Lasting Satellites**

Satellites are being used for both defence and civilian applications. These satellites utilise thruster rockets to remain in or change their orbits due to a variety of factors including the influence of gravitational forces exerted by the earth. Hence, these satellites are repositioned using these thrusters. The life of these satellites, to a large extent, is determined by the amount of fuel they can carry on board. In fact, more than 1/3 of the fuel carried aboard by the satellites is wasted by these repositioning thrusters due to incomplete and inefficient combustion of the fuel, such as hydrazine. The reason for the incomplete and inefficient combustion is that the onboard ignitors wear out quickly and cease to perform effectively. Nanomaterials, such as nanocrsytalline tungsten-titanium diboride-copper composite, are potential candidates for enhancing these ignitors' life and performance characteristics.

**P. Longer-Lasting Medical Implants**

Currently, medical implants, such as orthopaedic implants and heart valves, are made of titanium and stainless steel alloys. These alloys are primarily used in humans because they are biocompatible, i.e., they do not adversely react with human tissue. In the case of orthopaedic implants (artificial bones for hip, etc.), these materials are relatively non-porous. For an implant to effectively mimic a natural human bone, the surrounding tissue must penetrate the implants, thereby affording the implant with the required strength. Since these materials are relatively impervious, human tissue does not penetrate the implants, thereby reducing their effectiveness. Furthermore, these metal alloys wear out quickly necessitating frequent, and often very expensive, surgeries. However, nanocrystalline zirconia (zirconium oxide) ceramic is hard, wear-resistant, corrosion-resistant (biological fluids are corrosive), and biocompatible. Nanoceramics can also be made porous into aerogels (aerogels can withstand up to 100 times their weight), if they are synthesized by sol-gel techniques. This results in far less frequent implant replacements, and hence, a significant reduction in surgical

expenses. Nanocrystalline silicon carbide (SiC) is a candidate material for artificial heart valves primarily due to its low weight, high strength, extreme hardness, wear resistance, inertness (SiC does not react with biological fluids), and corrosion resistance.

**Q. Ductile, Machinable Ceramics**

Ceramics, per se, are very hard, brittle, and hard to machine. These characteristics of ceramics have discouraged the potential users from exploiting their beneficial properties. However, with a reduction in grain size, these ceramics have increasingly been used. Zirconia, a hard, brittle ceramic, has even been rendered superplastic, i.e., it can be deformed to great lengths (up to 300 % of its original length). However, these ceramics must possess nanocrystalline grains to be superplastic. In fact, nanocrystalline ceramics, such as silicon nitride ($Si_3N_4$) and silicon carbide (SiC), have been used in such automotive applications as high-strength springs, ball bearings, and valve lifters, because they possess good formability and machinabilty combined with excellent physical, chemical, and mechanical properties. They are also used as components in high-temperature furnaces. Nanocrystalline ceramics can be pressed and sintered into various shapes at significantly lower temperatures, whereas it would be very difficult, if not impossible, to press and sinter conventional ceramics even at high temperatures.

**R. Large Electrochromic Display Devices**

An electrochromic device consists of materials in which an optical absorption band can be introduced, or an existing band can be altered by the passage of current through the materials, or by the application of an electric field. Nanocrystalline materials, such as tungstic oxide ($WO_3.xH_2O$) gel, are used in very large electrochromic display devices. The reaction governing electrochromism (a reversible coloration process under the influence of an electric field) is the double-injection of ions (or protons, $H^+$) and electrons, which combine with the nanocrystalline tungstic acid to form a tungsten bronze. These devices are primarily used in public billboards and ticker boards to convey information. Electrochromic devices are similar to liquid-

crystal displays (LCD) commonly used in calculators and watches. However, electrochromic devices display information by changing colour when a voltage is applied. When the polarity is reversed, the colour is bleached. The resolution, brightness, and contrast of these devices greatly depend on the tungstic acid gel's grain size. Hence, nanomaterials are being explored for this purpose.

### 1.3 Bionanomaterials

Nanomaterial utilizes nanoscale engineering and system integration of existing materials to develop better materials and products. Applications of nanomaterials have made their presence strongly felt in various areas like healthcare, implants, and prostheses; smart textiles, energy generation and conservation with energy generating materials and highly efficient batteries, defence, security, terrorism, and surveillance. Bionanomaterial's research has emerged as a new exciting field, recognized as a new interdisciplinary frontier in the field of life science and material science. Great advances in nanobiochip materials, nanoscale biomimetic materials, nanomotors, nanocomposite materials, interface biomaterials, nanobiosensors, and nano-drug-delivery systems have the enormous prospect in industrial, defense, and clinical medicine applications.

A nanobiomaterial can be defined as a biomaterial substrate composed of nanometer-scale components. One example of a naturally occurring nanobiomaterial is inorganic bone matrix which is composed of hydroxyapatite crystals. Significant property changes can occur at the nanoscale, especially related to surface energy and reactivity. There are more atoms at the surface of nanostructured biomaterials which results in a marked increase in surface area to volume ratio when compared to micron scale biomaterials. Correlations of surface properties with stability, toxicity, and misdistributions are essential for in vivo applications. This is very important considering that, for example, cell adhesion, proliferation, and migration during tissue repair is dependent on protein adsorption on the surface of implanted biomaterials.

### 1.3.1 Biodegradability of Bionanomaterials

Biodegradation or biotic degradation or biotic decomposition is the chemical dissolution of materials by bacteria or other biological means. It is the natural process in which the degradation of materials results from the action of naturally-occurring microorganisms such as bacteria, fungi or algae. The term is often used in relation to ecology, waste management, biomedicine, and the natural environment (bioremediation) and is now commonly associated with environmentally friendly products that are capable of decomposing back into natural elements. Organic material can be degraded aerobically with oxygen, or anaerobically, without oxygen. A term related to biodegradation is biomineralisation, in which organic matter is converted into minerals. Biosurfactant, an extracellular surfactant secreted by microorganisms, enhances the biodegradation process.

Biodegradable matter is generally organic material such as plant and animal matter and other substances originating from living organisms, or artificial materials that are similar enough to plant and animal matter to be put to use by microorganisms. Some microorganisms have a naturally occurring, microbial catabolic diversity to degrade, transform or accumulate a huge range of compounds including hydrocarbons (e.g. oil), polychlorinated biphenyls (PCBs), polyaromatic hydrocarbons (PAHs), pharmaceutical substances, radionuclides and metals. Major methodological breakthroughs in microbial biodegradation have enabled detailed genomic, metagenomic, proteomic, bioinformatic and other high-throughput analyses of environmentally relevant microorganisms providing unprecedented insights into key biodegradative pathways and the ability of microorganisms to adapt to changing environmental conditions. Products that contain biodegradable matter and non-biodegradable matter are often marketed as biodegradable.

Biodegradable plastics break down completely into nonplastic and nontoxic constituent-substances like water, $CO_2$, $CH_4$ and biological materials. It is known that biodegradation is not significant in the first step of biological degradation of polyethylene, which has a good resistance to microorganisms. The oxidation is an important first degradation step for non-hydrolysable materials such as polyethylene.

Photo-oxidation increases the amount of low molecular weight material by breaking bonds and increasing the surface area. In the second degradation step, microorganisms may utilize the abiotic degradation products and low molecular weight polymer. Relatively inert polyethylene could become more degradable by introducing additives to it.

Starch is used as a biodegradation additive. Beside starch, the pro-oxidant formulation consisting of an unsaturated polymer, a transition-metal salt and thermal stabiliser, can also be used as additives for polyethylene. The major role of starch has been found to provide higher oxygen permeability as it is consumed by microorganisms. The matrix is hollowed out and the surface/volume ratio increases. Another effect of the higher permeability of the matrix is the facilitated release of degradation products from the samples. This is most obvious when the degradation is performed in an aqueous environment [10].

### 1.3.2 General Preparation of Bionanomaterials

Biodegradable nanoparticles can be prepared from a variety of materials such as proteins, polysaccharides and synthetic biodegradable polymers. The selection of the base polymer is based on various designs and end application criteria. It depends on many factors such as 1) size of the desired nanoparticles, 2) properties of the materials (aqueous solubility, stability etc.) to be encapsulated in the polymer, 3) surface characteristics and functionality, 4) degree of biodegradability and biocompatibility. Depending upon selection of desired criteria for the preparation of the nanoparticles, the methods can be classified as following 1) dispersion of preformed polymers, 2) polymerization of monomers and 3) ionic gelation method for hydrophilic polymers [11].

**Dispersion of Performed Polymers**

This technique can be used in several ways as described below:

(a) Solvent evaporation method

In this technique the polymer is dissolved in an organic solvent such as dichloromethane, chloroform or ethyl acetate. The drug is dissolved or dispersed in the preformed polymer solution followed by emulsification of the mixture to form an oil/water (o/w) emulsion using an appropriate surfactant/emulsifying agents.

Most commonly used surfactant/emulsifying agents for this purpose are gelatin and polyvinyl alcohol. After formation of a stable emulsion the organic solvent is evaporated by increasing the temperature or pressure along with continuous stirring of the solution. Process parameters such as stabilizer and polymer concentration and stirring speed have a great influence on the particle size of the nanoparticles (NPs) formed.

(b) Spontaneous emulsification/solvent diffusion method

This is a modified solvent diffusion method where a water-miscible solvent such as acetone or methanol along with a water-insoluble organic solvent such as dichloromethane or chloroform are used as an oil phase. Due to the spontaneous diffusion of solvents, an interfacial turbulence is created between the two phases leading to the formation of smaller particles. As the concentration of water- soluble solvent increases, smaller particle sizes of NPs can be achieved.

(c) Nanoprecipitation method

Polymers are dissolved in a polar, water-miscible solvent such as acetone, acetonitrile, ethanol, or methanol. The solution is then poured in a controlled manner (i.e. drop-by-drop addition) into an aqueous solution with surfactant. Nanoparticles are formed instantaneously by rapid solvent diffusion. Finally, the solvent is removed under reduced pressure. **Scheme 1.1** shows a schematic representation of this method.

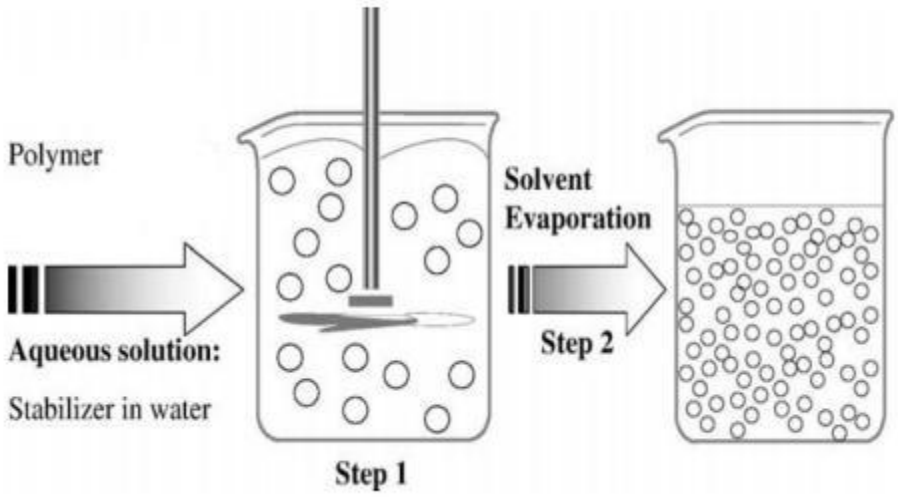


**Scheme 1.1** Schemetic representation of the nanoprecipitation technique [11]

**Polymerization Methods**

NPs are prepared from monomers that are polymerized to form NPs in an aqueous solution. Vaccines or drugs/therapeutic agents are incorporated in the NPs either by dissolving the drug in the polymerization medium or by adsorption/attachment of the drug onto the polymerized and fully formed NPs. The NPs suspension is then purified by removing stabilizers. The surfactants may be recycled for subsequent polymerization. This technique of NPs preparation has been reported for making poly-butylcyanoacrylate or poly-alkyl-cyanoacrylate NPs. The concentration of surfactant and the stabilizer determines the final size of the NPs formed.

**Ionic gelation method for hydrophilic polymers**

Some of the natural macromolecules have been used to prepare NPs. These polymers include gelatin, alginate, chitosan and agarose. They are hydrophilic natural polymers and have been used to synthesize biodegradable NPs by the ionic gelation method. This involves the transition of materials from liquid to gel due to ionic interaction at room temperature. An example of preparation of gelatin NPs includes hardening of the droplets of emulsified gelatin solution into gelatin NPs. The gelatin emulsion

droplets are cooled below the gelation point in an ice bath leading to gelation of the droplets into gelatin NPs. Alginate NPs are reported to be produced by drop-by-drop extrusion of the sodium alginate solution into the calcium chloride solution. Sodium alginate is a water-soluble polymer that gels in the presence of multivalent cations such as calcium. Chitosan NPs are prepared by spontaneous formation of complexes between chitosan and polyanions or by the gelation of a chitosan solution dispersed in an oil emulsion.

### 1.3.3 Bionanocomposites

Bionanocomposites (BNCs), a novel invention of nanocomposite materials, indicate a promising field in the frontiers of nanotechnology, materials and life sciences. A possible definition of a bionanocomposite can be established on the basis of the traditional acceptance of nanocomposite, as a multiphase material where one of the phases has at least one dimension of less than 100 nm, and adding one of the phases of biological origin. In many cases, a more restricted acceptance of the term considers that bionanocomposites contain at least one biological and one inorganic component, making them closely related to biohybrid systems. Under this assumption, two limit systems can be envisioned consisting either of inorganic colloids entrapped in a biomolecular network or of biological colloids incorporated within an inorganic matrix.

In other words, BNCs are composed of a natural polymer matrix and organic/inorganic filler with at least one dimension on the nanometer scale. BNCs has particular size, geometry, and surface chemistry properties. The polymers used are normally hydrocolloids, such as proteins, starches, pectins, and other polysaccharides. Various inorganic nano-particles have been recognized as possible additives to enhance the polymer performance. Nanofillers include solid layered clays, synthetic polymer nanofibers, cellulose nano-whiskers, and carbon nanotubes. Up to now only the layered inorganic solids like layered silicate have attracted the attention of the packaging industry [12].

In addition to these characteristics, BNCs show the extraordinary advantages of biocompatibility and biodegradability in various medical, drug release packaging, agricultural applications, and smart adsorbents. Among natural polymers, starch is one of the most promising biocompatible and biodegradable materials because it is a renewable resource that is universally available and of low cost. A number of researchers have presented work in the field of starch-based BNCs, which can be obtained by filling a thermoplastic starch matrix with nanofillers such as layer silicates. Montmorillonite and kaolinite are the usual layer silicates used in starch-based BNCs [13].

Up to now, degradable or biodegradable materials have been extensively tested in field trials in different countries and for different crops. Successful results have been obtained such as in maize, melon, strawberries, and cotton mulch film applications. The use of biodegradable materials in agriculture can promote sustainable and environmentally friendly cultivation reducing the contamination of the soil, enhancing the protection of the landscape in rural areas against pollution, and increasing the use of renewable non-oil raw materials such as starch [12].

When polymers are combined with nanofillers, the resulting in bionanocomposites exhibit significant improvements in mechanical properties, dimensional stability, and solvent or gas resistance with respect to the pristine polymer. BNCs also offer extra benefits like low density, transparency, good flow, better surface properties, and recyclability.

### 1.3.4 Preparative Techniques of Bionanocomposites

The techniques used to manufacture bio-nanocomposites are based largely on existing techniques for processing plastics or composite materials. There is considerable literature available devoted to developing bionanocomposites with different combinations, employing somewhat different technologies appropriate to each. The technologies are broadly classed into three main categories:

**Mechanical Mixing**

The simplest method to prepare bionanocomposites based on biopolymer hydrogels is to start from a physical mixture between the polymer and the particles both in a sol phase and then to induce gelation, either via a change in temperature (gelatin), pH (collagen and chitosan) or addition of crosslinking species (alginate and carragheenan) [**Scheme 1.2 (a)**]. The main advantage of this approach is that the size, morphology, and surface properties of the inorganic colloids are initially defined and designed. Moreover, if required, particles preparation can be performed in conditions that would not be compatible with the preservation of the biopolymer integrity or solubility, such as extreme pH, use of organic solvents, high temperature, or pressure. The main limitation of this technique is related to the achievable bio-organic/inorganic contents and ratios that depend (i) on the viscosity of the polymer sol that increases with biopolymer concentration but also upon addition of nanoparticles and (ii) on the colloidal stability of the inorganic particles, both in the initial media and in presence of the biomacromolecule sol. This will dramatically impact on the particle dispersion in the hydrogel and hence on the final homogeneity of the bionanocomposite. In certain cases, the addition of nanoparticles may even hinder the gelation process.

***In Situ* Synthesis of Particles and the Biotemplating Approach**

Biopolymers can be used as templates for the synthesis of nanoparticles. When compared with mechanical mixing, this strategy should limit diffusion issues met with preformed particles. This method starts from inorganic nanoparticle precursor species, ions or poly-ions, further converted into solids by a second reaction sequence [**Scheme 1.2 (b)**]. The first step is usually performed by addition of the inorganic precursor to the polymer sol before inducing gelation, but it is also possible to perform precursor impregnation once the hydrogel is obtained. The mineralization process can then be induced by pH modification, addition of reducing agent, carbonation or supplementation by any other suitable reagent, in the liquid phase or in the gas phase.

An alternative approach is to use bifunctional ions that act both as mineral precursors and network crosslinkers for the gelation of ionotropic systems [**Scheme 1.2 (c)**]. In contrast to the later synthetic procedure, the network crosslinkers can be distinguished from the particle precursors [**Scheme 1.2 (b)**] by their key role in hydrogel formation before particle templating. In this respect, Co, Ni, and CoNi nanoparticles have been formed within alginate matrices, where metal cations act as crosslinkers of gel networks, which in turn act as a confined medium that limits the growth of metal particles.

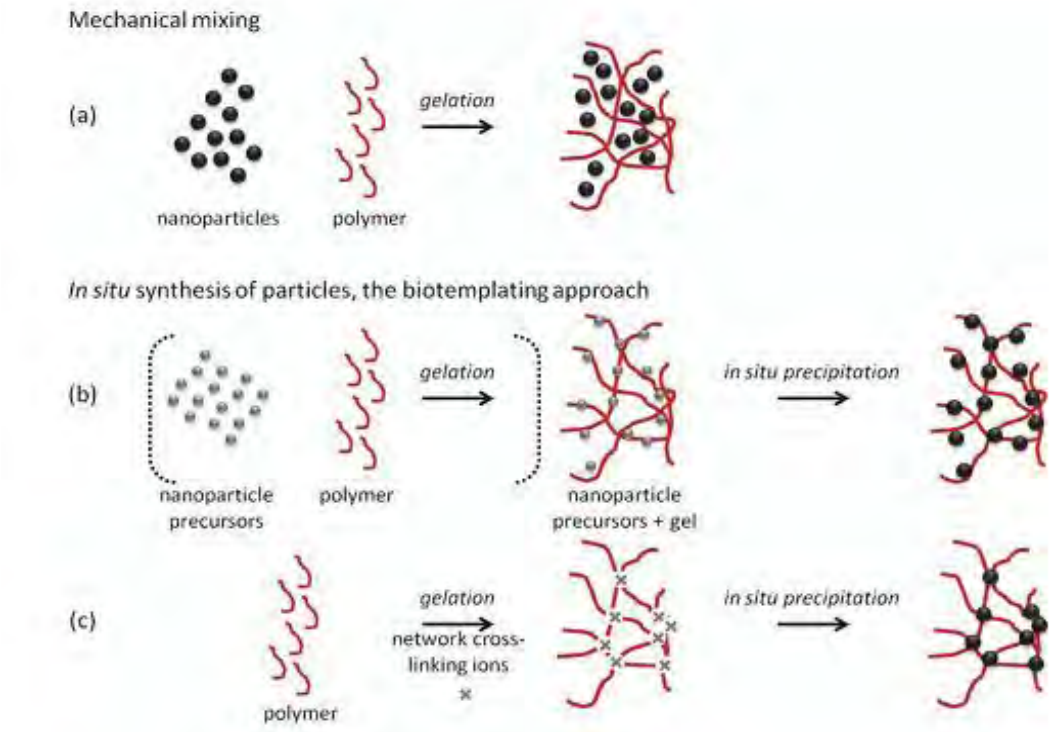


**Scheme 1.2** Schemetic representation of the preparation methods for the synthesis of bionanocomposites. (a) Mechanical mixing and (b and c) *in situ* synthesis of particles from nanoparticle precursors and network crosslinking ions, respectively [14].

### 1.3.5 Characterization of Nanocomposites

In addition to the SEM and XRD analyses, the thermal analyses (TA) are the most convenient means of nanocomposites' characterization. Thermal methods of analysis may be defined as those techniques in which changes in physical and/or chemical properties of a substance are measured as a function of temperature. There are of different types of thermal analyses namely thermogravimetry (TG), differential thermal analysis (DTA). In the former case, the results may be presented as a thermogravimetric (TG) curve, in which weight change is recorded as a function of temperature or time; or as a derivative thermogravimetric (DTG) curve, where the first derivative of the TG curve is plotted with respect to either temperature or time. The differential thermal analysis (DTA) is a technique in which the temperature difference between a substance and a reference material is measured as a function of temperature whilst the substance and the reference are subjected to a controlled temperature programme. **Fig. 1.1** shows the TG, DTG and DTA curves of pure starch.

In DTA, both the test sample and an inert reference material (usually α-alumina) undergo a controlled heating or cooling program which is usually linear with respect to time. There is a zero temperature difference between the sample and the reference material when the sample does not undergo any chemical or physical change. But if any reaction take place, then a temperature difference (ΔT) will occur between the sample and reference material. Thus in an endothermic change, e. g., when the sample melts or is dehydrated, the sample is at a lower temperature than the reference material. This condition is only transitory because, on completion of the reaction, the sample will again show zero temperature difference compared with the reference. Sharp endothermic peaks often signify changes in crystallinity or fusion processes, whereas broad endotherms arise from dehydration reactions. Physical changes usually result in endothermic curves whereas chemical reactions, particularly those of an oxidative nature, are predominantly exothermic [15].

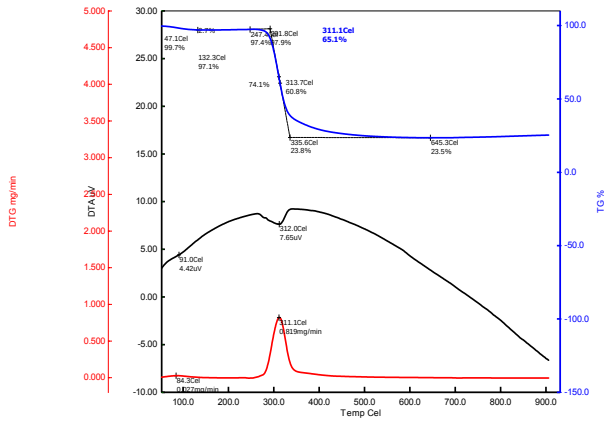


**Fig 1.1** Thermal behaviours of pure starch. The upper blue color shows TGA curve, the middle black color shows DTA curve and the bottom red color shows the DTG curve.

The advantages of TA over other analytical methods can be summarized as follows: (i) the sample can be studied over a wide temperature range using various temperature programmes; (ii) almost any physical form of sample (solid, liquid or gel) can be accommodated using a variety of sample vessels or attachments; (iii) a small amount of sample (0.1 µg-10 mg) is required; (iv) the atmosphere in the vicinity of the sample can be standardized; (v) the time required to complete an experiment ranges from several minutes to several hours; and (vi) TA instruments are reasonably priced. In polymer science, preliminary investigation of the sample transition temperatures and decomposition characteristics is routinely performed using TA before spectroscopic analysis is begun.

TA data are indirect and must be collated with results from spectroscopic measurements [for example NMR, Fourier transform infrared (FTIR) spectroscopy, X-ray diffractometry] before the molecular processes responsible for the observed behaviour can be elucidated.

## 1.4 Dyes and its Classification

A substance is referred to as a dye when it bears the following criteria [16]

1. It must have a desired color to match the object to be dyed.

2. It must be capable of being fixed to the fabrics or supports directly or indirectly with the help of certain reagents called mordant.

3. When fixed to the supports, the color must be fast to light and resistant to soap and water and to a certain extent to dilute acids and alkalis.

Dyes can be classified as anionic, cationic and nonionic according to their dissociation in an aqueous solution. According to the application they can be classified as bellow [17] –

**1. Acid dyes:** Acid dyes are anionic compounds that are mainly used for dyeing nitrogen containing fabrics like wool, polyamide, and silk and modified acryl. Most acid dyes are azo, anthraquinone or triarylmethane.

**2. Reactive dyes:** Dyes with reactive groups that form covalent bonds with $OH^-$, $NH^-$ or $HS^-$ groups in fibers are known as reactive dyes. The reactive group is often a heterocyclic aromatic ring substituted with chloride or fluoride (e.g., diclorotriazine).

**3. Metal complex dyes:** These are strong complexes of one metal atom (usually Cr, Cu, Co or Ni) and one or two dye molecules, respectively 1:1 and 1:2 metal complex dyes.

**4. Basic dyes:** Basic dyes are cationic compounds that are used for dyeing acid group containing fibers, usually synthetic fibers like modified polyacryl.

**5. Pigment dyes:** These insoluble, nonionic compounds or insoluble salts retain their crystalline or particulate structure throughout their application.

**6. Sulfur dyes:** Sulfur dyes are complex polymeric aromatics with heterocyclic S-containing rings.

**7. Solvent dyes:** Solvent dyes are nonionic dyes that are used for dyeing substrates in which they dissolve (e.g., plastics, varnish, ink, waxes and fats).

**8. Food dyes:** Food dyes are usually used in foods, soft drinks, medicines etc. These dyes should be used in such quantity that would not cause any health hazard to human

being. These dyes are prepared from coal tar such as tartrazine, sunset yellow, carmoisine, green-S, allura red, caramel aqua marine etc.

**9. Organic Ionic dyes:** Methylene blue (MB) and orange green (OG) are the typical organic ionic dyes. MB is cationic in nature while OG is an anionic one. Molecular weight of MB and OG are 355.89 and 452.38. $\lambda_{max}$ of MB and OG are 664 nm and 477 nm respectively. There chemical structures are shown in **Fig. 1.2**.

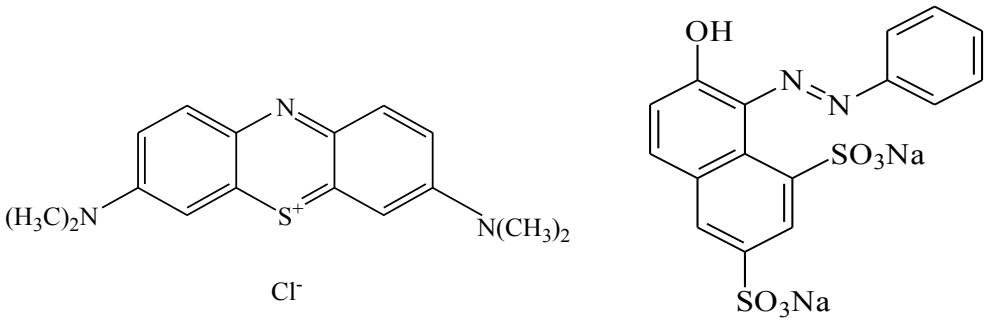


(a) (b)

**Fig. 1.2** Chemical structure of (a) MB and (b) OG.

### 1.4.1 Importance of Dye removing from Water

Industries such as textiles, paper, plastics, leather, food, and cosmetic are widely using various dyes and pigments to color products. These industrial wastes are the main sources of water as well as environmental pollution because these contain a lot of non-biodegradable organic dyes. In dyeing processes, 10-15 % of all dyestuffs is being lost directly to wastewater besides any pretreatment. The discharge of colored wastewater from these industries produces an eco-toxic hazard and introduces the potential danger of bioaccumulation [18]. That's why the removal of organic dyes from water is the prime challenge to the present world.

### 1.4.2 Dye Removal by Bio (nano) materials

Nanomaterials are applicable in the areas of reduction of environmental burden, reduction/treatment of industrial and agricultural wastes, and nonpoint source (NPS) pollution control. First, environmental burden reduction involves green process and engineering, emissions control, desulfurization/denitrification of nonrenewable energy sources, and improvement of agriculture and food systems. Second, reduction/treatment of industrial and agricultural wastes involves converting wastes into products, groundwater remediation, adsorption, delaying photocatalysis, and nanomembranes. Third, NPS pollution control involves controlling water pollution. NPS pollution derives from various sources, including automobile emissions, road dirt, leachate from agricultural fields, home gardens, construction runoff, and mining operations. NPS pollutants fall into seven major categories: sediment, nutrient, acid and salt, heavy metal, toxic chemical, pathogen, and contaminant.

Nanomaterials alter physical properties on a nanoscale due to their high specific surface area to volume ratio. They are used as catalysts, adsorbents, membranes, and additives to increase activity and capability due to their high specific surface areas and nano-sized effects. Thus, nanomaterials are more effective at treating environmental wastes because they reduce the amount of material needed. The use of natural biomaterials is a promising alternative due to their relative abundance and their low commercial value [19].

### 1.4.3 Dye Removal Techniques

Depending on the effectiveness, economic cost and environmental impact of the treatment process, several methods are developed to remove color from dyehouse effluent as shown in the **Fig. 1.3**. Among these biological treatment, membrane filtration, chemical oxidation, electrochemical techniques and adsorption are conventional paths for the treatment of wastewater. Biological treatments (aerobic–anaerobic) are relatively ineffective in effluent decolorization, because high molecular weight dyes can't effectively degraded by bacteria [20]. The latest developed low pressure chemical oxidation using Fenton's reagent ($H_2O_2$ + Fe (II) salts) decolorizes

both soluble and insoluble dyes but some biodegradable matter still remains. Another chemical treatment, ozonation, is at high cost because of the demand of continuous ozone supply. The electrochemical methods are very efficient with no chemical consumption but these techniques are relatively more expensive and thus economically unfavorable.

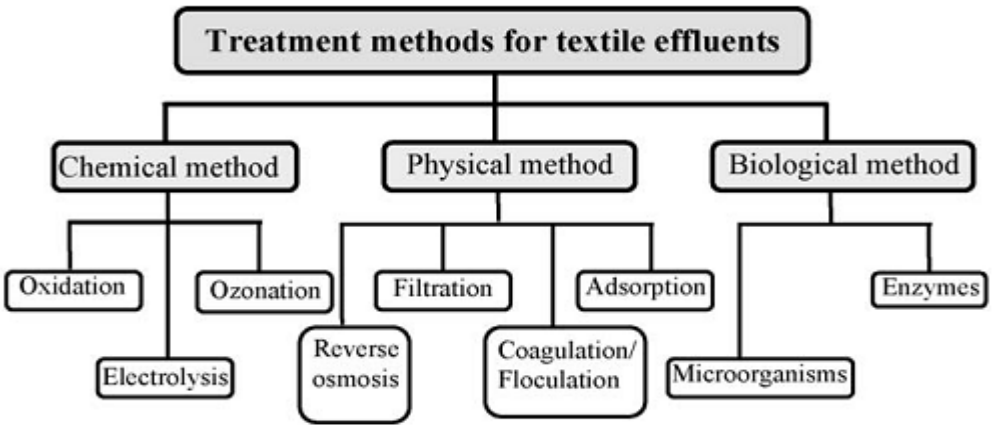


**Fig. 1.3** Treatment methods for the removal of dyes from wastewater effluents

Physical methods e.g., membrane filtration has the ability to clarify, concentrate and separate dye continuously from effluent but it has a high capital cost and the membranes are prone to clogging. The adsorption process has particular advantages because it removes the complete dye molecule, leaving no fragments in the wastewater. Thus it is the key choice due to the low generation of residues and the possibility of recycling and reuse of the adsorbents and/or dyes that are very important from the environmental and economical viewpoint [21].

### 1.4.4 Dye Removal by Natural Polysaccharides and its Composite with Conducting Polymers

Native starch is one of the most abundant biopolymers on earth and is present in living plants as energy storage material. Starches are mixtures of two polyglucans, amylopectin and amylose, but they contain only a single type of carbohydrate, glucose.

Chitin is a naturally abundant mucopolysaccharide extracted from crustacean shells, which are wastes products of seafood processing industries. Chitin is the second biopolymer in nature, after cellulose, in terms of abundance, but it is the most abundant amino polysaccharide.

Natural polysaccharides are used as adsorbents for removal of dye molecules from effluent. Naturally cationic polysaccharides such as chitin and chitosan gave excellent levels of color removal, and this is attributed to a combination of electrostatic attraction, van der waals forces, and hydrogen bonding. Nonionic galactomannans (locust bean gum, guar gum, cassia gum) are also highly effective in removing dye from effluent, whereas other nonionic polysaccharides, such as starch, are not so effective. This is attributed to the structure of the polysaccharides and the relative degree of inter- and intramolecular interactions between separate polymer chains as shown in the **Fig. 1.4**.

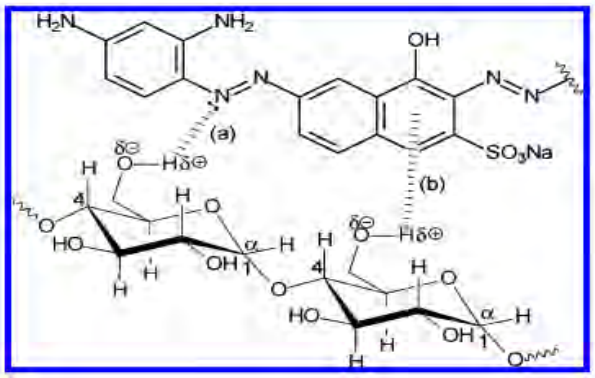


**Fig. 1.4** Dye-polysaccharide interactions: dipole-dipole hydrogen bonding interactions between polysaccharide hydroxyl groups and electronegative residues in the dye molecule; (b) H-bonding between polysaccharide hydroxyl groups and aromatic residues in dye [21].

The excellent adsorption behavior of polysaccharides is mainly attributed to: (1) high hydrophilicity of the polymer due to hydroxyl groups of glucose units; (2) presence of a large number of functional groups (acetamido, primary amino and/or hydroxyl groups); (3) high chemical reactivity of these groups; (4) flexible structure of the polymer chain.

Starch is a well known polymer naturally produced by plants in the form of granules (mainly from potatoes, corn, and rice). Starch granules vary from plant to plant, but in general are composed of a linear polymer, amylose (in most cases about 20 % of the granule), and a branched polymer amylopectin. Amylose is a semicrystalline biopolymer and is soluble in hot water, while amylopectin is insoluble in hot water during its biodegradation. Starch is produced by all green plants as an energy store.

Starch has received considerable attention during the past two decades as a biodegradable thermoplastic polymer and as biodegradable particulate filler. Indeed, products from agricultural sources such as starch, offers an attractive and cheap alternative in developing degradable materials. Starch is not truly thermoplastic as most synthetic polymers. However it can be melted and made to flow at high temperatures under pressure. If the mechanical shears become too high, then starch will degrade to form products with low molecular weight.

Addition of water or other plasticizers enables the starch to flow under milder conditions and reduces the degradation considerably. However, the thermo chemical stability is strongly due to the addition of plasticizers. By itself, starch is a poor choice as a replacement for any plastic. It is mostly water insoluble, difficult to process, and brittle. In principle some of the properties of starch can be significantly improved by blending it with synthetic polymers like polyaniline (PANI), polyolefin and so on.

Last few decades, the conducting polymers have opened a promising field in the charge storage materials, catalysts, and optoelectronic devices. Conducting polymers are consisted of π-conjugated system and offer unusual electronic properties such as electrical conductivity, low energy optical transitions, low ionization potential, and

high electron affinity. PANI is one of the most important and popular conducting polymer owing to its unique electrical and photoelectric properties which could be easily altered either by the oxidation of PANI chain or by the protonation of imine nitrogen backbone as shown in the **Fig. 1.5**. PANI shows high environmental stability and displays process feasibility.

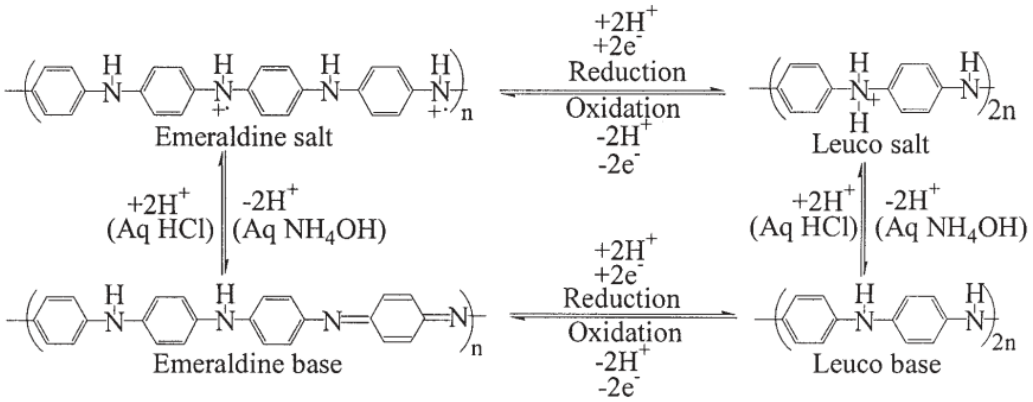


**Fig. 1.5** Interconversion of different forms of PANI depending on the variation of the pH of the solution [22]

It is reported that under light illumination, PANI gets excited and acts as electron donor materials in various catalytic and electrical process. Recently, the metal oxides and PANI nanocomposites have gained much attention as promising photocatalytic materials for the degradation of organic materials and organic dyes under light illumination [23].

### 1.5 Literature Survey and Plan of the Present Work

The efficiency of effluent treatment by adsorption processes depends on the capacity of an adsorbent, on its price and on the waste disposal technology. Activated carbon is the most commonly used method of dye removal by adsorption which is very pricey and reactivation of carbon loses 10-15 % of the sorbent.

Recently, an enormous curiosity has found on developing cheaper and effective adsorbents containing natural polymers to overcome the nonbiodegradability and high cost of the adsorbent resins. Among these, polysaccharides, such as chitin, chitosan and starch derivatives deserve great attention because of their ability to remove dyes and heavy metals from aqueous solutions [21, 24]. However, the usual method of extraction of chitin creates its own environmental pollution because it produces huge quantities of waste and the manufacture of chitosan consists of a chemical deacetylation process. But, below pH 5.5 chitosan forms gels and is not suitable for the dye removal [25].

Starches are very abundant, low-priced and renewable natural polymers which are widely available in many countries including Bangladesh. They have biological and chemical properties such as biodegradability, polyfunctionality, high chemical reactivity, and adsorption capacities which make them excellent materials for industrial use [26]. However, their application in dyes removal is limited due to the poor physical properties such as mechanical properties, hydrophilicity, dimensional stability and so on [5].

Nechwatal et al. [28] reported the capacity of starch products for the decolourisation of effluents containing hydrolysates of reactive dyestuffs. Native starch showed only a low absorbing capacity for reactive dyestuff hydrolysate. But cationic modified starch products were suitable in principle for the decolourising of reactive dyestuff hydrolysates, and they demonstrated the desired effect in the treatment of effluents containing direct dyestuffs, too.

Qayoom et al. [29] tested the overall ability of turmeric as a sequestering substance for copper (II) ions from aqueous solution as a function of initial concentration, contact time, pH and temperature. They established that turmeric powder can adsorb toxic metals and adsorption of metals ions by turmeric powder may be used as a natural remedy for the removal of toxic metal as well as other effluents.

The modification of polysaccharides also offers enormous opportunities. Through chemical reactions, in particular crosslinking and grafting reactions, polysaccharides can give interesting macromolecular superstructures, e.g. gels and hydrogels networks, polymeric resins, beads, membranes, fibers or composite materials. These polysaccharide-based materials can then be used as adsorbents [30]. Like other polysaccharides, starches and cyclodextrins can be crosslinked by a reaction between the hydroxyl groups of the chains with a coupling agent to form water-insoluble crosslinked networks.

Due to the hydrophilic nature of their crosslinking units, cross-linked starches also possess a remarkably high swelling capacity in water, and consequently their networks are sufficiently expanded to allow a fast diffusion process for the pollutants.

Khalil et al. [31] compared all types of cationic starch derivatives bearing different amine groups, that is, primary, secondary, and tertiary amino groups or a quaternary ammonium salt as dye adsorbers. The different factors affecting dye sorption, including pH-treatment time, dye type, amine type and content, and the chemical formula of the cationic starch (i.e., etherified form or grafted one), were studied. The maximum dye sorption values on with the acid dye depended on the amine type. The dye sorption value and the sorption efficiency percentage of the etherified cationic starch derivatives had higher values than that of the grafted cationic starch derivatives.

Klimaviciute et al. [32] examined adsorption of anionic dyes on the cross-linked with epichlorohydrin starches containing quaternary ammonium groups (CCS) and compared with that of modified starches containing only quaternary ammonium groups (CS). The adsorption occurs first of all due to an electrostatic interaction between the cationic groups of the modified starch and the anionic groups of the dyes. It was shown that CCS are more suitable for the anionic dye adsorption from a textile dyeing solution.

Cheng et al. [27] investigated the sorption performance of the ethylenediamine modified starch (CAS) for the removal of acid dyes from aqueous solutions. The influence of pH on adsorption of acid orange 10 (AO10), acid green 25 (AG25) and amido black 10B (AB10B) was evaluated. The different behaviors of individual dyes adsorption on CAS were largely dependent on the number of hydrophilic functional groups, which had strong tendency to form hydrogen bonds with the biosorbent. Dye release in sodium sulfate solutions was determined by the salt concentration and nature of dyes.

Cheng et al. [33] also published another report showing dithiocarbamate-modified starch (DTCS) as a commercially promising sorbent for the removal of anionic dyes from aqueous solutions. It is more effective than activated carbon for this purpose. The DTCS can effectively adsorb most heavy metals and positive particles. Furthermore, the metal bound DTCS strongly chelates dyes resulting in extensive use of the material. It was found that the capacity of DTCS for each dye is pH dependent, and the adsorption is governed by electrostatic attraction.

The addition of nano-scale particles into thermoplastic starch by chance can change the crystallization kinetics, the crystalline morphology, the crystal forms, and the crystallite size [34]. This difference in crystalline morphology, in turn, can significantly affect the overall mechanical and physical properties of the starch.

Ma et al. [35] prepared starch nanoparticles (SN), which are obtained by precipitating starch paste solution with ethanol as the precipitant. This SN could be used as a smart bionanosorbent because of its increased surface area to adsorb the pollutants.

Moreover, the conventionally used polymers like polypropylene, polystyrene, polyethylene and poly (methyl methacrylates) are non-biodegradable and recycling or reusing them is very challenging, thus contributing to piles of non-biodegradable wastes all over the world. Composites generated from these polymers share a similar fate. As most biodegradable polymers find their origin in other alternative renewable sources, their use in the polymer composites technology is attractive; however, their

use as an alternative to commercial nonbiodegradable polymers has emerged as both a dream and a challenge.

Park et al. [36] reported their efforts to develop environmentally friendly polymer hybrids to improve the properties of thermoplastic starch. Biodegradable thermoplastic starch/layered silicate nanocomposites were prepared by the melt intercalation method.

McGlashan and Halley [37] examined the melt intercalation of starch-polyester-nanocomposites and its usefulness in the addition of modified MMT in improving mechanical properties, clarity (via disruption of crystallinity) and film blowing processibility of the nanocomposites.

Physical incorporation of granular starch or starch derivatives, for example SN, as a functional additive and filler into synthetic polymers during processing has been largely used, since the first announcement of using starch in combination with synthetic polymer either as starch gel blends with ethylene acrylic acid copolymer or as a particulate starch dispersion in polyolefin or PANI. The starch-based nanocomposites are completely degradable in soil and water.

Conducting organic polymers such as polyaniline (PANI) were also tested in the adsorption of dye effluent [20, 38]. PANI is unique among the conducting polymers in that its electrical properties can be reversibly controlled by both charge-transfer doping and protonation. The wide range of associated electrical, electrochemical and optical properties coupled with good stability make PANI potentially attractive for application in various fields. Besides the many other interesting properties, PANI exhibits relatively high surface area and porosity and is reported to be utilized as adsorbent for adsorption of protein and DNA. Polypyrrole (PP) colloids stabilized by polyvinylphosphate dopant are also shown to adsorb metal ions from aqueous solutions [20].

Song et al. [39] synthesized the composite material of PANI/NiO/Sodium Dodecyl-Benzene-Sulfonate (SDBS) in SDBS micelles. Polyaniline particles doped with SDBS and NiO can form nanorods. The PANI nanoparticles synthesized in SDBS/Aniline/$H_2O$ micelles, self-assembled to form nano-lines after 3 days and nano-rods after a week.

In the SDBS micelles, Aniline (An) exists in the oil core and the palisade layer of the micelles, which can limit the size of the PANI particles. PANI particles prepared in the micelles vary in size from several nanometers to decades of nanometers. Due to the electrostatic interaction between the sulfonyl groups of SDBS, the protruded amino group of An and PANI in the An combine with each other to form a co-polymer. As a result, nano-rods are formed.

Xing et al. [40] reported the synthesis of Polyaniline–polypyrrole (PANI-PPy) composite by in situ polymerization of pyrrole in PANI dispersion using $FeCl_3.6H_2O$ as oxidant and sodium dodecyl benzene sulfonate (SDBS) as surfactant. PANI-PPy composite was successfully prepared from PANI dispersion using SDBS as surfactant. It showed that when the PANI dispersions were well formed through appropriately selecting the synthesis conditions, composites with high conductivity and excellent sponge-like morphology comprising of nanofibers could be obtained. Otherwise, the products presented aggregates with granular particle morphology and low conductivity.

Saikia et al. [41] Starch/polyaniline composites were synthesized using oxidative polymerization of polyaniline in an aqueous dispersion of starch isolated from Colocasia esculenta corn. Formation of new properties of the composites as compared to starch and poloyaniline was evident from the X-ray diffraction analysis (XRD). Characterization done using UV–Vis, FTIR and Differential Thermal analysis (DTA) provide evidence of composite formation.

The suitability of different kinds of low-cost materials to remove dye colors, the reaction involved and the factors governing the sorption are still not fully understood clearly. In this work PANI, two PANI/starch composites (i.e., named Composite-1 and Composite-2) and starch nanoparticles (SN) were prepared chemically and some natural raw adsorbents namely wheat powder (WP), turmeric powder (TP), and pure starch were introduced as low-cost bioadorbents. Adsorption behaviour of these raw bioadsorbents and synthetic adsorbents were compared for the two typical ionic dyes, specifically, methylene blue (MB) and orange green (OG) based on the removal of the dyes as a result of adsorption from their aqueous solution on the adsorbents. The dye, MB is cationic in nature while OG is an anionic one.

This study would be conducted to explore the possibility of regeneration and reuse of the adsorbents to minimize the environmental hazards and to establish a cost-effective alternative of the removal of organic dyes from water. The possible outcome may include the followings:

1. To collect some available starch-based low-cost biodegradable natural materials of different origin
2. To examine the biodegradability of the materials
3. To establish a facile chemical route for the preparation of starch nanoparticles (SN)
4. Synthesis of polyaniline (PANI) and *in situ* and *ex-situ* polymerization of the SN with the PANI matrix
5. Comparative adsorption capacity of the natural biomaterials with that of the synthetic PANI/starch nanocomposites and PANI
6. Detail batch dye adsorption study of the materials

## 1.6 References


1. Iijima, S. *Nature*, **1991**, *56*, 354.
2. *Science*, *294(5551)*, 2442-2443.
3. Klefenz, H. Nanobiotechnology: From Molecules to Systems. *Engineering in Life Sciences* **2004**, *4(3)*, 211–218.
4. Sawyer, C. N.; McCarty, P. L.; Parkin, G. F. Chemistry for Environmental Engineering. McGraw-Hill, New York, 4th Ed., **1994**.
5. Masciangioli, T.; Zhang, W. X. Environmental Technologies at the Nanoscale. *Environ. Sci. Technol*. **2003**, *37(5)*, 102A–108A.
6. Milo, S. P.; Shaffer, A .H. W. *Advanced Materials* **1999**, *11*, 937.
7. Dresselhaus, M. S.; Dresselhaus, G.; Avouris, P. Carbon Nanotubes Synthesis, Structure, Properties, and Applications. Berlin: Springer **2001**.
8. Osman, M. A.; Srivastava, D. *Nanotechnology* **2001**, *21*.
9. Dukhin, A. S.; Goetz, P. J. Ultrasound for Characterizing Colloids. Elsevier, **2002**.
10. Rutkowska, M.; Heimowska, A.; Krasowska, K.; Janik, H. Biodegradability of Polyethylene Starch Blends in Sea Water. *Polish Journal of Environmental Studies* **2002**, *11(3)*, 267-274.
11. Mahapatro, A.; Singh, D. K. Biodegradable Nanoparticles are Excellent Vehicle for Site Directed Delivery of Drugs and Vaccines. *Journal of Nanobiotechnology* **2011**.
12. Zhao, R.; Torley, P.; Halley, P. J. Emerging Biodegradable Materials: Starch- and Protein-based Bio-nanocomposites. *J. Mater. Sci*. **2008**, *43*, 3058–3071.
13. Ahmad, M. B.; Shameli, K.;Yunus, W. M. Z. W.; Ibrahim, N. A.; Darroudi, M. Synthesis and Characterization of Silver/Clay/Starch Bionanocomposites by Green Method. *Australian Journal of Basic and Applied Sciences* **2010**, *4(7),* 2158-2165.
14. Aim, C.; Coradin, T. Nanocomposites from Biopolymer Hydrogels: Blueprints for White Biotechnology and Green Materials Chemistry. *Journal of Polymer Science Part B: Polymer Physics* **2012**, *50*, 669–680.

15. Mendham, J.; Denney, R. C.; Barnes, J. D.; Thomas, M. Vogel's Textbook of Quantitative Chemical Analysis. Pearson Education Ltd., **2000**.

16. Hasnat, M. A.; Siddiquey, I. A.; Nuruddin, A. Comparative Photocatalytic Studies of Degradation of a Cationic and an Anionic Dye. *Dyes and Pigments* **2005**, *66,* 185–188.

17. Wu, T.; Liu, G.; Zhao, J.; Hidaka, H.; Serpone, N. Evidence for $H_2O_2$ Generation during the $TiO_2$-Assisted Photodegradation of Dyes in Aqueous Dispersions under Visible Light Illumination. *J. Phys. Chem. B.* **1999**, *103,* 4862-4863.

18. Ayad, M. M.; El-Nasr, A. A. Adsoption of Cationic Dye (Methylene Blue) from Water Using Polyaniline Nanotubes Base. *J. Phys. Chem. C* **2010**, *114*, 14377-14383.

19. Shan, G.; Surampalli, R. Y.; Tyagi, R. D.; Zhang T. C. Nanomaterials for Environmental Burden Reduction, Waste Treatment, and Nonpoint Source Pollution Control: A Review. *Front. Environ. Sci. Engin. China* **2009**, *3(3)*, 249–226.

20. Banat, I. M.; Nigam, P.; Singh, D.; Marchant, R. Microbial Decolourisation of Textile–Dye–Containing Effluents: A Review. *Journal of Bioresource Technology* **1996**, *58(3)*, 217– 227.

21. Blackburn, R. S. Natural Polysaccharides and their Interactions with Dye Molecules: Applications in Effluent Treatment. *Environ. Sci. Technol*. **2004**, *38*, 4905-4909.

22. Chowdhury, A. N.; Jesmeen, S. R.; Hossain, M. M. Removal of Dyes from Water by Conducting Polymeric Adsorbents. *Polym. Adv. Technol.* **2004**, *15*, 633–638.

23. Ameen, S.; Akhtar, M. S.; Kim, Y. S.; Yang, O. B.; Shin, H. S. An Effective Nanocomposite of Polyaniline and ZnO: Preparation, Characterizations, and its Photocatalytic Activity. *Colloid Polym. Sci.* **2011**, *289*, 415–421.

24. Mostafa, Kh. M.; Samarkandy, A. R.; El-Sanabary, A. A. Preparation of Poly (MMA)-Crosslinked Pregelled Starch Graft Copolymer and Its Application in Waste Water Treatments. *J. Appl. Polym. Sci.* **2009**, *112*, 2838-2846.

25. Crini, G.; Badot, P. M. Application of Chitosan, A Natural Aminopolysaccharide, for Dye Removal from Aqueous Solutions by Adsorption Processed using Batch Studies: A Review of Recent Literature. *Prog. Polym. Sci.* **2008**, *33*, 399–447.

26. Crini, G.; Badot, P. M. Starch-based Biosorbents for Dyes in Textile Wastewater Treatment. *Int. J. Environ. Technol. Manage*. **2010**, *12*, 129–150.

27. Cheng, R.; Ou, S.; Li, M.; Li, Y.; Xiang, B. Ethylenediamine Modified Starch as Biosorbent for Acid Dyes. *J. Hazard. Mater*. **2009**, *172*, 1665–1670.

28. Nechwatal, A.; Nicolai, M.; Mieck, K. P.; Rudolstadt. Use of Absorbers Based on Starch for the Effluent Treatment of Dyeing Liquors. *Starch/Stärke* **1999**, *51*, Nr. 8-9, 286–293.

29. Qayoom, A.; Kazmi, S. A.; Rafiq, N. Removal of Cu (II) Ions from Aqueous Solutions by Turmeric Powder. *J. Chem. Soc. Pak*. 2009, *31(6)*, 876-881.

30. Crini, G. Recent Developments in Polysaccharide-based Materials used as Adsorbents in Wastewater Treatment. *Prog. Polym. Sci*. **2005**, *30*, 38–70.

31. Khalil, M. I.; Aly, A. A. Use of Cationic Starch Derivatives for the Removal of Anionic Dyes from Textile Effluents. *Journal of Applied Polymer Science* **2004**, *93*, 227–234.

32. Klimaviciute, R.; Riauka, A.; Zemaitaitis, A. The Binding of Anionic Dyes by Cross-Linked Cationic Starches. *Journal of Polymer Research* **2007**, *14*, 67-73.

33. Cheng, R.; Xiang, B.; Li, Y.; Zhang, M. Application of Dithiocarbamate-Modified Starch for Dyes Removal from Aqueous Solutions. *J. Hazard. Mater*. **2011**, *188*, 254-260.

34. Okamoto, M.; Nam, P. H. *Nano Letters* **2001**, *1*, 295.

35. Ma, X.; Jian, R.; Chang, P. R.; Yu, J. Fabrication and Characterization of Citric Acid-Modified Starch Nanoparticles/Plasticized-Starch Composites. *Biomacromolecules* **2008**, *9,* 3314–3320.

36. Park, H. M.; Li, X. *Macromol. Mater. Eng.* **2002**, *287(8)*, 553.

37. McGlashan, S. A.; Halley, P. *J. Polym. Int.* **2003**, *52(11)*, 1767.

38. Mahanta, D.; Madras, G.; Radhakrishnan, S.; Patil, S. Adsorption of Sulfonated Dyes by Polyaniline Emeraldine Salt and Its Kinetics. *J. Phys. Chem. B* **2009**, *113*, 2293–2299.

39. Song, G.; Bo, J.; Guo, R. Synthesis of the Composite Materials of Polyaniline/NiO/Sodium Dodecylbenzene Sulfonate in Micelles. *Colloid Polym. Sci.* **2005**, *283*, 677-680.

40. Xing, S.; Zhao, C.; Zhou, T.; Jing, S.; Wang, Z. Preparation and Characterization of Polyaniline-Polypyrrole Composite from Polyaniline Dispersions. *Journal of Applied Polymer Science* **2007**, *104*, 3523–3529.

41. Saikia, J. P.; Banejee, S.; Konwar, B. K.; Kumar, A. Biocompatible Novel Starch/Polyaniline Composites: Characterization, Anti-cytotoxicity and Antioxidant Activity. *Colloids and Surfaces B: Biointerfaces* **2010**, *81*, 158-164.

## 2.1 Materials and Probes

### 2.1.1 Chemicals

The chemicals and reagents used in this work are listed below. These were analytical grade and used without further purification except aniline which was distilled twice prior to use. Doubly distilled water was used as solvent to prepare most of the solution of this work.

(a) Pure Starch [Merck, India]
(b) Aniline ($C_6H_6NH_2$) [ E. Merck, Germany]
(c) Ammonium peroxydisulphate $(NH_4)_2S_2O_8$ [Merck, Germany]
(d) Sulfuric acid ($H_2SO_4$) [Merck, India]
(e) Hydrochloric acid (HCl, 32% Extra Pure) [E. Merck, Germany]
(f) Sodium hydroxide (NaOH) [E. Merck, Germany]
(g) Sodium chloride (NaCl) [E. Merck, Germany]
(h) Anhydrous calcium chloride ($CaCl_2$) [India]
(i) Feric chloride hexahydrate ($FeCl_3.6H_2O$) [E. Merck, Germany]
(j) Methylene Blue (MB) [E. Merck, Germany]
(k) Orange Green (OG) [E. Merck, Germany]

### 2.1.2 Instruments

Analysis of the samples performed in this work employed the following tools:

(1) UV-Visible spectrophotometer (UV-Vis) [UV-1601 PC, Shimadzu, Japan]
(2) Infra red spectrophotometer (IR) [IR-470, Shimadzu, Japan]
(3) Differential Thermal Analyzer (DTA) [TG/DTA 6300]
(4) Scanning electron microscope (SEM)
[Hitachi S3400N and JSM-6700F (JEOL, Japan)]
(5) X-ray diffractometer (XRD) [Bruker D8 Advance]
(6) Centrifuge machine [Hermle, 2200 A, Germany]
(7) Sonicator [Model 50 T, VWR Scientific, USA]
(8) Digital balance [FR-200, Japan]
(9) Furnace [DK, Chino, England]
(10) Microburette [China]
(11) Filter Paper [Whatman]

## 2.2 Conditioning of Natural Adsorbents

We collected wheat powder (WP) and turmeric powder (TP) local market. Then the glutinous substances of the powder samples were removed by continuous washing with water and filtering followed by sonication to prepare their functional forms for the efficient adsorption of dyes from aqueous solution. The functional properties of these biological powders e.g., adsorption, rehydration, wetting properties are greatly dependent on the surface chemical composition of the particles rather than their bulk composition due to the powder manufacturing process by drying or milling.

## 2.3 Preparation of Starch Nanoparticles (SN)

The separation of starch and gluten proteins was conducted according to the Auger method as reported in **Scheme 2.1** [1]. Firstly, the flour was mixed with water at 25 ˚C with 80 rpm. The resulting dough was then diluted and the gluten-starch suspension obtained after the washing step was sieved by using a vibrating sieve. The gluten was recovered on the sieve, whereas the filtrate was collected in a separate container. Finally, to isolate the wheat starch, the previous filtrate was left overnight at 15 ˚C, washed by distilled water and centrifuged. After the last centrifugation, the starch fraction was dried overnight under a hood at 25 ˚C and then milled.

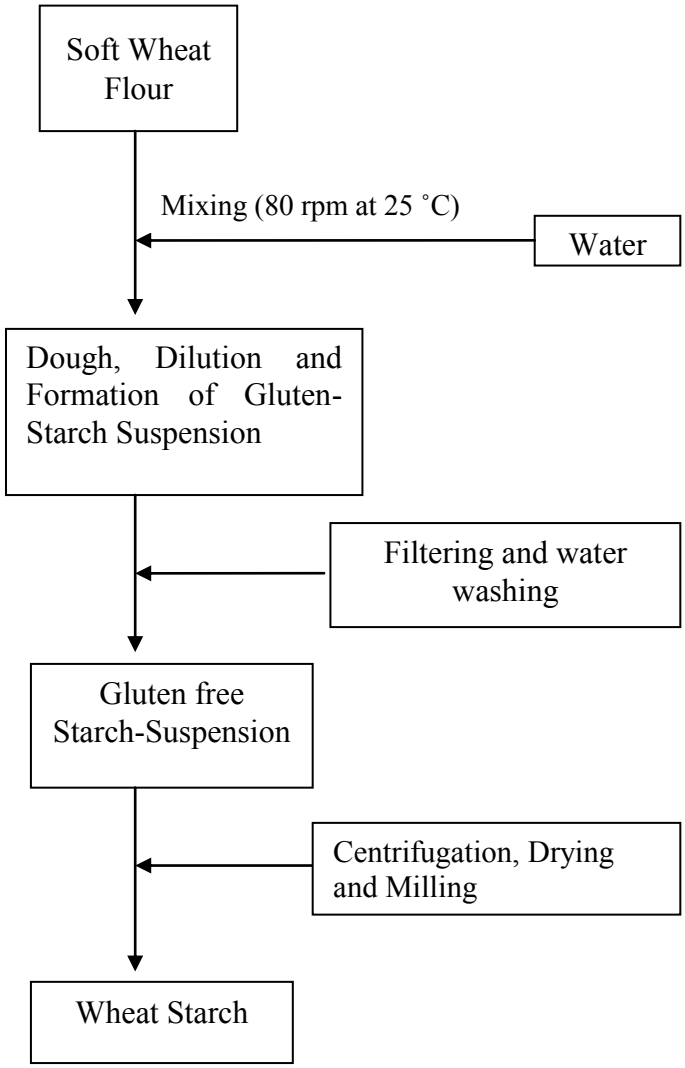


**Scheme 2.1** Process diagram for the extraction of the main components from wheat flour

For the preparation of starch nanoparticles (SN), we initially added 50 mL water to 2g of wheat starch. The mixture was heated at 90 °C for 1 h for the complete gelatinization of the starch with constant stirring, and then 50 mL of ethanol was added dropwise from a burette to the solution of gelatinized starch solution with constant stirring. The suspensions were then centrifuged at 2000 rpm for 10 minutes, and the settled SN was washed using ethanol to remove the water. After complete washing, the SN was dried at 50 °C to remove ethanol [2]. The whole procedure has shown in the flow chart in the **Scheme 2.2**.

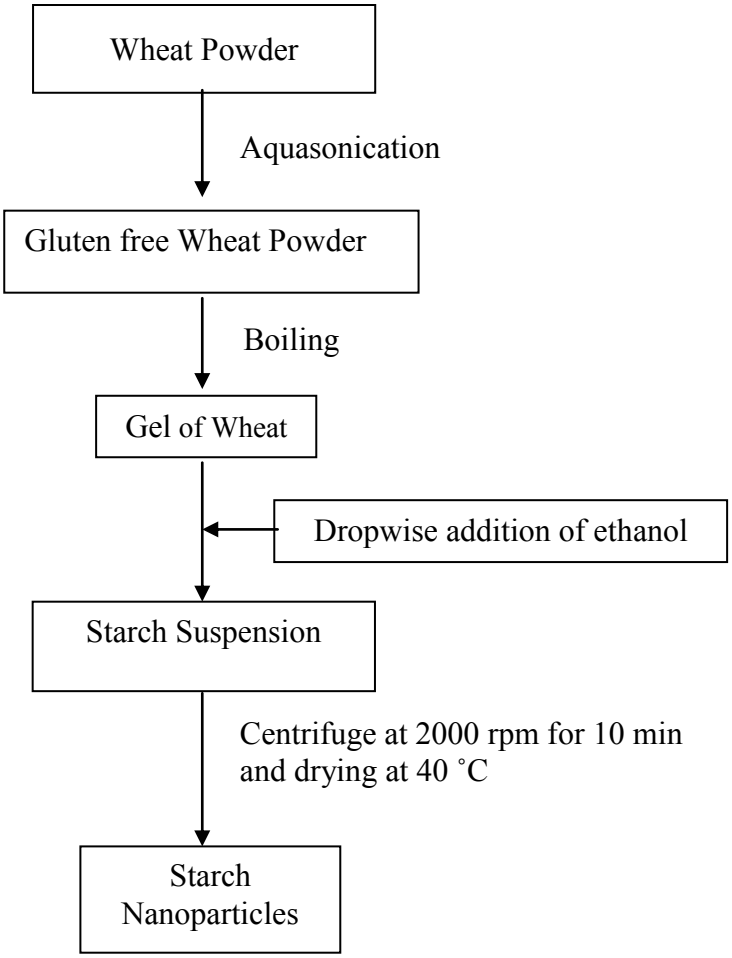


**Scheme 2.2** Preparation of starch nanoparticles (SN) by nanoprecipitation method

### 2.4 Preparation of Polyaniline (PANI)

PANI was prepared by chemical method at room temperature 29 ˚C (± 2˚) following the procedures described elsewhere [3-5]. In this study PANI was synthesized by using $(NH_4)_2S_2O_8$ as an oxidant, in which the ratio of $(NH_4)_2S_2O_8$ aniline was maintained to be 1.25 to minimize the presence of residual aniline and to obtain the best yield of PANI [6]. HCl was added in equimolar proportion to aniline to prepare aniline hydrochloride monomer. Then, 5 mL of distilled aniline, 5 mL of conc. HCl and 16 g of $(NH_4)_2S_2O_8$ were added to double distilled water maintaining the total volume of mixture 400 mL. The reaction is shown in the **Scheme 2.3**.

The reaction mixture was turned in to deep green polymeric sediment instantaneously. However, the content was left for overnight for completion of polymerization. The deep green sediment was then filtered and washed repeatedly with distilled water to remove excess acid content. The PANI substrate was then dried in air followed by vacuum drying. The dried mass was ground and then sieved using 100 mesh sieves and stored in a vacuum desiccator.

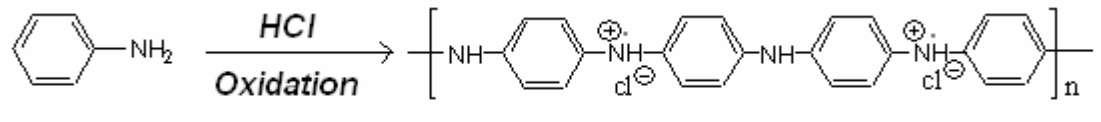


**Scheme 2.3** Formation of polyaniline by polymerization of aniline

### 2.5 *In situ* and *ex-situ* Preparation of Composites of PANI with Starch

For the preparation of Composite-1, 1.3 ml of conc. HCl was added to 1 ml of aniline to form anilinium salt. After that, we mixed 3 g of ammonium peroxydisulfate, $(NH_4)_2S_2O_8$ and various amounts of starch solution to the salt to prepare PANI/starch Composite-1 which can be summarized as follows (**Table 2.1**) [7]:

**Table 2.1** Starch loading capacity of polyaniline (PANI) with various amount of starch

| Amount of Starch(w/v) % | 0.02 | 0.1 | 0.2 | 1 |
|---|---|---|---|---|
| % yield of PANI/starch Composites with respect to 1 ml (1.02 g) of aniline | 92.97<br>* 92.07 | 95.42<br>* 91 | 95.08<br>*86.60 | 144.9<br>*97.3 |

*With respect to 1.02 g aniline and corresponding amount of starch

In contrary, for the preparation of Composite-2, initially we added 1.3 ml of conc. HCl to 1ml of aniline to form anilinium salt and then added 3 g of ammonium peroxydisulfate, $(NH_4)_2S_2O_8$, for its oxidative polymerization to form polyaniline (i.e. PANI). Finally, the as-prepared PANI is added in warm solution (0.5 g starch in 50 ml water) of starch at 20 ˚C under stirring condition for a day. The composite then washed with warm water to remove the adsorbed starch. Both of the preparation methods are shown in the **Scheme 2.4**.

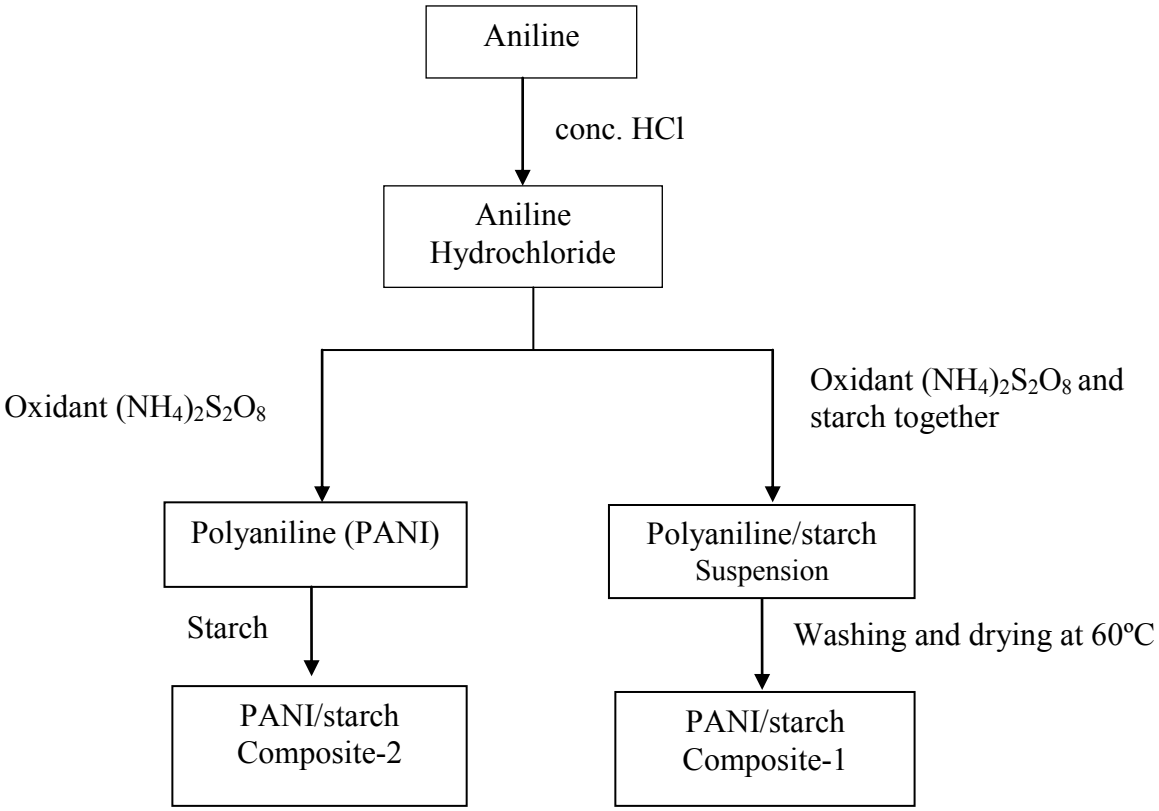


**Scheme 2.4** *In situ* and *ex-situ* preparation of Composite-1 and Composite-2, respectively

## 2.6 Characterization Methods

### 2.6.1 Infrared Spectroscopy

IR spectra of natural polymers WP, TP and synthetic polymeric materials SN, PANI/starch Composite-1 and PANI/starch Composite-2 were recorded on an IR spectrometer [IR-470, Shimadzu, Japan] in the region of 4000 - 400 $cm^{-1}$. IR spectra of the solid samples were frequently obtained by mixing and grinding a small amount of materials with dry and pure KBr crystals. Thorough mixing and grinding were done in a mortar by a pestle. The powdered mixture was then compressed in a metal holder under a pressure of 8-10 tons to make a pellet. The pellet was then placed in the path of IR beam for measurements.

### 2.6.2 Ultraviolet-Visible Spectroscopy

The UV-Vis spectral analysis of the sample solutions employed a double beam spectrophotometer [UV-1601 PC, Shimadzu, Japan]. We used water as solvent in the UV-Vis spectroscopic analysis of dye adsorption on the adsorbents. The reference aqueous solutions were also used for preparing the adsorbate solutions of different pH. The determination of the amount of dye adsorbed by an adsorbent was done by spectroscopy in the visible region. The UV-Visible spectrum of methylene blue was obtained for 10 μM solution in the range of 200 nm to 700 nm. The maximum absorbance was found at 664 nm ($\lambda$ max = 664 nm) and photometric measurements were carried out at 664 nm. Moreover, the dye orange green shows maximum absorbance at 478 nm.

### 2.6.3 X-ray Diffraction (XRD)

A D8 Advance Bruker analytical X-ray system was operated at the Cu Kα wavelength of 32.297 nm, 40 mA, and 40 keV. XRD diffractograms were acquired at 25 ˚C over a 2θ range of 5–60˚ with a step size of 0.020˚ and a step time of 1s.

We analyzed WP, TP, SN, PANI/starch Composite-1 and PANI/starch Composite-2 for their X-ray diffraction pattern in the powder state. The powder samples were pressed in a square aluminum sample holder (40 mm × 40 mm) with a 1 mm deep rectangular hole (20 mm × 15 mm) and pressed against an optical smooth glass plate. The upper surface of the sample was labeled in the plane with its sample holder. The sample holder was then placed in the diffractometer.

### 2.6.4 Scanning Electron Microscopy (SEM)

WP, TP, SN, PANI/starch Composite-1 and PANI/starch Composite-2 samples were prepared and treated for their surface morphology. For this purpose, SEM was adopted. The SEM images were found from instruments of two models i.e., Hitachi S3400N and JSM-6700F (JEOL, Japan). In the former device, the dried powders of these samples were dispersed on a conducting carbon glued strip and sample-loaded strip was then mounted to a chamber that evacuated to ~ $10^{-3}$ to $10^{-4}$ torr. In the latter machine, a very thin gold layer (~ few nanometers thick) was sputtered on the sample additionally to ensure the conductivity of the sample surface. The sample was then placed in the main SEM chamber to view its surface in both cases. The systems were computer interfaced and thus provide recording of the surface images in the computer file for its use as hard copy.

### 2.6.5 Thermal Analyses

Thermal gravimetric analysis (TGA) and differential thermal analysis (DTA) were performed with a TG/DTA 6300 instrument. Samples were placed in an alumina cup and heated from 30 to 900 ˚C at a heating rate of 20 ˚C $min^{-1}$ in a nitrogen atmosphere. A purge gas was flowing dry nitrogen at a rate of 100 ml $min^{-1}$. α-$Al_2O_3$ was used as reference.

## 2.7 Adsorption Study

### 2.7.1 Preparation of Methylene Blue (MB) and Orange Green (OG) Dye Solutions

#### A. Stock dye solutions

$1\times10^{-3}$ M 500 mL stock MB solution was prepared by dissolving 0.0356 g solid MB in double distilled water and raising the volume up to the mark while $1\times10^{-3}$ M 250 mL OG stock solution was prepared by dissolving 0.113 g solid OG in double distilled water raising the volume up to the mark.

#### B. Dilution of dye stock solutions

With help of these stock solutions, dilute solutions of various concentrations were prepared by using the formulae:

$$V_1 S_1 = V_2 S_2$$

The chemical structure and typical UV-Visible spectral feature of MB are represented in **Scheme 2.5** and **Fig. 2.1** and of OG are represented in **Scheme 2.6** and **Fig. 2.2** respectively. The calibration curves of MB and OG are given in **Fig. 2.3** and **Fig. 2.4**. The effect of pH on MB and OG are also given in **Fig. 2.5** and **Fig. 2.6**.

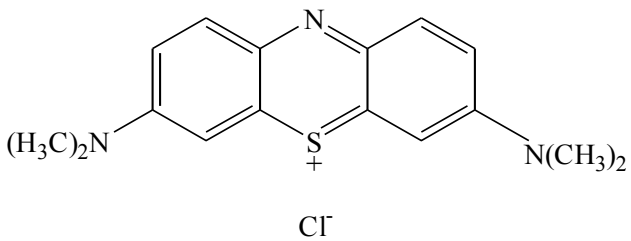


**Scheme 2.5** Chemical Structure of MB

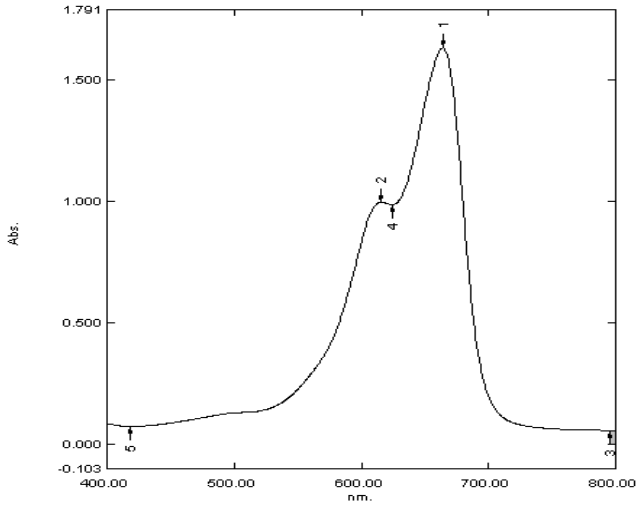


**Fig. 2.1** UV-Visible spectrum of an aqueous $2\times10^{-5}$ M solution of MB at pH 6.86

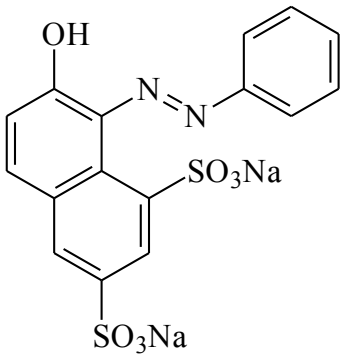


**Scheme 2.6** Chemical structure of OG

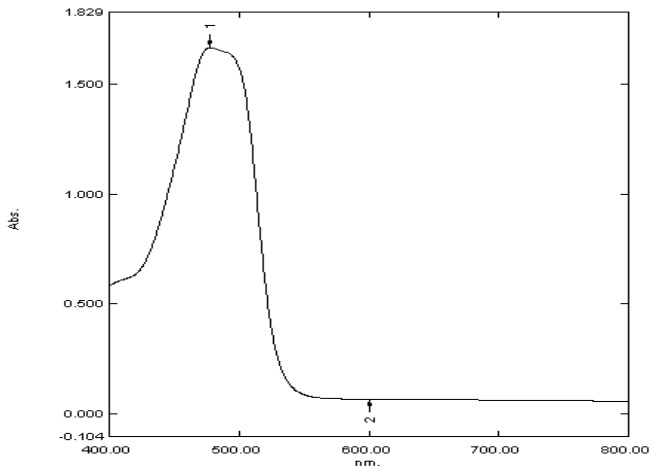


**Fig. 2.2** UV-Visible spectrum of an aqueous $1\times10^{-4}$ M solution of OG at pH 6.86

**C. Determination of molar absorption co-efficient of MB**

Reference : Water

$\lambda_{max}$ for MB solution : 664 nm

Temperature : 29 ˚C

pH : 6.83

**Table 2.2** Absorbance of MB solution at different concentration

| Run No | Concentration $M/10^{-6}$ | Absorbance | Regression Coefficient, \|R\| |
|---|---|---|---|
| 1 | 1.0 | 0.08 | 0.998 |
| 2 | 2.5 | 0.19 | |
| 3 | 5.0 | 0.40 | |
| 4 | 7.5 | 0.55 | |
| 5 | 10.0 | 0.73 | |

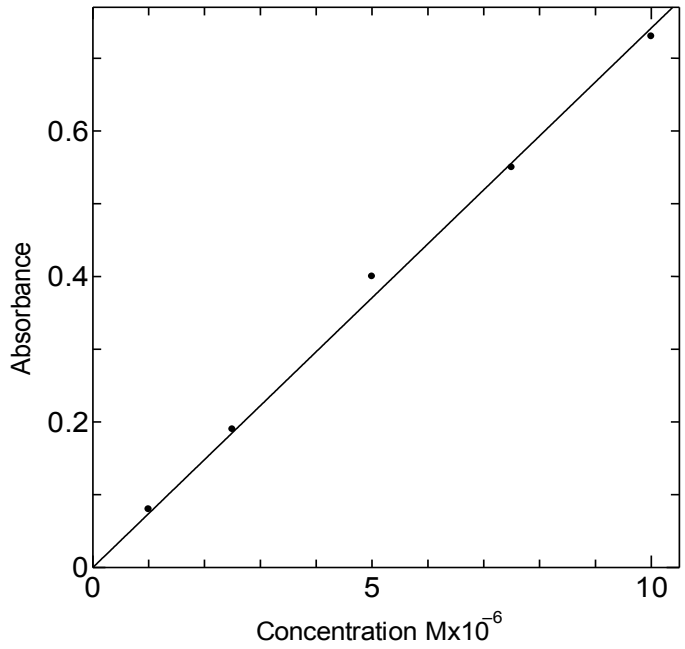


**Fig. 2.3** Calibration Curve for MB

Result: The molar absorption co-efficient (ε) is 74164 L $mol^{-1}$ $cm^{-1}$

**D. Determination of molar absorption co-efficient of OG**

Reference : Water

$\lambda_{max}$ for OG solution : 478 nm

Temperature : 29 ˚C

pH : 6.83

**Table 2.3** Absorbance of OG solution at different concentration

| Run No | Concentration $M/10^{-5}$ | Absorbance | Regression Coefficient, \|R\| |
|---|---|---|---|
| 1 | 1.0 | 0.14 | 0.999 |
| 2 | 2.0 | 0. 28 | |
| 3 | 4.0 | 0.57 | |
| 4 | 6.0 | 0.68 | |
| 5 | 8.0 | 1.14 | |
| 6 | 10.0 | 1.42 | |

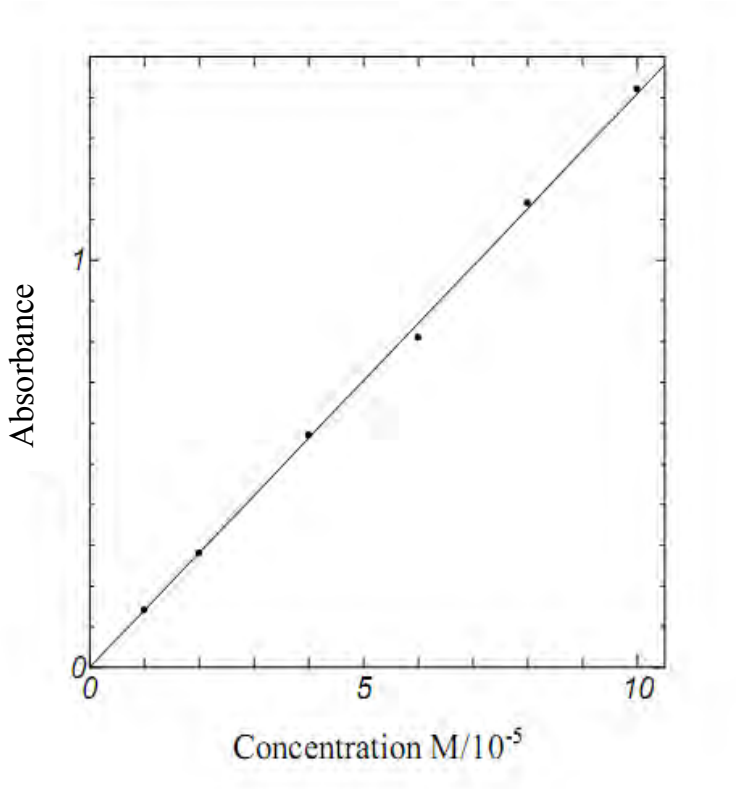


**Fig. 2.4** Calibration Curve for OG

Result: The molar absorption co-efficient (ε) is 13750 L $mol^{-1}$ $cm^{-1}$.

**E. Effect of pH on the spectral behavior of MB**

Reference : Water

Temperature : 29 ˚C

pH : 6.83

**Table 2.4** Absorbance of MB solution at different pH of the medium

| Run No | Concentration $M/10^{-5}$ | pH | Instant Abs. | Abs. after 24 hrs. |
|---|---|---|---|---|
| 1 | 2 | 2.9 | 1.356 | 1.356 |
| 2 | | 4.29 | 1.356 | 1.356 |
| 3 | | 6.83 | 1.356 | 1.356 |
| 4 | | 8.3 | 1.356 | 1.356 |
| 5 | | 10.9 | 1.356 | 1.356 |

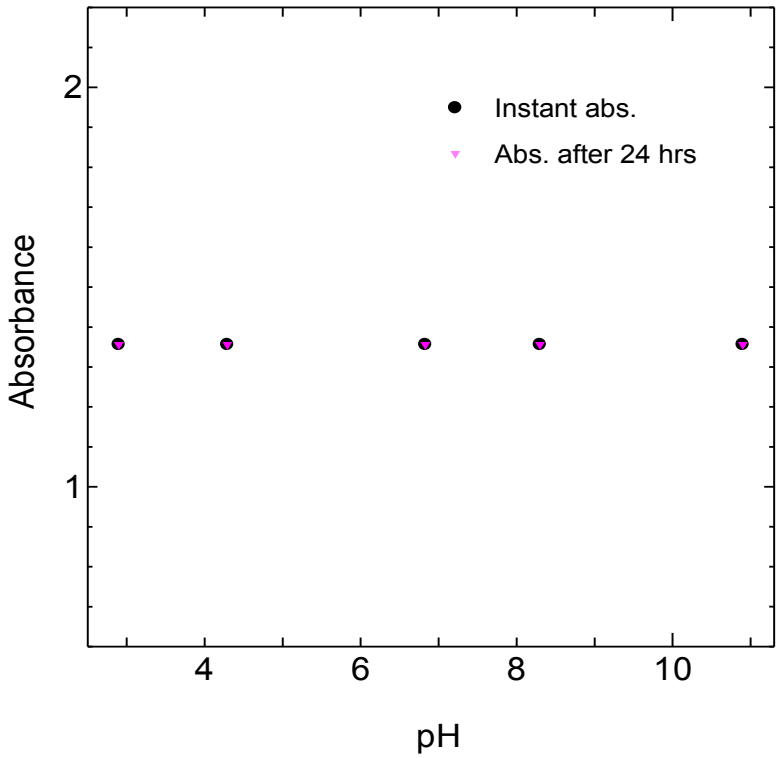


**Fig. 2.5** Effect of pH on the behaviour of MB

**F. Effect of pH on the spectral behavior of OG**

Reference : Water

Temperature : 29 ˚C

pH : 6.83

**Table 2.5** Absorbance of OG solution at different pH of the medium

| Run No | Concentration $M/10^{-4}$ | pH | Instant Abs. | Abs. after 24 hrs. |
|---|---|---|---|---|
| 1 | 1 | 2.90 | 1.61 | 1.61 |
| 2 | | 4.29 | 1.61 | 1.61 |
| 3 | | 6.83 | 1.61 | 1.61 |
| 4 | | 8.30 | 1.61 | 1.61 |
| 5 | | 10.9 | 1.61 | 1.61 |

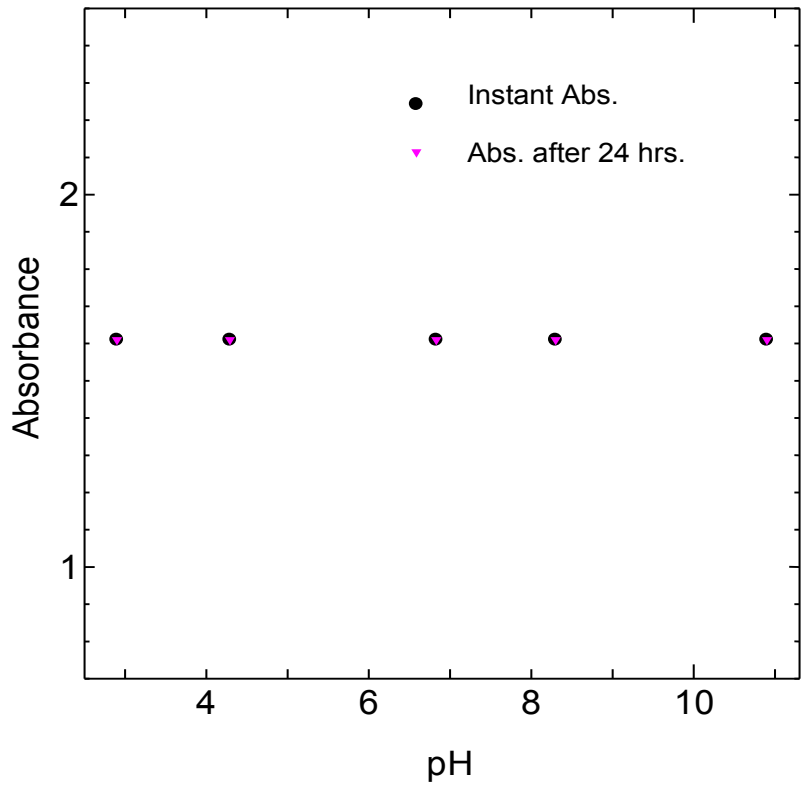


**Fig. 2.6** Effect of pH on the behaviour of OG

### 2.7.2 Batch Adsorption Experiments

The biosorption experiments were carried out by batch sorption method with the influence of solution pH, adsorbent dosage, temperature and initial dye concentration [8]. Adsorption was performed by agitating a given dose of the adsorbent with 50 mL of the MB and OG dye solutions of desired concentration at (29 ± 1) ºC in different shaker flasks in a thermostat shaker. The shaking speed was maintained at 235 rpm throughout the study to ensure equilibrium was reached. At the end of preset time intervals, samples were withdrawn and the changes in concentration of dye solution was analyzed by using UV-spectrophotometer. Since the solution pH has a considerable effect on bioadsorption studies, the pH change of the solution could also be monitored to know the adsorption behavior of dyes onto adsorbents. The pH was regulated by adding incremental amounts of either dilute HCl or NaOH to the solution. The biosorption studies were also carried out at different temperature of 10, 20, 30, 40 and 45 ºC to study the effect of temperature to evaluate the adsorption thermodynamic parameters.

The percentage of removal of dye can be calculated by using the following relationship

$$\% \text{ Dye removal} = \frac{(C_i - C_t)}{C_i} \times 100 \qquad (2.1)$$

where, $C_i$ (mol/L) and $C_t$ (mol/L) are the initial and terminal concentrations of dye in the adsorption solution, respectively.

The adsorption capacity of the adsorbent at time *t*, $q_t$ (mol/g), was calculated by

$$q_t = \frac{(C_i - C_t)V}{m} \qquad (2.2)$$

where, V is the volume of the adsorption solution (L) and m is the dose of adsorbent used in gram.

The amount of dye adsorbed at equilibrium, $q_e$ (mol /g) was calculated by

$$q_e = \frac{(C_i - C_t)V}{m} \qquad (2.3)$$

where, $C_i$ (mol/L) and $C_e$ (mol/g) are initial and equilibrium concentrations of the dye respectively.

Influence of concentration of dye, pH, contact time, presence of electrolytes and the confirmation of biodegradability of the WP and TP adsorbents were carried out through this study are listed below:

a) Dye (MB and OG) adsorption as a function of time
b) Influence of pH on dye adsorption
c) Effect of concentration of dye (MB and OG) on adsorption
d) Influence of electrolytes
e) Biodegradability of the WP and TP adsorbents

### 2.7.3 Desorption Study of MB Adsorbed onto WP

100 mL $4.0\times10^{-6}$ M MB solution was taken in two 200 mL beakers and 2.5 g WP was added in each of the beakers. The beakers were allowed for 54 h for complete adsorption of MB on WP. Then, the solutions were filtered using filter paper. After that, the resulting dye-adsorbed residues, MB-WP, were allowed to desorb into two new beakers containing fresh aqueous solution raising the volume of each beaker 50 mL maintaining one beaker at 29 ºC and other at 37 ºC. Finally, the solutions were taken for UV-spectroscopic analysis to determine absorbance of MB solution after desorption.

The amount desorbed MB was determined by the following equation:

$$\text{Amount desorbed} = \frac{C\times M}{1000\times m} \times V \qquad (2.4)$$

where , C represents the concentration of MB after desorption, M is the formula mass of MB, V is the volume of the solution, m is the amount of adsorbent.

## 2.8 References


1. Saad, M.; Gaiani, C.; Mullet, M.; Scher, J.; Cuq, B. X-ray Photoelectron Spectroscopy for Wheat Powders: Measurement of Surface Chemical Composition. *J. Agric. Food Chem*. **2011**, *59*, 1527–1540.
2. Corre, D. L.; Bras, J.; Dufresne, A. Starch Nanoparticles: A Review. *Biomacromolecules* **2010**, *11*, 1139-1153.
3. Stejskal, J.; Gilbert, R. G. Polyaniline. Preparation of a Conducting Polymer. *Pure Appl. Chem.* **2002**, *74*, 857-867.
4. Stejskal, J.; Sapurana, I. *Pure Appl. Chem.* **2005**, *77*, 815-826.
5. MacDiarmid, A. G.; Chiang, J. C.; Richter, A. F.; Epstein, A. *J. Synth. Met.***1987**, *8(1-3)*, 285-290.
6. Armes, S. P.; Milles, J. F. *Synth. Met.* **1988**, *22*, 385.
7. Saikia, J. P.; Banejee, S.; Konwar, B. K.; Kumar, A. Biocompatible Novel Starch/Polyaniline Composites: Characterization, Anti-cytotoxicity and Antioxidant Activity. *Colloids and Surfaces B: Biointerfaces* **2010**, *81*, 158-164.
8. Hameed, B. H.; ElKhaiary, M. I. Batch Removal of Malachite Green from Aqueous Solutions by Adsorption on Oil Palm Trunk Fibre: Equilibrium Isotherms and Kinetic Studies. *J. Hazard. Mater.* **2008**, *154*, 237–244.

## 3.1 General Consideration

After collection of wheat powder (WP) and turmeric powder (TP) from the local market, the glutinous substances of the powder samples were removed by continuous washing with water. Then their functional forms were prepared by filtering followed by aquasonication. The functional properties of these natural powders e.g., adsorption, rehydration, wetting properties are greatly dependent on the surface chemical composition of the particles rather than their bulk composition as a result of the powder manufacturing process by drying or milling.

## 3.2 Characterization of Wheat Powder (WP), Turmeric Powder (TP) and Starch Nanoparticles prepared from WP

### 3.2.1 Infrared Spectral Analysis

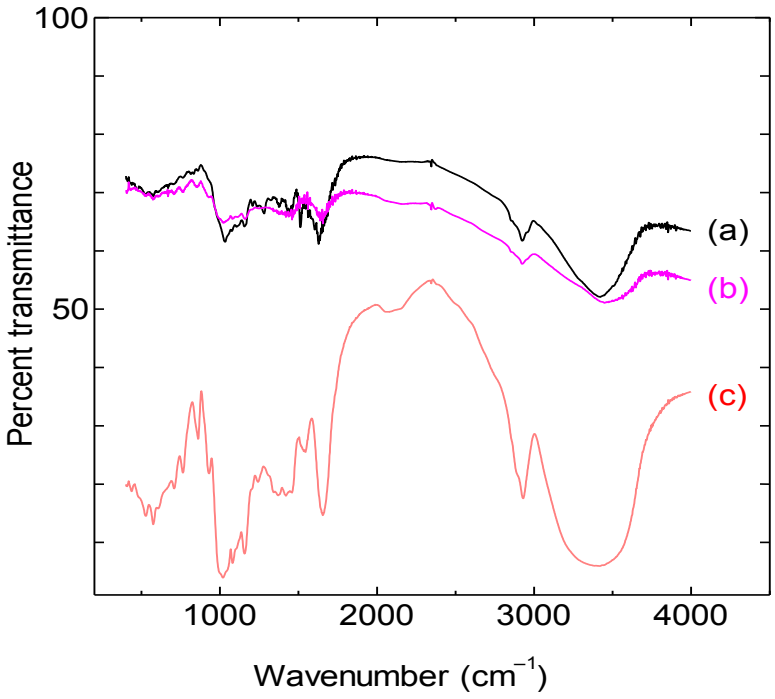


**Fig. 3.1** FTIR spectra of (a) TP, (b) SN and (c) WP

The IR spectrum of starch indicated it to be sensitive to changes in molecular structure (short-range order), such as starch chain conformation, helicity, crystallinity, and the retrogradation process as well as moisture content [1].

**Fig. 3.1** shows the FTIR spectra of (a) TP, (b) SN and (c) WP. In all cases, the broad absorption peaks in the range of 3000–3600 $cm^{-1}$ are raised due to the H-bonded O-H stretching and the peaks between 1600 and 1660 $cm^{-1}$ are for the tightly bounded water present in starch. Absorption bands between1000-1200 $cm^{-1}$ are characteristic of the –C-O- bond stretching of the C-O-C group in the anhydroglucose ring on the polysaccharide skeleton [2]. Moreover, the peaks around 2927 $cm^{-1}$ come from $–CH_2$- asymmetric stretching [3].

The broad absorption band of H-bonded O-H stretching appears at 3422 $cm^{-1}$ for TP which is at 3424 $cm^{-1}$ and 3383 $cm^{-1}$ for SN and WP respectively shown in **Fig. 3.1** (a), (b) and (c). The peaks at 1628 $cm^{-1}$ for TP, at 1643 $cm^{-1}$ for SN and at 1657 $cm^{-1}$ for WP are attributed to the tightly bounded water in these starch materials.

Moreover, the bands of TP at 1032 $cm^{-1}$ and 1154 $cm^{-1}$, at 1018 $cm^{-1}$ and 1159 $cm^{-1}$ for SN and at 1018 $cm^{-1}$ and 1157 $cm^{-1}$ for WP could be attributed to the coupling of C–O, C–C, and O–H bond stretching, bending and asymmetric stretching of the C–O–C glycosidic bridge in the anhydroglucose ring of starch. Therefore, the **Fig. 3.1** conform that all these samples are starch containing adsorbents and reveal that the starch existed in the native pure form in all the cases unless a little changes in IR peak positions due to the changes in chain conformation, helicity, crystallinity and moisture content of the starch origins.

### 3.2.2 X-Ray Diffraction

#### 3.2.2.1 Selection of Diffraction Peaks

Starch generally shows two types of characteristic X-ray patterns viz., A-type and B-type. Although both the types are based on parallel standard double helices but the major difference between the two types is in the packing of the helices (A-type starch being more closely packed); and differ in the content of intra-helical water (B > A).

For pure starch, single peaks at 2θ of 148˚8' and 22˚54' and double peaks at 16˚86' and 17˚78' are observed. This pattern corresponds to the typical A-type X-ray diffraction pattern of corn starch. In the case of gelatinized starch, the areas of the peaks, which correspond to the crystalline region, decrease in comparison with pure starch, which lead to a decrease of crystallinity [4].

X-ray diffraction pattern of (a) WP, (b) TP and (c) SN is shown in **Fig. 3.2**. Indexing of powder diffraction pattern is made and miller indices (h k l) to each peak is assigned and summarized in **Table 3.1**.

**Table 3.1** Selection of diffraction peaks of (a) WP, (b) TP and (c) SN in XRD analysis with the help of peak-fitting procedure.

| **Sorbent** | **Diffraction Angle, 2θ (Degree)** | **Intensity (cps)** | **Miller Indices (h k l)** |
|---|---|---|---|
| WP | 14.96 | 556 | (-220) |
| | 16.8 | 643 | (301) |
| | 17.8 | 651 | (020) |
| | 22.9 | 581 | (121) |
| TP | 14.98 | 369 | (120) |
| | 17.3 | 491 | (121) |
| | 22 | - | (-132) |
| | 24 | - | (041) |
| | 26.52 | 368 | (132) |
| SN | 15.26 | 486 | (-220) |
| | 17.08 | 554 | (301) |
| | 22.94 | 404 | (121) |

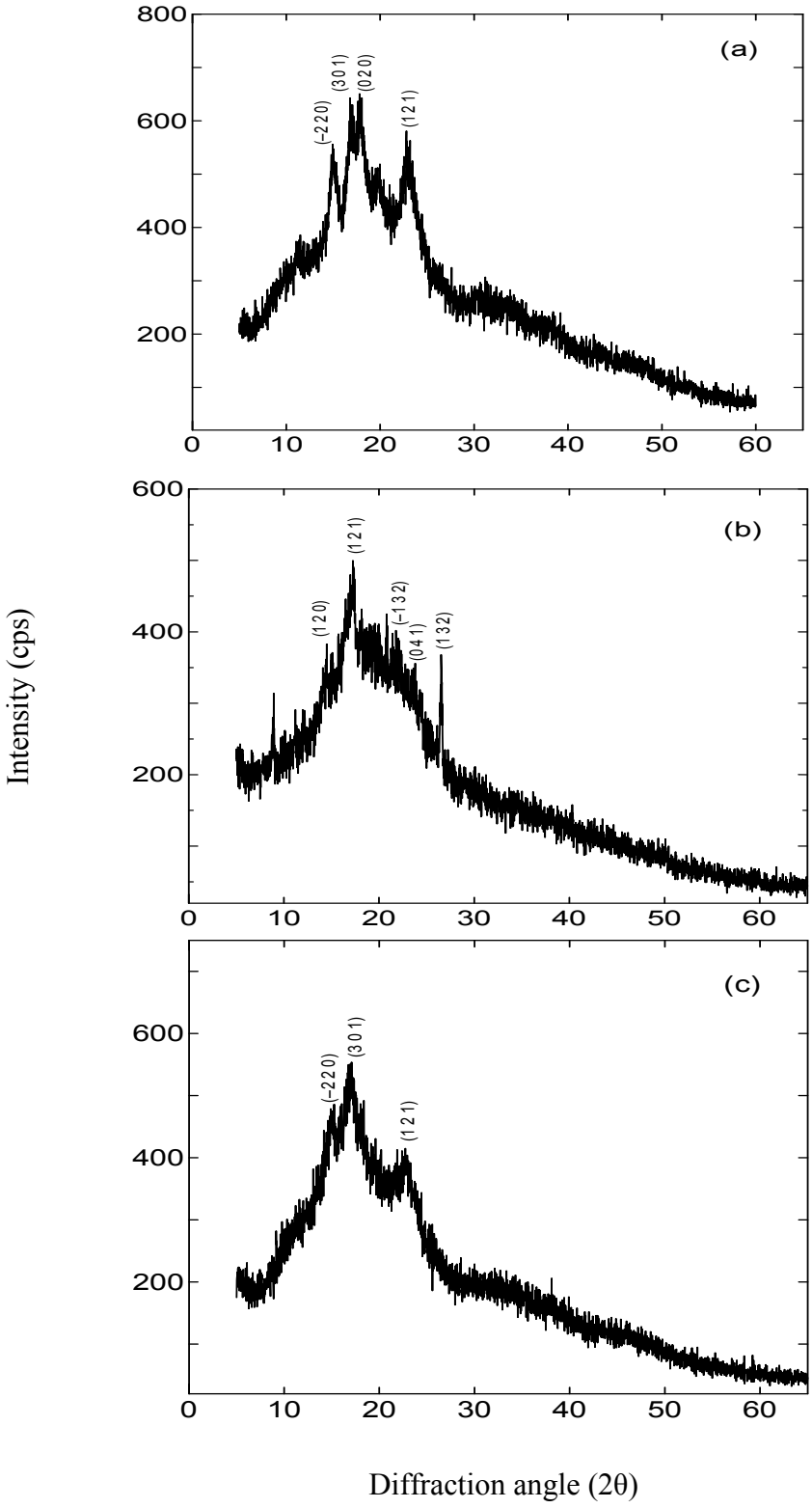


**Fig. 3.2** X-ray diffraction spectrum of (a) WP, (b) TP and (c) SN showing peak indices and 2θ positions

X-ray diffractogram of WP shows a typical A-type pattern of cereal starch (**Fig. 3.2a**). It shows strong Bragg reflections at 2θ = 14.96˚, 16.8˚, 17.8˚, and 22.9˚ which corresponds to the (-220), (301), (020) and (121) reflections [5]. An identical observation has reported by Rubio et al. [6]. Moreover, an additional peak at 2θ = 19.96˚ corresponding to the presence of crystalline V-type amylose-lipid complexes.

The Bragg diffraction pattern of TP is attributed to B-type starch. It reveals a strong peak at 2θ of 17.3˚ with a maximum intensity and weak peaks at 2θ = 14.98˚ and 26.52˚ as in **Fig. 3.2b**. These peaks are assigned by indices (121), (120) and (132), respectively [6]. TP also gives weak peaks at around 22˚ (-132) and 24˚ (041). These observations are similar to that of earlier reported type on starches from curcuma species (*C. zedoaria*, *C. malabarica*, and *C.amad*). Although the X-ray diffraction pattern of TP resembles to the isolated native starch but it gives lower intensity (a maximum 491 cycles per second (cps) at 2θ = 17.3˚) [3].

In case of SN, the $V_H$-style crystallinity is different from A-style crystallinity of WP, could originate from a single-helical structure "inclusion complex" made up of amylose and plasticizer as can be seen from the **Fig. 3.2c**. The similar $V_H$-style crystallinity also appears in the plasticized wheat starch. When ethanol was delivered dropwise to starch-paste solution, gelatinized starch nanoparticles was precipitated. Therefore, the gelatinization destroyed A-style crystallinity of wheat starch, and SN exhibits the $V_H$-style crystallinity with single Bragg diffraction peaks at 2θ of 15.26˚, 17.08˚ and 22.94˚ which are attributed to the crystal planes (-220), (301) and (121) [2, 6]. Moreover, the broader diffraction peaks of SN indicating that the crystallite size of SN is very smaller than those of WP and TP.

### 3.2.2.2 Particle Size Calculation of Starch Nanoparticles (SN)

Powder X-ray diffraction has become a cornerstone technique for deriving crystallite size in nanoscience due to speed and simplicity. This technique does not rely on any underlying order, so it is suited to poorly crystalline and amorphous materials. In the study of nanomaterials the crystallite size is usually the sole factor of interest [7].

The ancient methodology developed for the starch crystallinity determination named Two Phase concept assumes that relatively perfect crystalline domains (crystallites) are interspersed with amorphous regions. With slight modifications, most researchers in the starch field continue to use the same methodology and, thus, consider starch structure as a two-phase system.

However, this simplified picture is not compatible with improved understanding of polymeric structures that encompasses intermediate crystalline objects, chain folding, lamellar crystalline growths, lattice dislocations, and other phenomena. Therefore, a more appropriate way of approaching the crystalline structure of starch is to use the crystal-defect concept as opposed to the two-phase concept typically used. According to the crystal defect concept of polymer structure, a portion of the X-ray scattering from the crystalline domains is diffuse and contributes to the so-called amorphous background [8].

Rubio et al. [6] applied a peak fitting methodology to calculate crystallinity in native starch varieties to take into account the irregularities in crystal that are expected to exist in semicrystalline materials. This procedure is very famous for the XRD analysis of synthetic polymers.

An accurate determination of crystallinity cannot be fulfilled without a proper decomposition of crystalline and amorphous intensity profiles from the total corrected intensity profile, no matter what method is employed for crystallinity calculation. For synthetic polymers, this is normally achieved by a curve fitting technique, in which the crystalline and amorphous components in a crystal defect structure are assumed to be a Gaussian, Lorentzian, or other related function e.g., Voigt functions [6].

Most modern X-ray diffractometers include software for peak profile fitting. For well behaved samples, e.g., of proper particle size and free of strain, stress or stacking faults the Pseudo-Voigt function gives a good representation of the profile and it is used today in most programs for Rietveld refinements and also in the Two Stage method. This software greatly helps in calculating the intensities, positions, widths and shapes of the peaks with a far greater precision than is possible with manual measurements [9]. Moreover, particle size, strain/stress and domain size in a sample could be determined by analyzing the broadening of the peaks, full width at half maxima (FWHM) [10]. The FWHM was measured by the 7.03 version of Leptos software of the D8 Advance Bruker Diffractometer [11].

The determination of particle size is treated already by the so-called Scherrer equation developed in the course of Scherrer's Ph.D. thesis in 1918. This equation is now frequently used to estimate the particle sizes of both cubic and noncubic materials [12]. The Debye modified Scherrer formula applied in the particle size estimation of SN is

$$D = \frac{k\lambda}{\beta\cos\theta} \qquad (3.1)$$

Here,

D = Average particle size measured in a direction perpendicular to the surface of the specimen in the unit of nm.

k = A constant, which varies from 0.8 to 0.98 (usually 0.94) depending on the crystal structure.

$\lambda$ = Wavelength of the X-rays used (0.1541 nm)

$\beta$ = Full width at half maxima (FWHM) in radians

$\theta$ = Bragg angle in radians

The particle size detail of SN is tabulated in **Table 3.2**. The average size of starch nanoparticles estimated from Debye-Scherrer formula is 9 nm. Corre, D. L. et al. [13] also have been reported that SN displays a spherical or oval shape, with diameters in the range of 10-20 nm.

**Table 3.2** SN mean diameter from Scherrer equation at different positions

| Peak | Position Peak (2θ) | Intensity (cps) | FWHM (rad) | Diameter (nm) |
|---|---|---|---|---|
| 1 | 15.04 | 460 | 0.1739 | 0.81 |
| 2 | 16.94 | 551 | 0.0248 | 5.66 |
| 3 | 22.76 | 401 | 0.0982 | 1.44 |
| 4 | 96.39 | 46 | 0.0224 | 9.28 |

### 3.2.3 Scanning Electron Microscopy

The scanning electron micrographs of WP, TP and SN were taken at different magnifications (×500 and ×10,000) and different high voltages (15 kV and 20 kV) which have been shown in the **Fig. 3.3**. The SEM micrograph for starch reveals hexagonal starch granules with average size of the order of 2 μm, the surface being quite smooth and well defined. It is important to know about the granule structure, size and their distribution because they affect the functional properties of starch.

Wheat powder (WP) revealed large disk-like or lenticular shaped A-granules and small, roughly spherical, B- and C-granules in all the starches shown in **Fig. 3.3A** [5]. The granule size distribution is classified into A- (>15 μm), B- (5-15 μm), and C-granules (< 5 μm). The dried turmeric powder (TP) in **Fig. 3.3B** appeared in an irregular shape. It mainly consists of starch with some other components like protein, crude fiber and fat which are visible but difficult to identify. Particle size remains in 3-20 μm for small and 20-50 μm for large size particles [3].

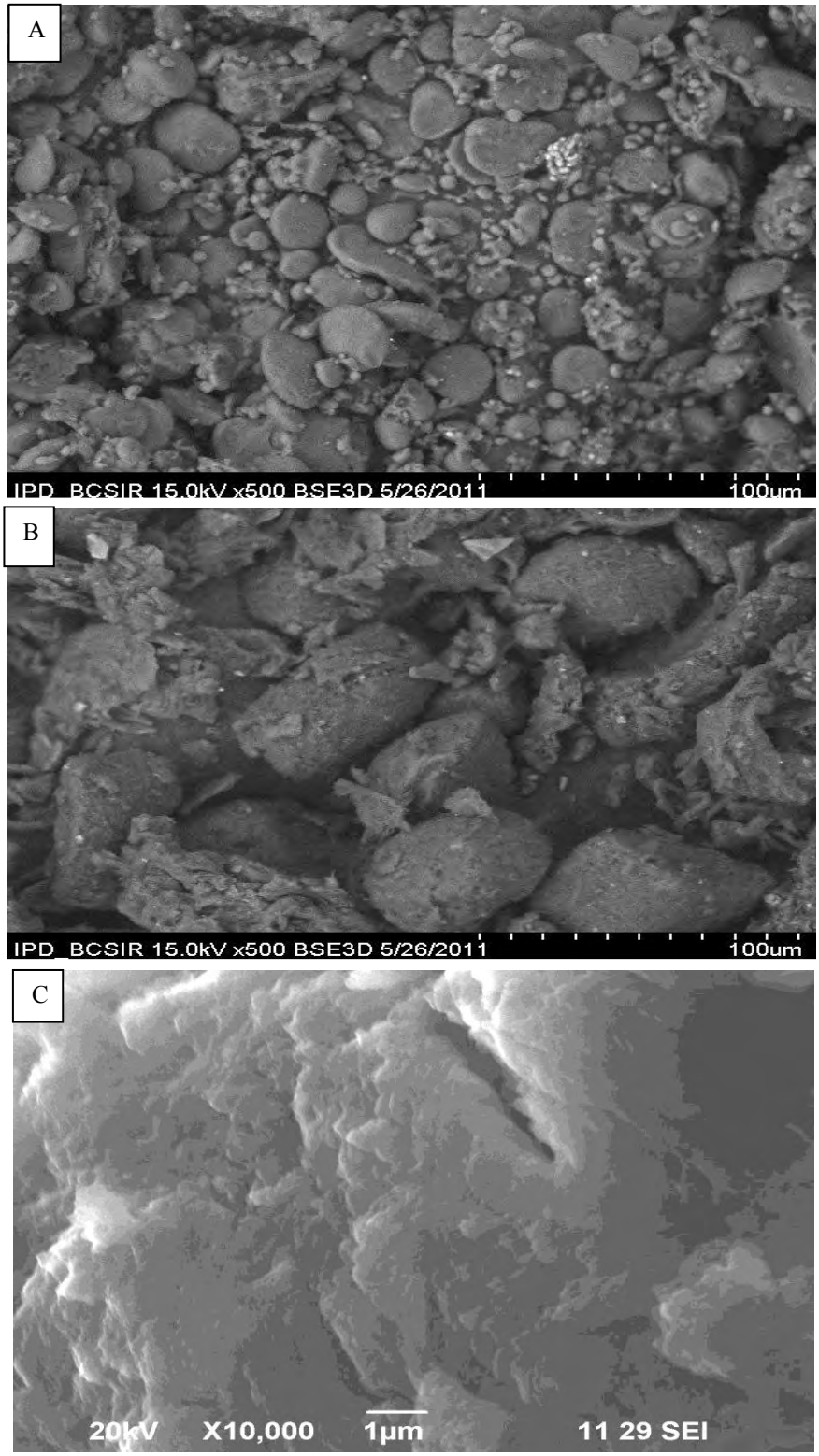


**Fig. 3.3** SEM (Scanning Electron Microscopic) image of (A) WP, (B) TP and (C) SN

Finally **Fig. 3.3C** shows the SEM micrograph of starch nanoparticles (SN). Most of the SN usually possesses sizes in the range from 50 to 300 nm [2]. We actually found a SEM image of agglomerated SN because of the lack of dispersion of the particles on the substrate. In the preparation of SN, firstly the native wheat powder was gelatinized in water and formed starch paste. The SN was formed by dropwise addition of ethanol in the resultant solution. The agglomeration of the SN may result from the inadequate stirring and reaction temperature. However, the interaction of hydrogen bond between SN and starch paste play the important role on the stability of the precipitated SN in the suspension. It is also noticeable that the samples were not pre-treated with any kind of milling which would change the shape of particles and consequently reduce the particle sizes.

## 3.3 Characterization of PANI and its Composite with Starch

### 3.3.1 IR Spectral Analysis

The FTIR spectra of (a) pure starch, (b) PANI and (c) PANI/starch composite are shown in **Fig. 3.4**. The characteristic broad band for O-H group (in the presence of H-band) of starch appears at 3423 $cm^{-1}$. A peak around 2927 $cm^{-1}$ is attributed to an asymmetrically stretching vibration of C-H band in pyranoid ring. The several absorption bands between 828 $cm^{-1}$ and 1158 $cm^{-1}$ are attributed to the contribution of various functional groups, such as C-O and C-O-C [2].

The typical feature of pure PANI is very familiar in literature [14]. The main peaks at 1564.2 $cm^{-1}$ and 1481.2 $cm^{-1}$ can be assigned to the stretching vibrations of quinine and benzene rings respectively. The peaks at 1303 $cm^{-1}$ and 1244 $cm^{-1}$ corresponds to the C-N stretching vibrations. The 1220-500 $cm^{-1}$ is the region of the in-plane and out of plane bending of C-H bonds on aromatic ring. The main absorption bands for intrinsic PANI are located at 1113 $cm^{-1}$ and 822 $cm^{-1}$.

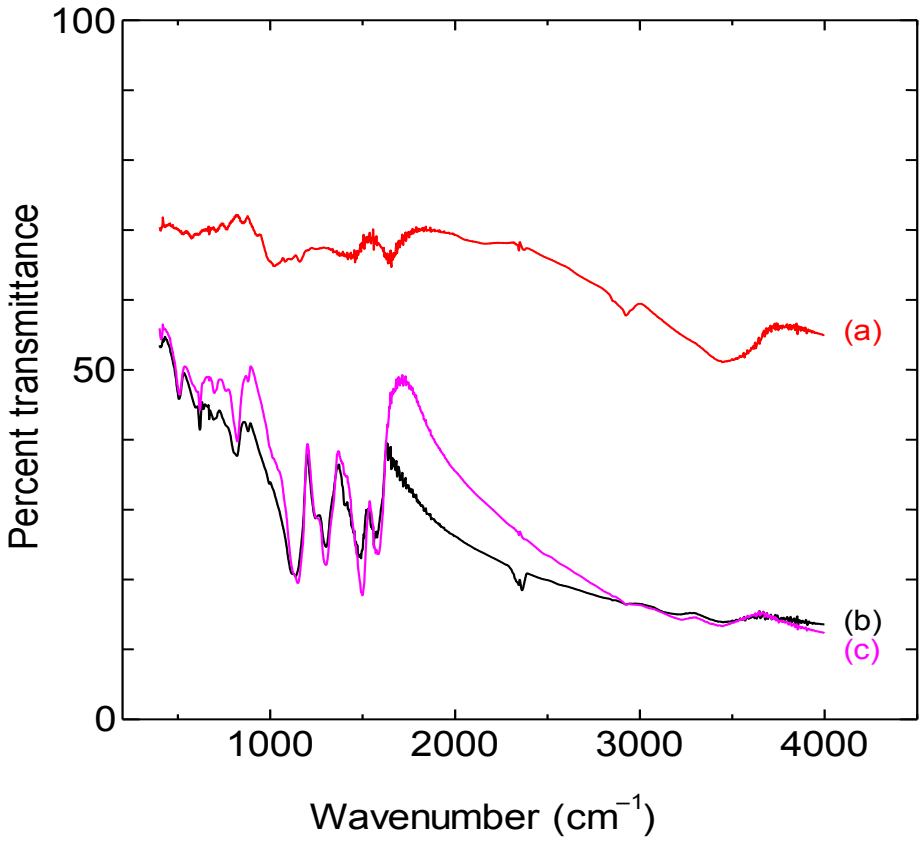


**Fig. 3.4** FTIR spectra of (a) pure starch, (b) PANI and (c) PANI/starch Composite

The characteristic absorption bands of pure starch (3423 $cm^{-1}$) and PANI (1571, 1488, 1296, 1240, 1124 and 821 $cm^{-1}$) have been both present in the spectrum of their composite, PANI/starch. Comparing the relative intensity band around 3423 $cm^{-1}$, we also find that the band of the stretching vibration of -OH group in the composite is apparently weaker than the same band in pure starch. Furthermore, the absorption peak at 3423 $cm^{-1}$ in the spectrum of pure starch is blue-shifted to 3452 $cm^{-1}$ in the spectrum of the composite.

### 3.3.2 Thermal Analyses

The thermal behaviour of pure starch and PANI (**Fig. 3.5a**) and PANI/starch Composite-1 and Composite-2 (**Fig. 3.5b**) are very clearly exhibited by the thermograms (TG), derivatograms (DTG) and differential thermograms (DTA). The onset temperatures of PANI and pure starch are 250 ˚C and 247 ˚C and for the PANI/starch composites it is 216 ˚C. The maximum decomposition temperature ($T_{max}$) of PANI and pure starch are 315 ˚C and 311 ˚C and for the PANI/starch composites the $T_{max}$ is 230 ˚C. All these materials differ widely in the onset temperature of decomposition, the maximum decomposition temperature ($T_{max}$) and % weight loss for the different stages.

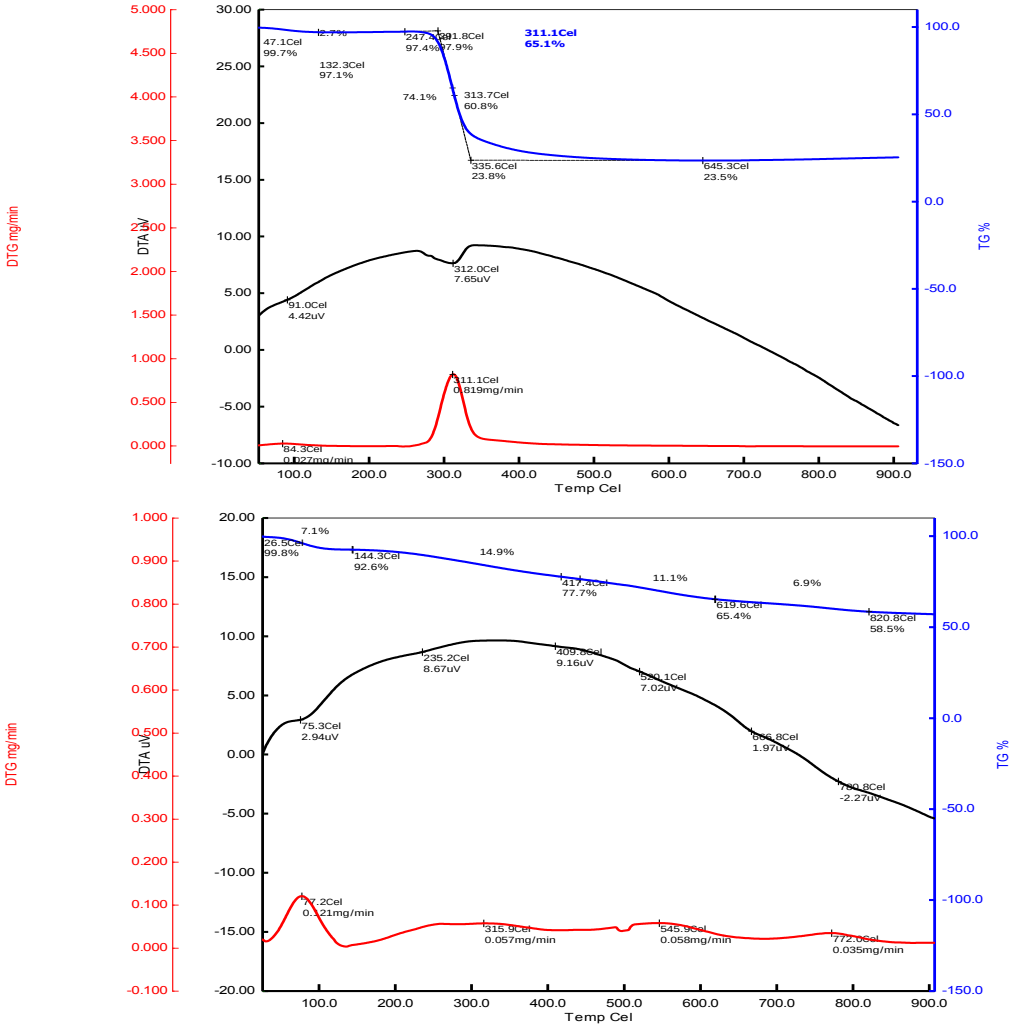


**Fig. 3.5a** Thermal behaviours of pure starch (top panel) and PANI (bottom panel). The upper blue color shows TGA curve, the middle black color shows DTA curve and the bottom red color shows the DTG curve.

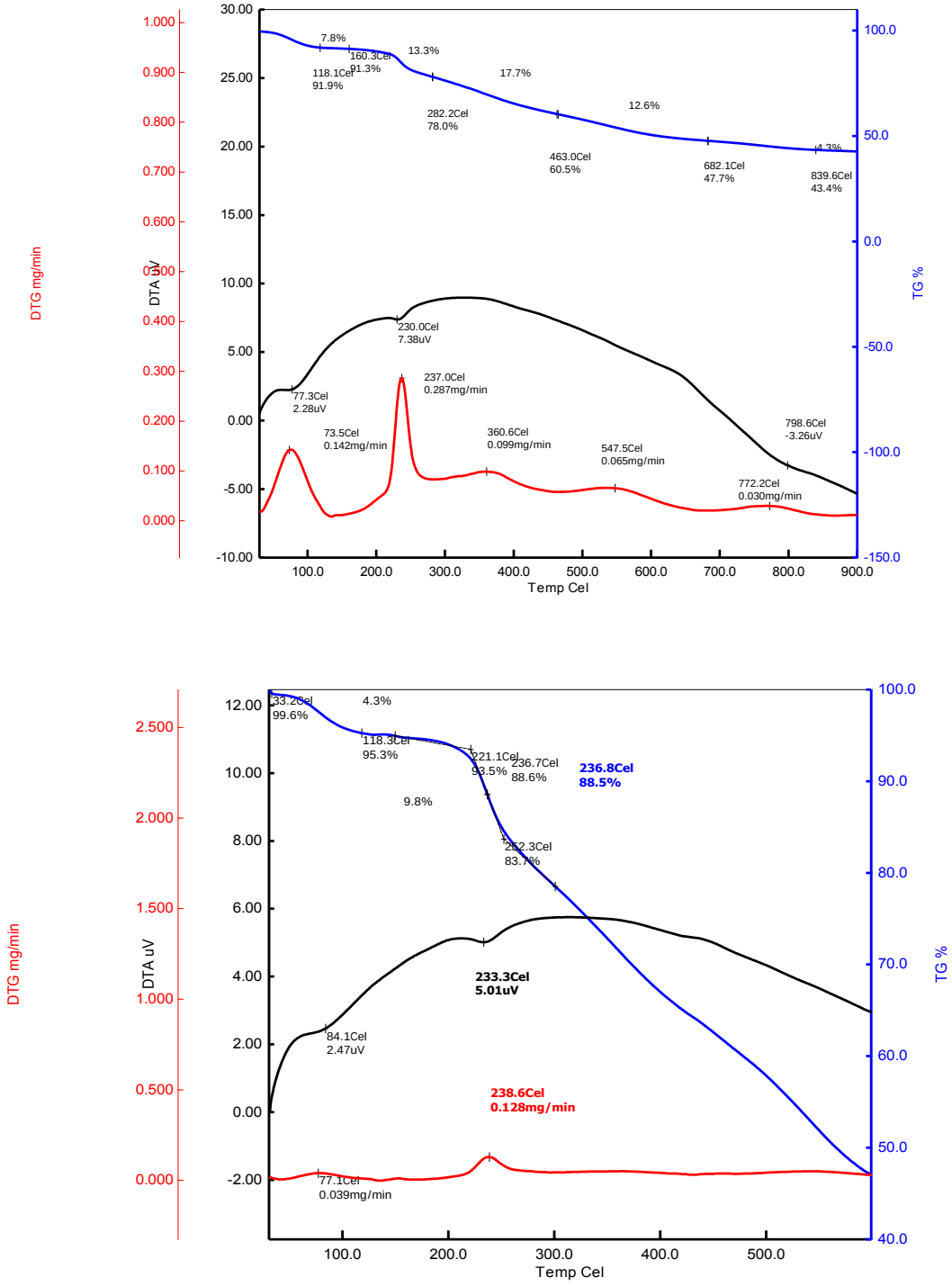


**Fig. 3.5b** Thermal behaviours of PANI/starch Composite-1 (top panel) and PANI/starch Composite-2 (bottom panel). The upper blue color shows TGA curve, the middle black color shows DTA curve and the bottom red color shows the DTG curve.

It has long been reported that the main decomposition mechanism of starch is the dehydration reaction between starch molecules [15]. Pure starch shows a characteristic three-step thermogram, wherein the major 61 % weight loss occurs in the second step within the temperature range of 247-340 ˚C [16]. The derivatogram gives the $T_{max}$ 311 ˚C. The third stage of decomposition is rather slow and results in a small weight loss up to 440 ˚C. DTA curve of the starch shows a broad endothermic peak at 312 ˚C with a small endothermic peak at 91 ˚C. This prominent endotherm at 312 ˚C appeared to involve further elimination of the polyhydroxy1 groups, accompanied by depolymerization and decomposition of starch [15, 17].

On the other hand, in the redoped PANI (PANI-HCl) the weight loss below 150 ˚C has been assigned to water loss [18] and at a higher temperature (>150 ˚C), due to the loss of bonded water and dopant [19]. Above 420 ˚C, the weight loss is associated with the degradation of the polymer chain structure, in agreement with the literature [20]. It does not show any significant endothermic peak in DTA curve.

In case of the both PANI/starch Composites i.e., Composite-1 and Composite-2, the onset temperature of starch decomposition for the second step is as low as 216 ˚C as against 247 ˚C for that of pure starch. All the steps for PANI are obvious from the derivatogram of the PANI/starch Composites. Therefore, the PANI/starch Composites are thermally less stable than the pure starch. Besides, in the DTA thermograms in the **Fig. 3.5 (C, D)**, both PANI/starch Composites have broad endothermic peaks both at identical temperature of 230 ˚C but the peak of Composite-2 is lower in intensity. It can be seen that PANI/starch Composites have one prominent endothermic peak, whereas PANI shows no significant endothermic peak. This is an indication of the presence of starch in the structure of the composites. Thus both of the composites are merely composed of starch and PANI and are indistinguishable in structure [21].

### 3.3.3 X-Ray Diffraction

#### 3.3.3.1 Diffraction Peak Indexing

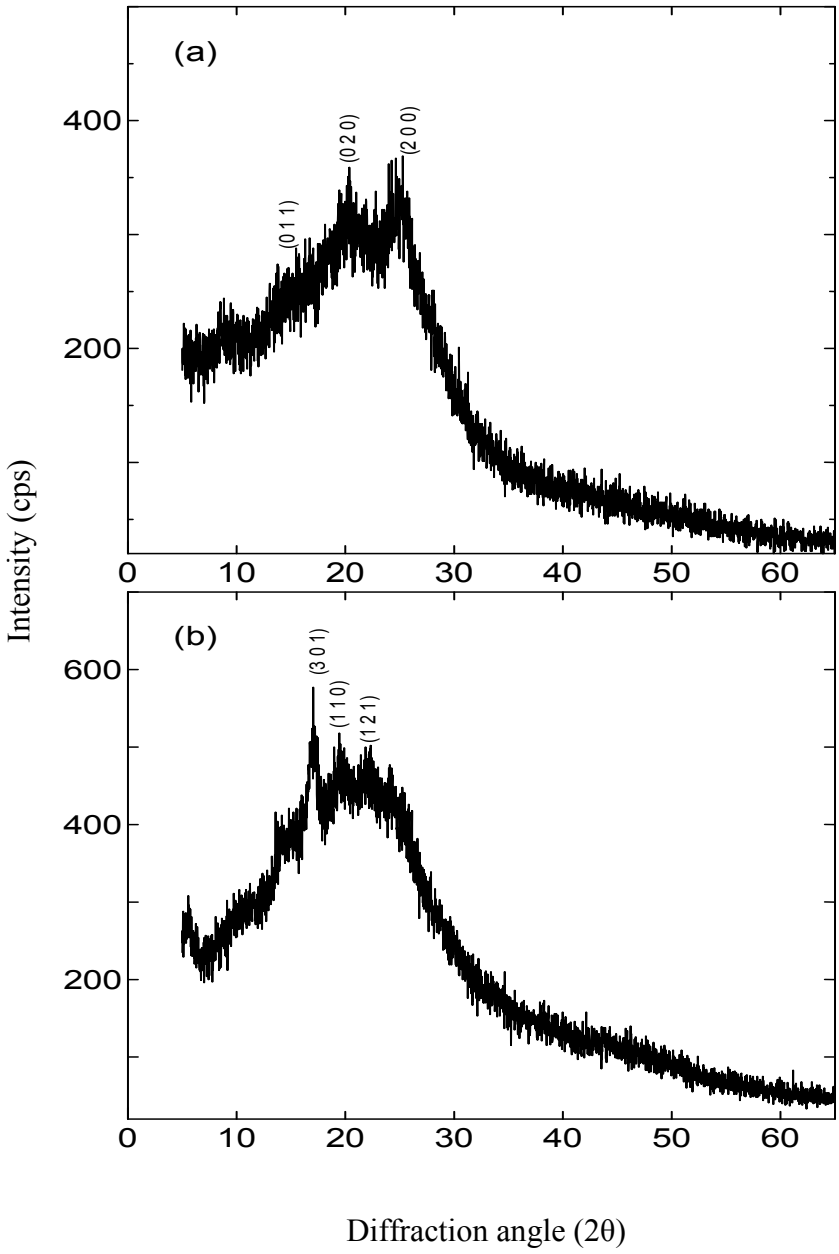


**Fig. 3.6** X-ray diffraction spectrum of (a) PANI and (b) PANI/starch Composite exhibiting peak indices and 2θ positions

**Fig. 3.6** shows X-ray diffraction spectra of (a) PANI and (b) PANI/starch Composite. In the case of PANI, two broad peaks at 2θ = 21˚and 25.28˚ and another peak at 2θ of 15.14˚are observed as in **Fig. 3.6a**.

The peaks centered at 2θ = 21˚and 25.28˚ are ascribed to the periodicity parallel and perpendicular to the polymer chains of PANI respectively. The peak at 2θ = 21˚ also represents the characteristic distance between the ring planes of benzene rings in adjacent chains or the close contact interchain distance [22, 23].

The X-ray patterns for the PANI/starch Composite (**Fig. 3.6b**) exhibits the evolution of the peaks corresponding to polyaniline with the increase of starch concentration which is quite obvious. A sharp diffractive peak centered at an angle of 21˚ in **Fig. 3.6a** indicates the usual neutral PANI to be amorphous, whereas **Fig. 3.6b** shows a higher degree of crystalline PANI in the composite. Therefore, the XRD pattern shows nearly semicrystalline structure of PANI/starch Composite [21, 22].

**Table 3.3** Diffraction peak indexing of PANI and its composite with starch in XRD analysis

| **Material** | **Scattering Angle, 2θ (Degree)** | **Intensity (cps)** | **Miller Indices (h k l)** |
|---|---|---|---|
| PANI | 15.14 | 266 | (011) |
| | 21 | 337 | (020) |
| | 25.28 | 369 | (200) |
| PANI/starch Composite | 17.04 | 577 | (301) |
| | 19.44 | 518 | (110) |
| | 22.32 | 502 | (121) |

### 3.3.3.2 Particle Size of PANI and PANI/starch Composite

The average particle size of polyaniline (PANI) and PANI/starch Composite are also calculated and represented in **Table 3.4** and **Table 3.5**, respectively, by using the Debye-Scherrer equation (**Eq. 3.1**). The average particle size of PANI/starch Composite is about 18 nm which is a smaller than that of PANI (20 nm). A similar finding was found by Zareh, E. N. et al. [24]. They firstly prepared polyaniline/starch blend structure and then introduced polystyrene of commercial type into the blend.

**Table 3.4** Mean diameter of PANI from Scherrer equation at different positions

| Peak | Position Peak (2θ) | Intensity (cps) | FWHM (rad) | Diameter (nm) | Average Particle size (nm) |
|---|---|---|---|---|---|
| 1 | 20.36 | 359 | 0.066 | 2.13 | |
| 2 | 25.28 | 369 | 0.058 | 2.45 | |
| 3 | 57.22 | 44 | 0.023 | 6.86 | |
| 4 | 60.7 | 48 | 0.014 | 11.8 | |
| 5 | 64.34 | 40 | 0.014 | 11.8 | |
| 6 | 65.56 | 36 | 0.018 | 8.76 | |
| 7 | 71.54 | 40 | 0.005 | 35.7 | |
| 8 | 74.2 | 36 | 0.011 | 15.6 | 19.8 |
| 9 | 75.29 | 42 | 0.004 | 41.8 | |
| 10 | 77.75 | 34 | 0.011 | 16.8 | |
| 11 | 90.21 | 39 | 0.017 | 11.7 | |
| 12 | 91.54 | 29 | 0.007 | 27.1 | |
| 13 | 95.9 | 34 | 0.007 | 30.9 | |
| 14 | 96.56 | 37 | 0.006 | 35.0 | |
| 15 | 98.13 | 34 | 0.013 | 16.7 | |

**Table 3.5** Mean diameter of PANI/starch from Scherrer equation at different positions

| Peak | Position Peak (2θ) | Intensity (cps) | FWHM (rad) | Diameter (nm) | Average Particle size (nm) |
|---|---|---|---|---|---|
| 1 | 17.04 | 577 | 0.023 | 6.18 | 17.75 |
| 2 | 19.44 | 518 | 0.010 | 13.9 | |
| 3 | 21.86 | 500 | 0.024 | 58.7 | |
| 4 | 24.07 | 452 | 0.188 | 0.75 | |
| 5 | 85.80 | 59 | 0.020 | 9.26 | |

### 3.3.4 Scanning Electron Microscopy

**Fig. 3.7** shows the scanning electron micrographs of polyaniline and it's composite with starch exhibiting at 10,000 magnification and at high voltage of 20 kV. When PANI is treated with double-distilled water (neutral PANI), the aggregates seem to exhibit a granular morphology (**Fig. 3.7A**) in which grains seem to be aggregated into a stonelike body and distributed nonuniformly over the substrate [25].

In the preparation of PANI/starch Composite (**Fig. 3.7B**), the polymerization of aniline took place over the surface of the starch granules forming a layer over it. With increasing the added amount of starch, polymerization begins in the bulk beyond the surface which is obvious from the SEM micrograph of the composite. Starch is well dispersed in the polyaniline matrix of the composite [14]. The agglomeration of the PANI/starch Composite might be resulted from improper mixing of its constituents. This fault could be mitigated by high energy ball milling of the material.

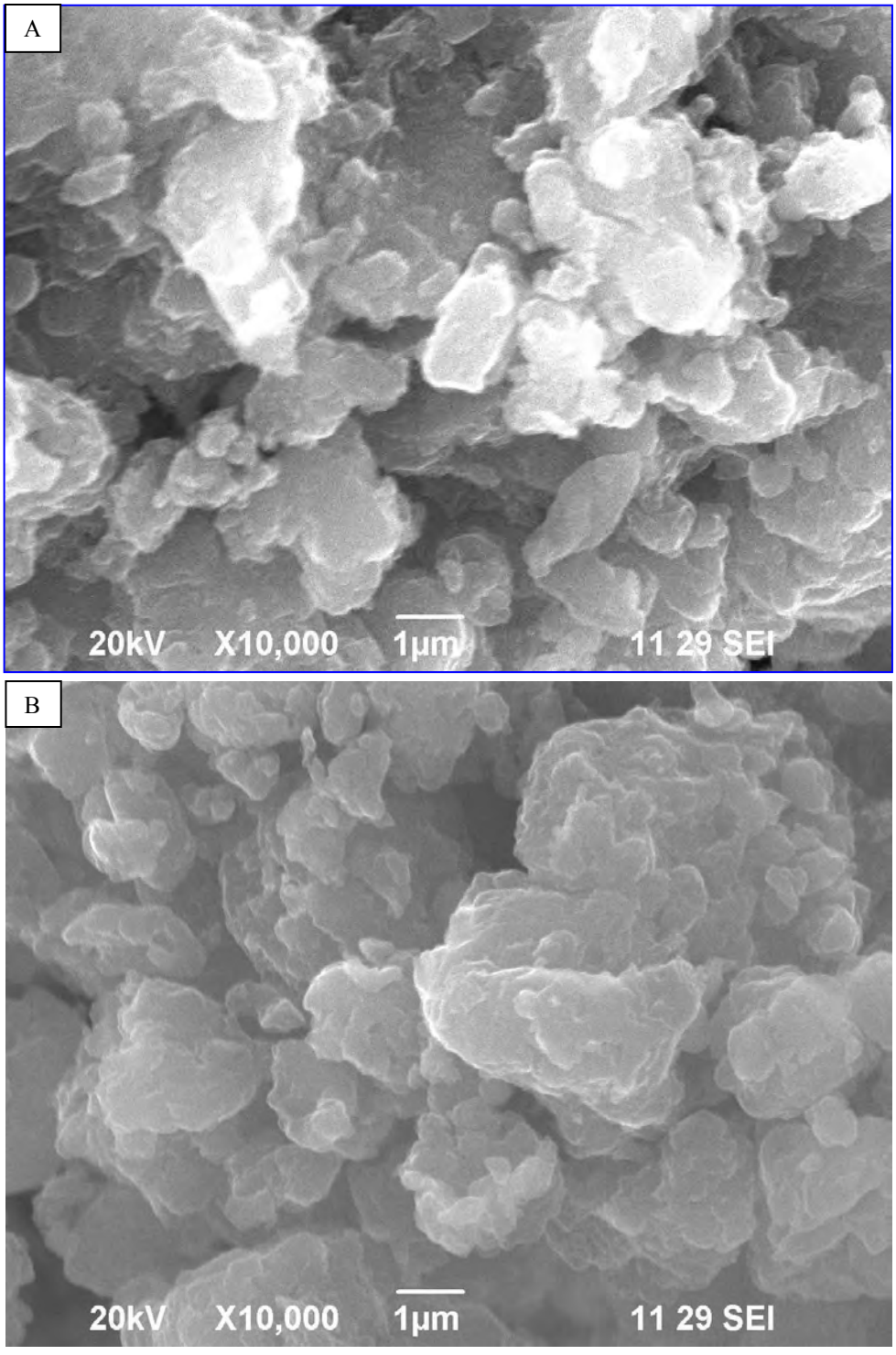


**Fig. 3.7** SEM (Scanning Electron Microscopic) image of (A) PANI and (B) PANI/starch Composite

### 3.4 Choice of Degradable and Cost Effective Adsorbents

#### 3.4.1 Selection of Degradable Adsorbents

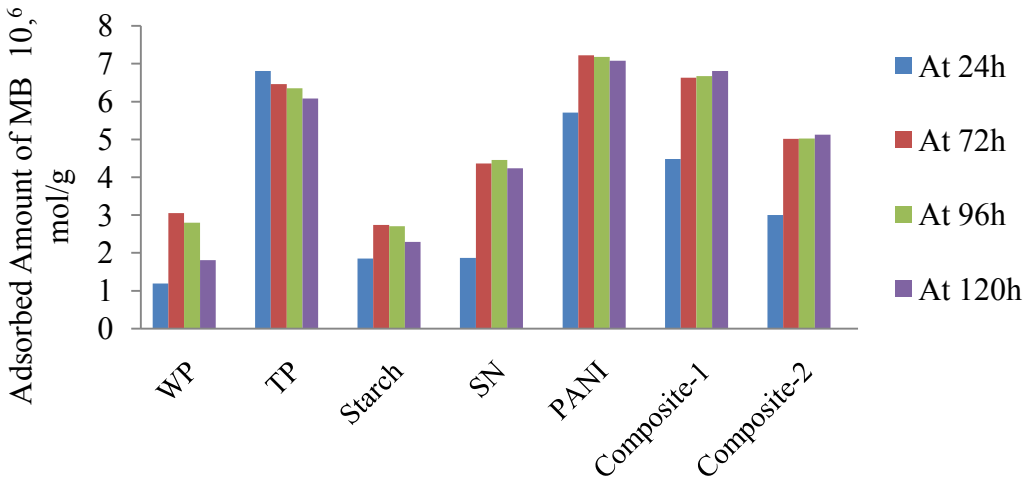


**Fig. 3.8** Comparative adsorption of methylene blue (MB) onto the starch-based biosorbents and conducting polymer adsorbents. Initial [MB] = $1\times10^{-5}$ M, pH = 6.86, adsorbent dose = 1.2 g/L and temperature = 29 ˚C

**Fig. 3.8** shows the comparative adsorption of MB onto starch-based biosorbents named wheat powder (WP), turmeric powder (TP), starch and starch nanoparticles (SN) and onto some synthetic conducting polymer adsorbents named polyaniline (PANI), two PANI/starch composites i.e., Composite-1 and Composite-2 at different time intervals in double distilled water solution. The adsorption efficiencies of TP, PANI, Composite-1 and Composite-2 were found maximum and were comparable. The efficiencies of WP, pure starch and SN were reasonably low, but the efficiency of SN was higher than that of pure starch. High adsorption efficiency of SN was revealed by SEM and XRD analysis to be due to the smaller particle size.

Interestingly, it was observed that the adsorption of MB on WP was raised a maximum at 72 h and then decreased gradually. In the case of TP, the adsorption became to the maximum within 24 h and declined subsequently with time. The adsorption on WP at 120 hrs (about 3.05 x $10^{-6}$ mol/g) is decreased by about 50 % of that observed at 72 hrs (about 1.81 x $10^{-6}$ mol/g), indicating that the adsorbents get

biodegraded and hence the MB gets desorbed. The biodegradation of the adsorbents WP and TP is revealed in a clear view in the **Fig. 3.9** which also exhibits that the synthetic adsorbent PANI remains undegraded with time.

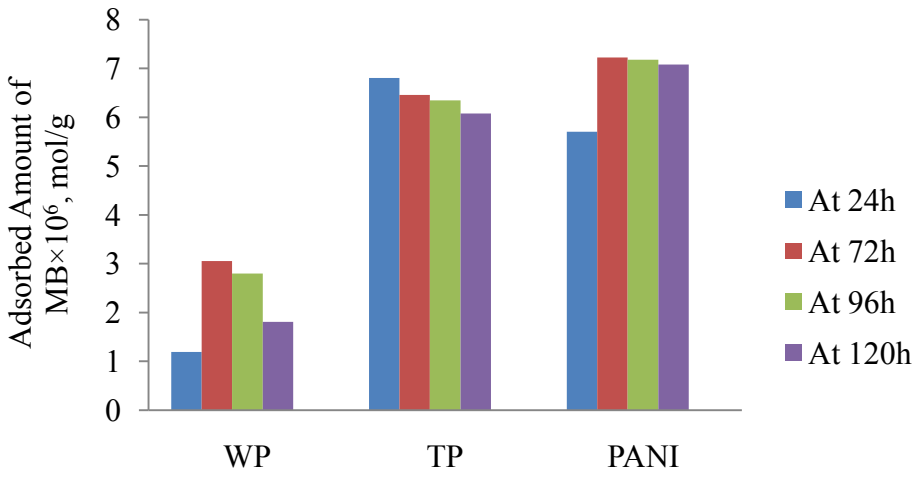


**Fig. 3.9** Conformation of the biodegradation of wheat powder (WP) and turmeric powder (TP) with expend of time compared to the synthetic adsorbent polyaniline (PANI) which remains undamaged with time. (Reproduced from the **Fig. 3.8**).

Biodegradation involves enzymatic and chemical degradation by living microorganisms. Degradation of all polymers follows a sequence in which the polymer is first converted to its monomers, after which the monomers are mineralized. Most polymers are too large to pass through cellular membranes, so they must first be depolymerized to small monomers before they can be absorbed and biodegraded within microbial cells. The initial breakdown of a polymer can result from a variety of physical, chemical, and biological forces with chemical hydrolysis probably being the most important. Physical forces, such as heating/cooling, freezing/thawing, or wetting/drying, can cause mechanical damage such as the cracking of polymeric materials. The growth of many fungi can also cause small-scale swelling and bursting, as the fungi penetrate the polymer solids.

The speed of degradation depends on the specific environmental conditions. For example, a ready supply of nutrients, oxygen, and water are needed for soil microorganisms to rapidly degrade cellulose and starch, while the fungi which degrade wood are actually more active under poor nutrient conditions. Soil microbes can initiate the depolymerization of many natural polymers such as starch, cellulose, and hemicelluloses. They secrete a variety of enzymes into the soil water and these enzymes then begin the breakdown of the polymers [26].

Starch digesting enzymes include α-amylases, glucoamylases, α-glucosidases, isoamylases, β-amylases and maltogenic β-amylases. There are two endo amylase families: (i) α-amylases that randomly hydrolyze α-1, 4-linkages between adjacent glucose units in the amylose and amylopectin polymers to produce dextrins and (ii) isoamylases that hydrolyze α-1, 6-linkages at branch points in amylopectin. Cereal α-amylases randomly attack high molecular weight substrate and nonrandomly attack short dextrins. Amylases capable of raw starch digestion are found throughout the animal and plant kingdom. Amylases from cereals such as maize, barley, wheat, rice, and sorghum have raw starch hydrolytic capabilities that are essential to the breakdown of stored carbohydrates for plant development. Many species produce multiple α-amylases: as many as 10 in rice and five in potato. Wheat produces an α-amylase isoform early in germination that digests raw starch and an isoform late in germination that only digests soluble starch [27].

In our study, biodegradation of WP and TP was carried out in aqueous medium in presence of MB dye. Although MB dye is a photodynamic antimicrobial agent, very low concentrations of MB are able to kill or inhibit the growth of microorganisms e.g., fungi, yeasts in the aqueous solution even under light conditions.

On contrary microbial reduction of the phenothiazinium chromophore of MB causes decolourisation. The bactericidal activity of MB is weak due to chromophoric reduction by bacterial enzymes. Moreover, the starch content of the biosorbents has the potential to induce the growth of microorganisms. Starch secretes α-amylase isoform that also digests raw starch in a considerable extent [27, 28].

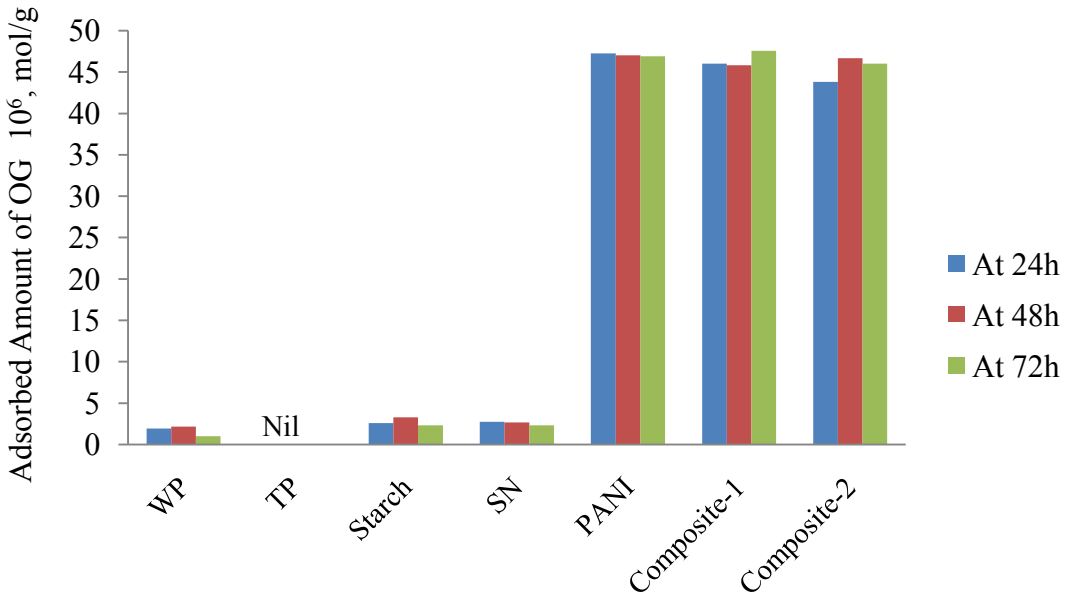


**Fig. 3.10** Adsorption of orange green (OG) dye on the natural and synthetic adsorbents (Initial [OG] = $5\times10^{-5}$ M, pH = 6.86, adsorbent dose = 1.2 g/L and temperature = 29 ˚C)

**Fig. 3.10** reveals the adsorption of the anionic azo dye OG onto starch-based biosorbents and synthetic adsorbents as described for the **Fig. 3.8**. The OG dye was not adsorbed onto TP and other starch-based biosorbents i.e., WP, starch and SN had very little adsorption capacities compared to the synthetic adsorbents PANI, Composite-1 and Composite-2. The WP and starch experienced biodegradation as explained in the **Fig. 3.9**. It is noticeable that there is no report regarding the antimicrobial activity of OG dye.

### 3.4.2 Rationalization of the Efficacy of the Prepared Adsorbents through their Relative Cost Estimation

#### 3.4.2.1 Effectiveness of the Adsorbents

The adsorption capacity of our investigated adsorbents is compared to the efficacy of some recognized adsorbents and summarized in **Table 3.6**.

**Table 3.6** Amount of the MB dye adsorbed on the adsorbents of our choice of interest and onto some other reported adsorbents.

| Adsorbents | Prepared Adsorbents | | | | | | Other reported Adsorbents | | |
|---|---|---|---|---|---|---|---|---|---|
| | Starch | WP | SN | TP | PANI | PANI/starch Composite | Basic PANI | PANI Nanotube Base | Basic PANI /$SiO_2$ |
| Amount adsorbed MB×$10^6$ (mol/g) | 2.9 | 3.3 | 4.3 | 6.81 | 7.07 | 6.83 | 35 | 14 | 39 |

Among the adsorbents, the starch-based bisorbents starch, WP and SN were shown comparable adsorption capacities. Even though the SN had a higher efficacy than the pure starch, it has no experience of biodegradation as shown in **Fig. 3.8** and **Fig. 3.10**. A similar finding was observed by Taghi, M. et al. [29] in the study of enzymatic degradation and water absorption of the nanocomposites of starches with clay. They established that nanoparticles hinder degradation. Moreover, starch-based TP exhibited a compatible adsorption to the synthetic PANI and it's composite with starch.

Chowdhury, A.-N. et al. [25] reported that basic-PANI can adsorb $35\times10^{-6}$ mol/g MB dye. Another report of the same author in 2008 published that basic PANI/$SiO_2$ composite exhibit $39\times10^{-6}$ mol/g adsorption capacity towards MB [30]. Moreover, Ayad, M. M. et al. [31] introduced PANI Nanotube Base which has $14\times10^{-6}$ mol/g capacity for cationic MB dye.

All these three synthetic adsorbents have much higher efficacies than that of our adsorbents. But the cornerstone of our interest was the biodegradability of the starch-based biosorbents. That's why we choice to study the adsorption of WP and TP in a more detail. It could be possible to recover the adsorbed dyes and to recycle the biosorbents through fermentation process which would be a very cost effective and eco-friendly way of the waste water treatments.

### 3.4.2.2 Cost Effective Adsorbents

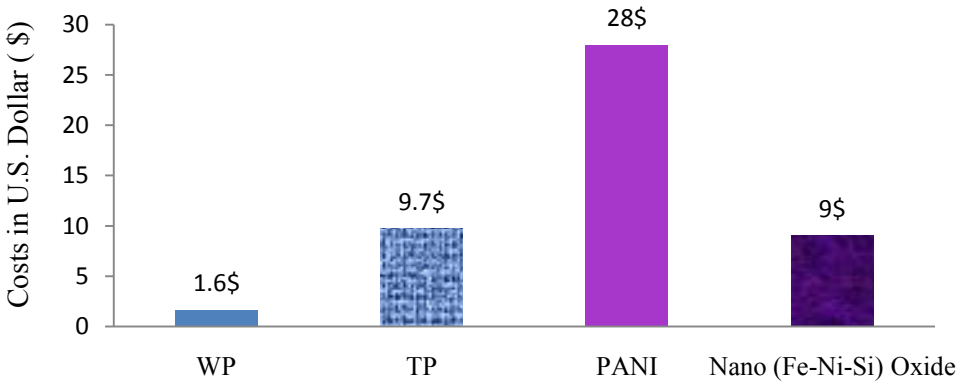


**Fig. 3.11** Comparative costs of the adsorbents to remove 1 ton (~1000L) $1\times10^{-5}$ M methylene blue (MB) dye

We estimated a rough calculation of the expenses of the biosorbents comparing with that of the synthetic conducting polymer adsorbents shown in the **Fig. 3.11**. To remove about 1000 L $1\times10^{-5}$ M MB dye, WP expenses 1.6 $ whereas TP, PANI and nano-mixed (Fe-Ni-Si) oxide cost 9.7 $, 28 $ and 9 $ currency respectively. It is very obvious that WP and TP are too cheaper adsorbents. Moreover these adsorbents are biodegradable. Thus we were interested in the adsorption study of these low-cost, biodegradable adsorbents which could also be recycled to various useful by-products like alcohol and to recover the dyes for reuse.

### 3.5 Detail Adsorption Behaviors of MB on WP and TP

#### 3.5.1 Influential Parameters of Adsorption

##### 3.5.1.1 Effect of pH

The pH is an important parameter for biosorption studies and affects not only the biosorption capacity, but also the color and solubility of dye solutions. **Fig. 3.12** shows the effect of solution pH on the removal of MB dye by TP and WP. The most important feature of TP as an adsorbent is that it works in a wide range of pH of dye solutions i.e., from pH 4 to11 [32]. Only when the pH of the dye solution exceeded 10, the amount of the dye adsorbed by TP considerably decreased as shown in **Fig. 3.12a**. As can be seen from **Fig. 3.12b**, the MB dye adsorption capacity of WP was found to increase with the increase in solution pH giving a maximum at pH 11. For simplicity, neutral aqueous solution (pH = 6.86) was used in further studies.

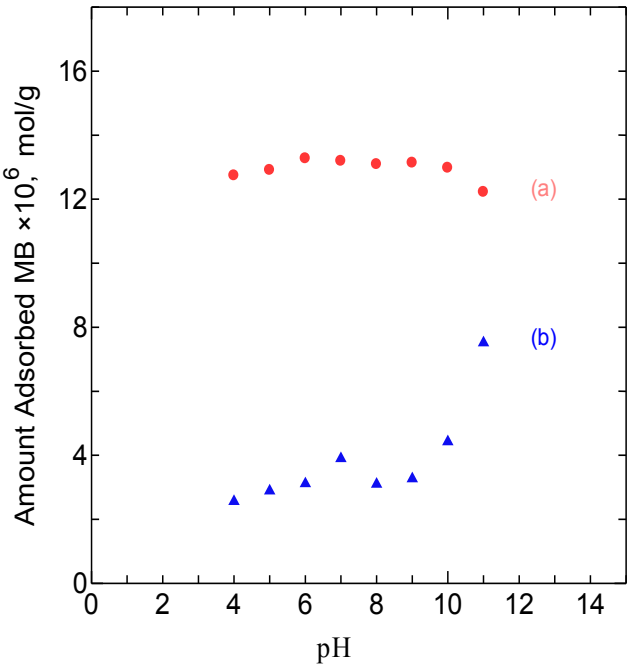


**Fig. 3.12** Effect of pH on adsorption of MB onto (a) TP and (b) WP. Initial [MB] = $2\times10^{-5}$ M, adsorbent dose = 1.2 g/L, agitation time = 60 min, temperature = 29 ˚C, stirring rate = 235 rpm.

The effect of pH on the adsorption process can be explained with the protonation of the functional groups on the adsorbents and adsorbates [33]. There are two possible mechanisms for adsorption of dye on the adsorbent which may be considered as (a) electrostatic interaction between the adsorbent and the dye molecule and (b) a chemical reaction between the dye and the adsorbent. At pH 4 the $H^+$ ion concentration in the system increased and the surface of WP acquired positive charge by absorbing $H^+$ ions. As the adsorbent surface was positively charged at lower pH, a significantly high electrostatic repulsion existed between the positively charged surface of the adsorbent and MB, a cationic dye molecule, resulting lower dye adsorption. But as the pH of the system increases, the number of negatively charged sites increases and the number of positively charged sites decreases. Negatively charged surface sites on WP favor the adsorption of dye cations due to the electrostatic attraction leading to maximum adsorption.

### 3.5.1.2 Time Dependencies of the Adsorbed Amounts

The influence of agitation time for the adsorption of MB by the adsorbents turmeric powder (TP) and wheat powder (WP) is shown in **Fig. 3.13**. The dye was rapidly adsorbed in the first 5-10 min. and then the extent of adsorption was reached in a plateau and finally reached in equilibrium in about 45 min. for TP as shown in **Fig. 3.13a** [34].

At the beginning of adsorption, the rate was fast as the dye ions were adsorbed by the exterior surface of the TP. When the adsorptions of the exterior surface reached saturation then the dye ions exerted onto the pores of the adsorbent particles and were adsorbed by the interior surface of the particles. **Fig. 3.13b** shows that in the WP adsorbent, the adsorption started rather steadily than TP and reached at the saturation within 60 min. [35]. The adsorption of the MB dye was about five times higher in the TP than the WP adsorbent.

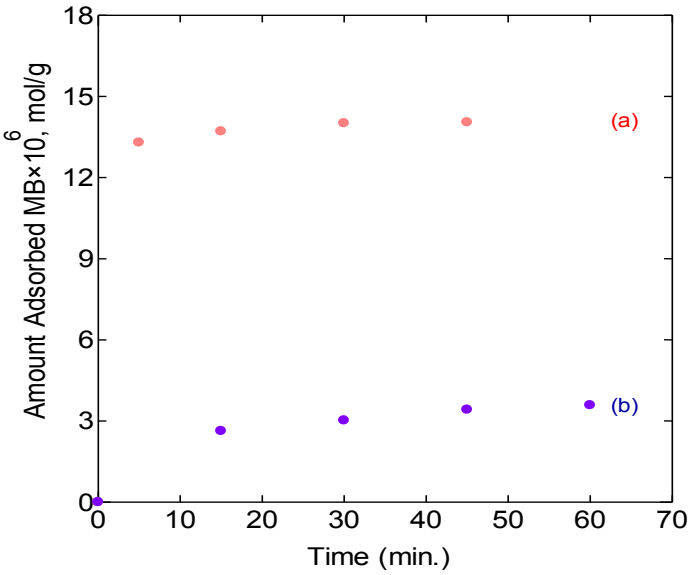


**Fig. 3.13** Effect of agitation time on adsorption of MB onto (a) TP and (b) WP. [MB] = $2\times10^{-5}$ M, adsorbent dose = 1.2 g/L, pH = 6.86, temperature = 29 °C, stirring rate = 235 rpm.

### 3.5.1.3 Effect of Electrolytes on Adsorption-Desorption of Dyes

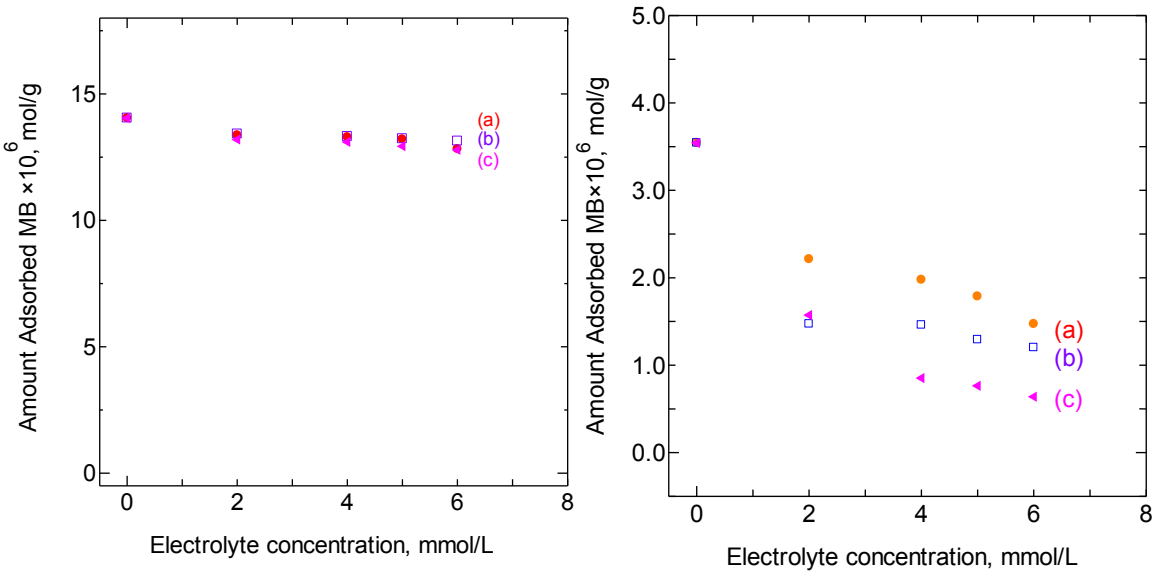


**Fig. 3.14** Effect of electrolytes (a) NaCl, (b) $Na_2SO_4$ and (c) $CaCl_2$ on the adsorption of MB dye onto TP (left panel) and WP (right panel). [MB] = $2\times10^{-5}$ M, adsorbent dose = 1.2 g/L, pH = 6.86, agitation time = 60 min, temperature = 29 ˚C, stirring rate = 235 rpm.

Wastewater contains various salts besides pollutants. So, it was worthy to study the effects of different electrolytes like (a) NaCl, **(**b) $Na_2SO_4$ and (c) $CaCl_2$ on adsorption. These electrolytes have both of discouraging and encouraging impact on the adsorption. Studies on dye desorption from the dye saturated starch-based biosorbents (WP and TP) contribute to well understanding the interaction mechanism and repeatedly utilize adsorbents [32].

**Fig. 3.14** shows the influence of these electrolytes on MB dye adsorption onto TP and WP bioadsorbents by varying the concentration of the electrolytes from 0 to 6 mM. From the left panel of **Fig. 3.14**, it was found that with increasing the concentration of each of the above electrolytes from 0 to 6 mM, the adsorption of MB dye onto TP was not decreased mostly. That is the adsorption of MB dye was not hampered due to the presence of these electrolytes up to 6 mM in the dye solution.

On contrary, from the right panel of the **Fig. 3.14** it was observed that with the gradual increase in concentration of each electrolyte, the adsorption of MB dye onto WP was declined drastically. The decrease in adsorption of MB dye onto WP was about 55 %, 66 % and 80 % in presence of 6 mM each of sodium chloride, sodium sulfate and calcium chloride respectively.

It also be concluded that the adsorption reduced 55 % in the case of monovalent anion chloride ion which was lower than the reduced adsorption of 66 % in presence of divalent anion sulfate ion. Similarly the MB dye desorption from the dye-saturated WP adsorbent was higher (80 %) in presence of divalent cation calcium ion rather in the presence of monovalent cation sodium whether desorption was 55 %.

The adsorption capacity in presence of these ions might also block the active sites of the adsorbents surface thus quite deactivating TP and WP towards MB dye. Similar observations were found for the adsorption of Reactive Blue 19 on native starch [35] and for the adsorption of acid dyes on ethylenediamine modified starch [32].

### 3.5.1.4 Effect of Initial Dye Concentration

Initial concentration provides an important driving force to overcome resistances encountered when all molecules were transferred between the aqueous and solid phases [36]. **Fig. 3.15** shows the influence of initial dye concentration on amount adsorption of MB dye at variable concentration ranging from 8 to 40 µM. By increasing the initial dye concentration, the amount of dye adsorbed per unit mass of TP and WP was increased with the increase in initial concentration. But at initial concentration beyond 39 µM the dye uptake capacity per unit mass of TP was decreased (**Fig. 3.15a**) and for the WP biosorbent it occurred at 30 µM as shown in **Fig. 3.15b**.

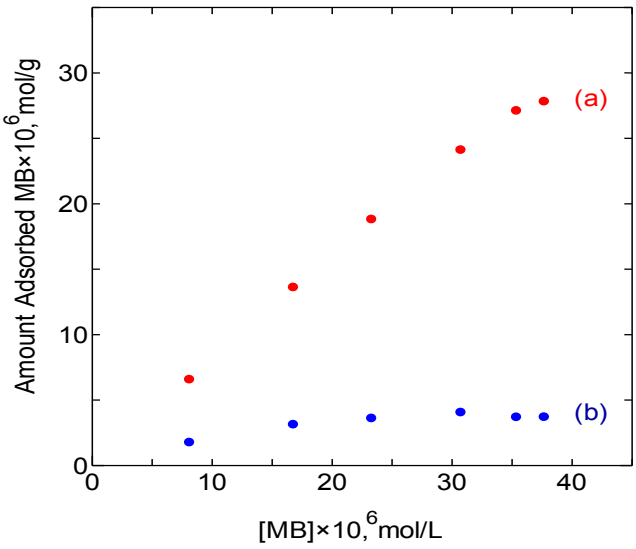


**Fig. 3.15** Effect of initial concentration of dye on adsorption of MB onto (a) TP and (b) WP. Adsorbent dose = 1.2 g/L, pH = 6.86, agitation time = 60 min, temperature = 29 ˚C, stirring rate = 235 rpm.

This effect could be explained as follows: At lower initial dye concentrations, all dye molecules could interact with the binding sites on the biomass surface and thus higher adsorption yields were obtained. At high initial dye concentrations, binding sites on the adsorbent surface were saturated and no further biosorption was occurred. A decrease observed on the biosorption capacity was mainly due to the repulsive forces between dye molecules at adjacent sites on the cell surface [31].

### 3.5.1.5 Effect of Temperature

The temperature has two main effects on the sorption processes. Firstly, increasing temperature is known to increase the diffusion rate of the adsorbate molecules within the pores as a result of decreasing solution viscosity. Secondly, it also modifies the equilibrium capacity of the adsorbent for a particular adsorbate [37]. To investigate the effect of temperature, the equilibrium biosorption capacity of MB dye onto (A) TP and (B) WP were studied at constant temperatures of 10, 20, 30, 40 and 45 ˚C (**Fig. 3.16**). As seen in **Fig. 3.16A**, the amount of adsorbed MB dye onto TP biosorbent was enlarged with increase in the temperature from 10 to 30 ˚C and raised to a maximum at 30 ˚C. It was followed by a fall until 45 ˚C under optimum conditions of pH and equilibrium time.

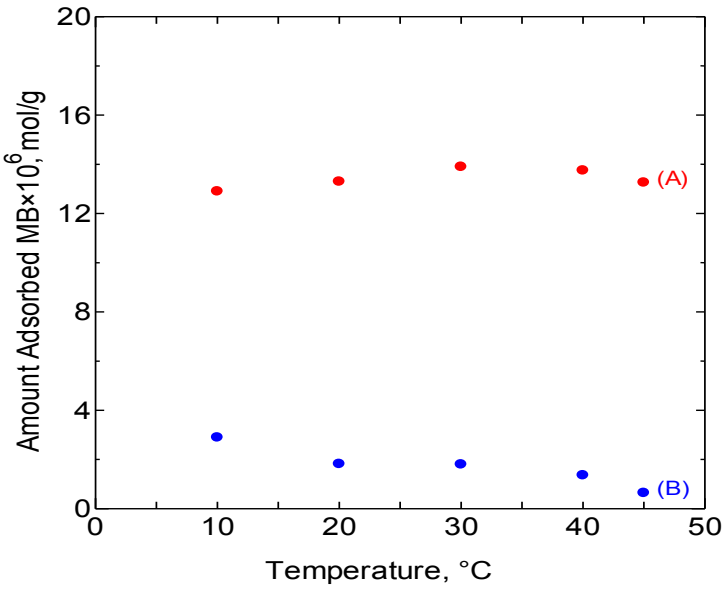


**Fig. 3.16** Effect of temperature on the adsorption of MB onto (A) TP and (B) WP. [MB] = $2\times10^{-5}$ M, adsorbent dose = 1.2 g/L, pH = 6.86, agitation time = 60 min, temperature = 29 ˚C, stirring rate = 235 rpm.

The increase in the uptake capacity up to 30 ˚C could be explained by the availability of more binding sites or the energy of adsorption sites has been an exponential distribution and a higher temperature enables the energy barrier to be overcome for MB adsorption onto TP. Therefore, the adsorption follow an endothermic process up to 30 ˚C but the following decrease could be resulted from the disruption of the TP surface because of the high temperature [38].

On the other hand in case of WP adsorbent, the adsorption gradually decreased with the increase of temperature which is obvious from the **Fig. 3.16B**. This is also can happen for the disruption of the WP surface at higher temperature. A similar finding was reported for removal of dyes from aqueous solutions by dithiocarbamate-modified starch [39].

### 3.5.2 Adsorption Kinetics

The adsorption of a solute by a solid in aqueous solution is a phenomenon with often complex kinetics. The adsorption rate has strongly influenced by several parameters related to the state of the solid, generally having very heterogeneous reactive surface, and to the physico-chemical conditions under which adsorption is carried out.

Several steps can be used to examine the controlling mechanism of adsorption process such as chemical reaction, diffusion control and mass transfer. Kinetic data are used to test experimental data from the adsorption of MB onto TP and WP is required for selecting optimum operating conditions for the full-scale batch process. The kinetic parameters, which are helpful for the prediction of adsorption rate, give information designing and modeling the adsorption process. In order to evaluate the kinetic mechanism which controls the solid/liquid adsorption systems, the pseudo-first-order [40], pseudo-second order [41, 42], and intraparticle diffusion [43] models were verified by the linear equation analysis: $\ln(q_e - q_t)$ vs t, $\frac{t}{q_t}$vs t and $q_t$ vs $t^{1/2}$, respectively.

The conformity between experimental data and model predicted values was expressed by the co-relation coefficients ($R^2$, values closed to equal to 1). Good correlation with the kinetic data explains the dye adsorption mechanism in the solid phase. The relative higher values are the applicable model to the kinetics of dye adsorption onto TP and WP. The required derived data for these kinetics models is listed below in **Table 3.7** and in **Table 3.8**.

**Table 3.7** Comparison of the first and second order constants and experimental and calculated adsorption capacity, $q_e$ for MB adsorption onto TP and WP.

| Sorbent | Experimental adsorption capacity $q_e \times 10^6$ (mol $g^{-1}$) | Pseudo-first-order kinetic model (Calculated) | | | Pseudo-second-order kinetic model (Calculated) | | |
|---|---|---|---|---|---|---|---|
| | | $k_1 \times 10^2$ (L $mol^{-1}$) | $q_e \times 10^6$ (mol $g^{-1}$) | $R^2$ | $k_2 \times 10^4$ g $(mol\ min)^{-1}$ | $q_e \times 10^6$ (mol $g^{-1}$) | $R^2$ |
| TP | 14.04 | 12.7 | 1.7 | 0.978 | 17 | 14.2 | 0.999 |
| WP | 3.58 | 6.28 | 2.9 | 0.975 | 2.35 | 4.2 | 0.998 |

**Table 3.8** Parameters of intra-particle diffusion model for the adsorption of MB onto TP and WP.

| Adsorbents | Parameter of intra-particle diffusion | | |
|---|---|---|---|
| | $k_i \times 10^7$, (mol $g^{-1}$ $min^{-1/2}$) | $C \times 10^6$, (mol $g^{-1}$) | $R^2$ |
| TP | 1.7 | 13 | 0.934 |
| WP | 3.9 | 0.763 | 0.912 |

### 3.5.2.1 Pseudo-first-order Model

Lagergren's rate equation is the one widely used [39, 40] mean for the sorption of solute from liquid solution. The pseudo–first–order model was described by Lagergren which is given bellow:

$$\frac{dq_t}{dt} = k_1(q_e - q_t) \qquad (3.2)$$

where $q_e$ and $q_t$ refer to the amount of dye adsorbed (mol $g^{-1}$) at equilibrium and at any time, t (min), respectively and $k_1$ is the equilibrium rate constant of pseudo–first–order adsorption in L $mol^{-1}$.

Integration of Eq. (3.2) for the boundary conditions t = 0 to t and $q_t$ = 0 to q gives

$$\ln(q_e - q_t) = \ln q_e - k_1 t \qquad (3.3)$$

The values of ln ($q_e$ −$q_t$) were linearly correlated with t shown in the **Fig. 3.17**. The plot of ln ($q_e$ −$q_t$) vs. t should give a linear relationship from which the values of $k_1$ were determined from the slope of the plot **(Table 3.7)**. In many cases, the first-order equation of Lagergren does not fit well with the whole range of contact time and is generally applicable over the initial stage of the adsorption processes [33]. The values of equilibrium rate constants are presented in **Table 3.7**. The regression coefficients of pseudo–first–order data were found to be ($R^2 \geq 0.975$). This result shows that the pseudo-first order kinetic model was tested but the straight lines could not be obtained for the entire adsorption period.

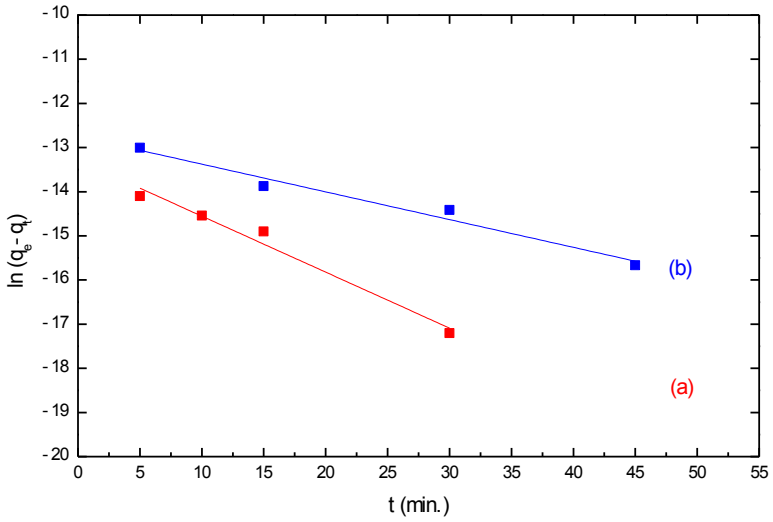


**Fig. 3.17** Lagergren plot for MB adsorption onto (a) TP and (b) WP.

### 3.5.2.2 Pseudo-second-order Model

The pseudo-second-order model is represented by the following differential equation

$$\frac{dq_t}{dt} = k_2(q_e - q_t)^2 \qquad (3.4)$$

where, $k_2$ is the equilibrium rate constant of pseudo-second-order adsorption (g $mol^{-1}$ $min^{-1}$). Integrating Eq. (3.4) for the boundary condition t = 0 to t and $q_t$ = 0 to q, gives

$$\frac{t}{q_t} = \frac{1}{k_2 q_e^2} + \frac{1}{q_e} t \qquad (3.5)$$

The plots gave linear relationships which allowed computation of kinetic parameters without having to know any parameter beforehand. The rate parameters $k_2$ and $q_e$ can be directly obtained from the intercept and slope of the plot of $t/q_t$ versus t **(Fig. 3.18)**. The values of equilibrium rate constant ($k_2$) are presented in **Table 3.7**. The regression coefficients of all examined data were found very high ($R^2 \geq 0.99$). This shows that the model can be applied for the entire adsorption process and confirms that the sorption of MB dye onto TP and WP follows the pseudo-second-order kinetic model.

The calculated $q_e$ values from the model were also consistent with experimental data, underlining the efficiency of the model. These results suggested that the pseudo-second order adsorption mechanism was predominant, and that the overall rate of the dye adsorption process appeared to be controlled by the physisorption process. In both cases, the phenothiazinium chromophores of MB were interacted with the polyhydroxy functional groups of the adsorbents surface. The adsorption of dye takes place probably via surface exchange reactions until the surface functional sites are fully occupied; thereafter dyes molecules diffuse into the polymer network for further interactions.

Although the pseudo-second order model proposed by Ho and McKay [42] is a simplified model, this equation is commonly used to describe the kinetics of the adsorption of dyes onto solid materials. For example, the kinetics of adsorption of many dye species onto various bioadsorbents was also found to be of second order in

the literature. Specifically it was observed for the adsorption of acid dyes onto ethylenediamine modified starch as biosorbent [32], in the removal of C. I. Acid Blue 25 from aqueous solutions by using cationized starch-based material as a new ion-exchanger adsorbent [44] and on the adsorption of MB dye from water onto the Polyaniline Nanotubes Base [31].

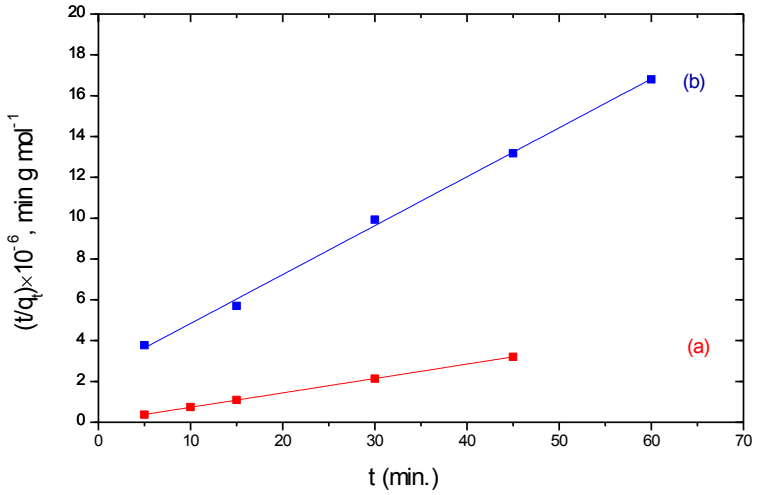


**Fig. 3.18** Ho's plot of pseudo-second order kinetics of MB dye adsorption onto (a) TP and (b) WP.

### 3.5.2.3 Intra-particle Diffusion Model

During the adsorption of a solute over an adsorbent, there are three possible cases: particle diffusion governance of rate when external transport > internal transport; film diffusion governance of rate when external transport > internal transport; and a third case when external transport < internal transport. The third case may be excluded and possibility can be explored for governance of rate from film or particle diffusion. In diffusion studies, the rate can be expressed in terms of the square root time. In order to investigate the possibility of intra-particle diffusion resistance affecting the adsorption intra-particle diffusion model [43] was explored

$$q_t = k_i t^{1/2} + C \qquad (3.6)$$

where, $k_i$ is the intra-particle diffusion rate parameter in the unit mol $g^{-1}$ $min^{-1}$, C = Value of the intercept in the unit mol $g^{-1}$ and $t^{1/2}$ is the square root time in min. **Fig. 3.19** represents a plot of $q_t$ vs. $t^{1/2}$ for the adsorption of MB onto (a) TP and (b) WP.

**Fig. 3.19** shows the amount of dye adsorbed versus $t^{1/2}$ for intraparticle transport of MB by starch containing adsorbents (a) TP and (b) WP at different initial dye concentrations. As seen from this figure, the plot for TP was linear over the whole time range but it was not linear for WP sorbent. The plot of WP (**Fig. 3.19B**) presented a multilinearity which indicated that three steps took place in the process. The first sharper portion was attributed to the diffusion of dye molecules through the solution to the external surface of material (or the boundary layer diffusion of dye molecules). The second portion described the gradual adsorption stage where intraparticle diffusion was the rate limiting step. The third portion was attributed to the final equilibrium stage for which the intraparticle diffusion started to slow down due to the low dye concentration left in the solution.

It can also be observed that the plots do not pass through the origin (the values of the intercept, C, are reported in **Table 3.8**). The intercept also give an idea about the boundary layer thickness: the larger the intercept, the greater is the boundary layer effect. These results show that the intraparticle diffusion is not the only rate-limiting step, but other processes may control the rate of adsorption. The slope of the second linear portion characterizes the rate parameter, $k_i$, corresponding to the intraparticle diffusion (the values for are given in **Table 3.8**). The $R^2$ values for this diffusion model are high (**Table 3.8**), suggesting that the adsorption of MB onto WP can be followed thanks to an intraparticle diffusion model.

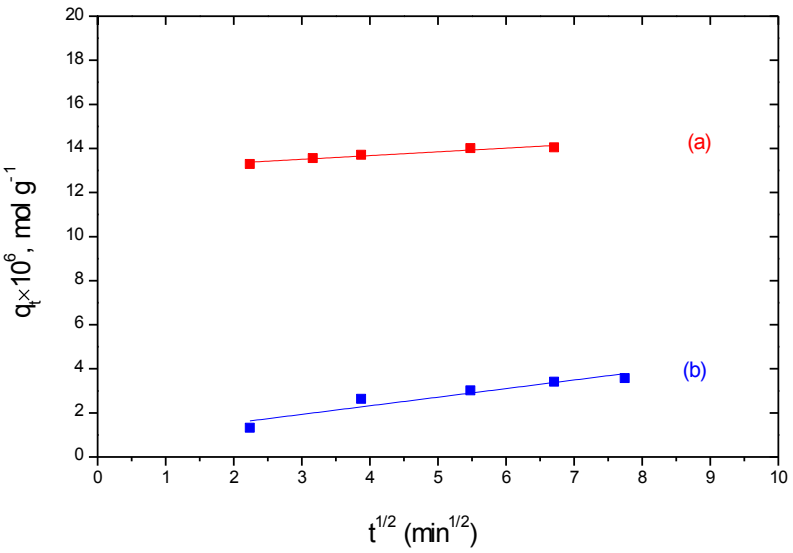


**Fig. 3.19** Weber-morris plot for intrapaticle diffusion of MB onto (a) TP and (b) WP.

### 3.5.3 Adsorption Equilibrium

Adsorption isotherms are usually determined under equilibrium conditions. Adsorption properties and equilibrium data, commonly known as adsorption isotherms, describe how adsorbate molecules (pollutants) interact with adsorbent particles and are thus critical in optimizing the use of solid materials. Analysis of isotherm data is important in order to develop an equation that accurately represents the results and which could be used for design purpose. It expresses the relation between the concentrations of solute in the solution at dynamic equilibrium with concentration of the solute adsorbed onto the adsorbent.

The Langmuir, Freundlich, and Tempkin isotherm models were used to describe the relationship between the amount of MB adsorbed and its equilibrium concentration in solutions. The Langmuir equation, which is valid for monolayer adsorption onto a completely homogenous surface with a finite number of identical sites and with negligible interaction between adsorbed molecules, is represented in the linear form as follows [45].

$$\frac{C_e}{q_e} = \frac{C_e}{q_m} + \frac{1}{aq_m} \qquad (3.7)$$

where a is the Langmuir adsorption constant (L $mol^{-1}$) and $q_m$ is the theoretical monolayer adsorption capacity (mol $g^{-1}$). **Fig. 3.20** shows the Langmuir ($C_e/q_e$ vs. $C_e$) plots for adsorption of MB onto (a) TP and (b) WP. The value of the constants $q_m$ and a and the correlation coefficients for Langmuir isotherm are presented in **Table 3.9**.

The value of $q_m$ were found $3\times10^{-5}$ mol/g and $5.22\times10^{-6}$ mol/g for TP and WP respectively. The linearized forms of the isotherms are found to be linear over the whole concentration range studied, and the regression coefficients were extremely high i.e., $R^2 = 0.99$ for TP and $R^2 = 0.95$ for WP, as shown in **Table 3.9**. These $R^2$ values strongly support the fact that the dye-material adsorption data closely follow the Langmuir model of adsorption.

The Freundlich isotherm model describes the heterogeneous multilayer surfaces of adsorption due to the different trends supporting the surface sites. It supports that occupation will occur at the first stage through stronger binding, and will later decrease with the increasing degree of sites occupation [46]. The linearized form of Freundlich isotherm can be is given by the following equation

$$\ln q_e = \ln K_F + \frac{1}{n}\ln C_e \qquad (3.8)$$

where $K_F$ (mol $g^{-1}$) is the relative indicator of adsorption capacity and n indicates the intensity of adsorption called Freundlich constant respectively. **Fig. 3.21** exhibits deviation from linearity on the Freundlich plot for the adsorption of MB onto the adsorbent (a) TP and (b) WP for the whole concentration range. It is known that the Freundlich model is generally applicable for low concentrations. **Table 3.9** shows the Freundlich adsorption isotherm constant and correlation coefficients.

The value of 1/n ranges between 0 and 1, and indicates the degree of non-linearity between solution concentration and adsorption as follows: if the value of 1/n is equal to unity, the adsorption is linear; if the value is below unity, this implies that the adsorption process is chemical; if the value is above unity, adsorption is a favorable physical process; the more heterogeneous the surface, the closer 1/n value is to 0. The value of 1/n for Freundlich isotherm were found 0.38 for TP and 0.48 for the WP adsorbent indicating that MB dye is favorably adsorbed by TP and WP by a chemical means [44].

Tempkin and Pyzhev [46] considered the effects of some indirect adsorbate/adsorbate interactions on adsorption isotherms. They suggested that, because of these interactions and ignoring very low and very large values of concentration, the heat of adsorption of all molecules in the layer would decrease linearly with coverage. The adsorption is characterized by a uniform distribution of binding energies, up to certain a maximum binding energy.

The Tempkin isotherm equation is given as

$$q_e = \frac{RT}{b}\ln K_t C_e \qquad (3.9)$$

Eq. (3.9) can be linearized as

$$q_e = B\ln K_t + B\ln C_e \qquad (3.10)$$

where B = RT/b, T is the absolute temperature in kelvin, R is the universal gas constant, 8.314 J $mol^{-1}$ $K^{-1}$, $K_t$ the equilibrium binding constant (L $mol^{-1}$) and B is related to the heat of adsorption. A plot of $q_e$ vs. ln $C_e$ at studied temperature is given in **Fig. 3.22**.

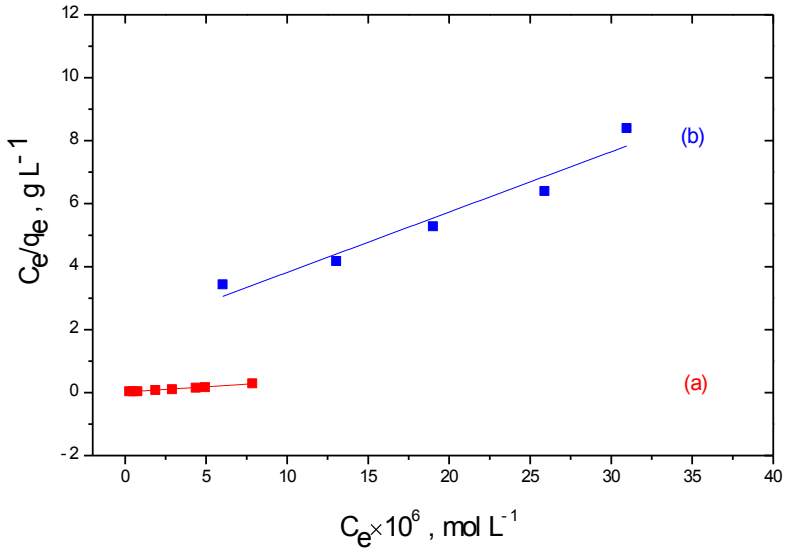


**Fig. 3.20** Langmuir plots for the adsorption of MB onto (a) TP and (b) WP. [MB] =$2\times10^{-5}$ M, adsorbent dose = 1.2 g/L, pH = 6.86, agitation time = 60 min, temperature = 29 ˚C, stirring rate = 235 rpm.

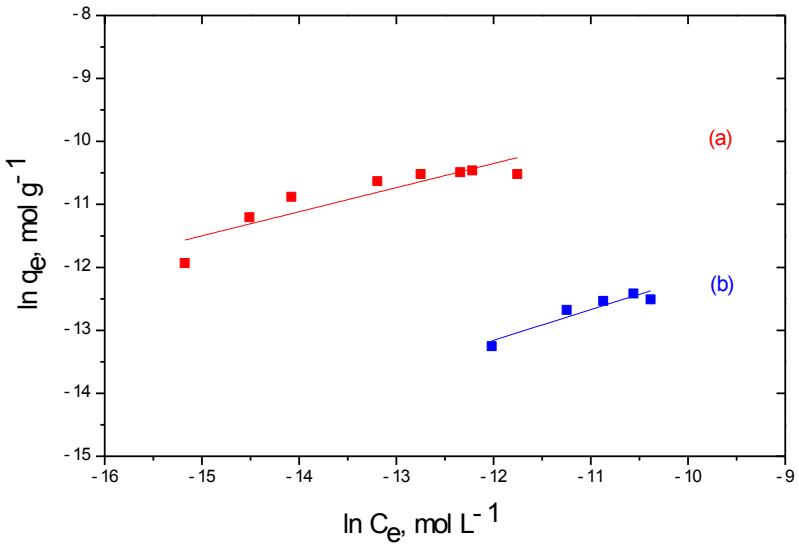


**Fig. 3.21** Freundlich plots for the adsorption of MB onto (a) TP and (b) WP. [MB] =$2\times10^{-5}$ M, adsorbent dose = 1.2 g/L, pH = 6.86, agitation time = 60 min, temperature = 29 ˚C, stirring rate = 235 rpm.

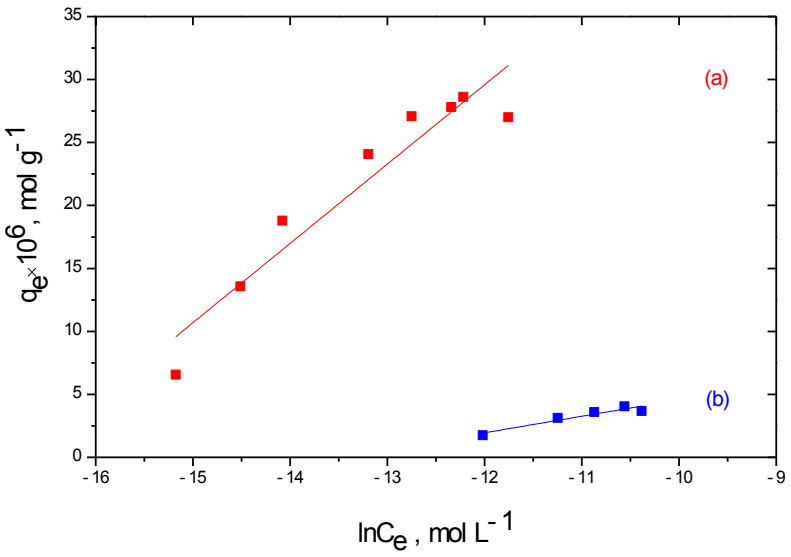


**Fig. 3.22** Tempkin plots for the adsorption of MB onto (a) TP and (b) WP. [MB] = $2\times10^{-5}$ M, adsorbent dose = 1.2 g/L, pH = 6.86, agitation time = 60 min, temperature = 29 ˚C, stirring rate = 235 rpm.

The constants obtained for Tempkin isotherm are shown in **Table 3.9**. From Table it can be found that the values of B and $K_t$ are $6.29\times10^{-6}$ and $1.77\times10^{7}$ (L/mol) for TP and $1.32\times10^{-6}$ and $7.08\times10^{5}$ (L/mol) for WP, respectively. The low value of heat energy means that there is a high adsorbate–adsorbent interaction in the coverage layer of adsorption. The Tempkin coefficient correlations ($R^2 \approx 0.911$) for the adsorption of MB were lower than that of the Langmuir correlation coefficients ($R^2 \geq 0.95$), indicating non-favorable MB adsorption onto TP and WP [47].

**Table 3.9** Constant parameters and regression coefficients calculated for various adsorption models for TP and WP.

| Type of Isotherm | Sorbents | Isotherm parameters | | |
|---|---|---|---|---|
| **Langmuir** | | $a\times10^{-5}$ (L/mol) | $q_m\times10^{6}$ (mol/g) | $R^2$ |
| | TP | 18.70 | 30.00 | 0.990 |
| | WP | 1.00 | 5.22 | 0.950 |
| **Freundlich** | | $K_F\times10^{4}$ (mol/g) | n | $R^2$ |
| | TP | 32.00 | 2.61 | 0.882 |
| | WP | 6.66 | 2.05 | 0.894 |
| **Tempkin** | | $B\times10^{6}$ | $K_t\times10^{-7}$ (L/mol) | $R^2$ |
| | TP | 6.29 | 1.77 | 0.910 |
| | WP | 1.32 | 708 | 0.911 |

### 3.5.4 Thermodynamic Studies

The adsorption equilibrium can be regarded as the distribution equilibrium of adsorbate between adsorbents and the solution of adsorbate. In order to determine thermodynamic parameters, experiments were carried out at different equilibrium concentrations of the MB (Methylene Blue) dye at the four different temperatures in the range of 283–318K. The thermodynamic parameters such as standard Gibb's free energy change (ΔG˚), enthalpy change (ΔH˚) and entropy change (ΔS˚) were estimated to evaluate the feasibility and nature of the adsorption process. The Gibb's free energy change, of the process is related to equilibrium constant by the equation

$$\Delta G^{\circ} = -RT \ln Kc \qquad (3.11)$$

where, T is temperature in kelvin, R ideal gas constant having value as 8.314 J $mol^{-1}$ $K^{-1}$ and $K_c$ is thermodynamic equilibrium constant. The thermodynamic equilibrium constant ($K_c$) of the adsorption is defined as

$$K_c = \frac{q_e}{C_e} \qquad (3.12)$$

where, $q_e$ is the adsorption capacity at equilibrium in mol $g^{-1}$ and $C_e$ is the equilibrium concentration of solution in the unit mol $L^{-1}$ .

According to thermodynamics, the Gibb's free energy change is also related to the enthalpy change (ΔH˚) and entropy change (ΔS˚) at constant temperature by the Van't Hoff equation

$$\ln K_c = \frac{\Delta S^\circ}{R} - \frac{\Delta H^\circ}{RT} \qquad (3.13)$$

The values of enthalpy change (ΔH˚) and entropy change (ΔS˚) were calculated from the slope and intercept of the plot $\ln K_c$ vs. 1/T. The calculated values of thermodynamic parameters are reported in **Table 3.10**.

**Table 3.10** Thermodynamic parameters for adsorption of MB by WP and TP.

| Temperature T (K) | Parameters | | | | | |
|---|---|---|---|---|---|---|
| | WP | | | TP | | |
| | ΔG˚ (kJmol$^{-1}$) | ΔH˚ (kJmol$^{-1}$) | ΔS˚ (kJmol$^{-1}$K$^{-1}$) | ΔG˚ (kJmol$^{-1}$) | ΔH˚ (kJmol$^{-1}$) | ΔS˚ (kJmol$^{-1}$K$^{-1}$) |
| 283 | 3.66 | -35.350 | -0.137 | -4.34 | 37.305 | 0.147 |
| 293 | 5.04 | | | -5.82 | | |
| 303 | 6.42 | | | -7.29 | | |
| 318 | 8.49 | | | - | | |

**Fig. 3.23** shows the Van't Hoff plot for the adsorption of MB onto (a) WP and (b) TP. The calculated values of the thermodynamic parameters are tabulated in the **Table 3.10**. In case of WP, the negative value of ΔH˚ and the increase in ΔG˚ with the increase temperature show that the adsorption process is more favorable at low temperature. A similar observation was found in the adsorption of aniline on cross-linked starch sulfate from aqueous solution [33].

Conversely for TP, the negative values of ΔG° (**Table 3.10**) indicate that the adsorption of the dyes is spontaneous. The positive value of ΔH° and the increase in the negative value of ΔG° with the increasing temperature show that the adsorption process is more favorable at higher temperatures. In many cases, the change in Gibbs energy for physisorption is between −20 and 0 kJ $mol^{-1}$, but chemisorption is in a range of −80 to −400 kJ $mol^{-1}$ [39]. The values of ΔG° obtained in this study are within the ranges of −20 to 0 kJ $mol^{-1}$, indicating that physisorption is the dominating mechanism.

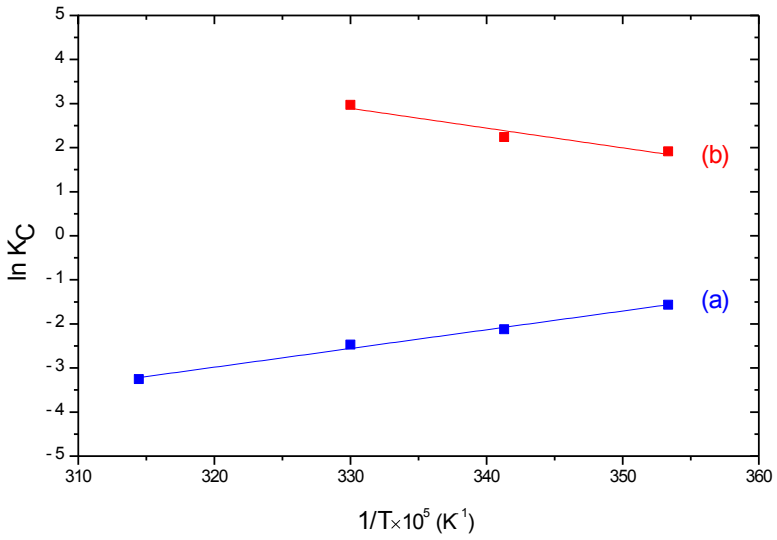


**Fig. 3.23** Van't Hoff plot for the adsorption of MB dye onto (a) WP and (b) TP.

### 3.5.5 Adsorption Mechanism

The quantitative behavior of acids and bases in solution can be understood from the Henderson–Hasselbalch equation only if their $pK_a$ (= -log $K_a$) values are known where $K_a$ is the acid dissociation constant. In particular, the pH of a solution can be predicted when the analytical concentration and $pK_a$ values of all acids and bases are known. On contrary, it is possible to calculate the equilibrium concentration of the acids and bases in solution when the pH is known. The Henderson–Hasselbalch equation is

$$p^H = p^{K_a} + \log\left(\frac{\propto}{1-\propto}\right) \qquad (3.14)$$

where, α is degree of dissociation.

From the knowledge of pH and $pK_a$, the degree of dissociation of MB and starch were calculated by using the Henderson–Hasselbalch equation and summarized in **Table 3.11**.

**Table 3.11** Degree of dissociation of aqueous solution of wheat starch and two dyes named methylene blue and orange green at 29 ˚C.

| Substances | pH | $pK_a$ | Calculated α |
|---|---|---|---|
| Wheat Starch | 6.86 | 13.3 | 0.78 |
| Methylene blue | | 2.6 | 0.99 |
| | | 11.2 | 0.85 |
| Orange Green | | 12.8 | 0.54 |

From the **Table 3.11**, it is obvious that the larger the value of $pK_a$ the smaller the extent of dissociation. The pKa value of wheat starch (pKa = 13.3) is much higher than that of MB (pKa = 2.6) [48, 49]. Thus in the aqueous solution of pH 6.86, the MB dissociates in much higher extent (α = 0.99) than the wheat starch (α = 0.78). As a consequence, wheat starch acts as a strong base and MB acts as a weak acid in the solution.

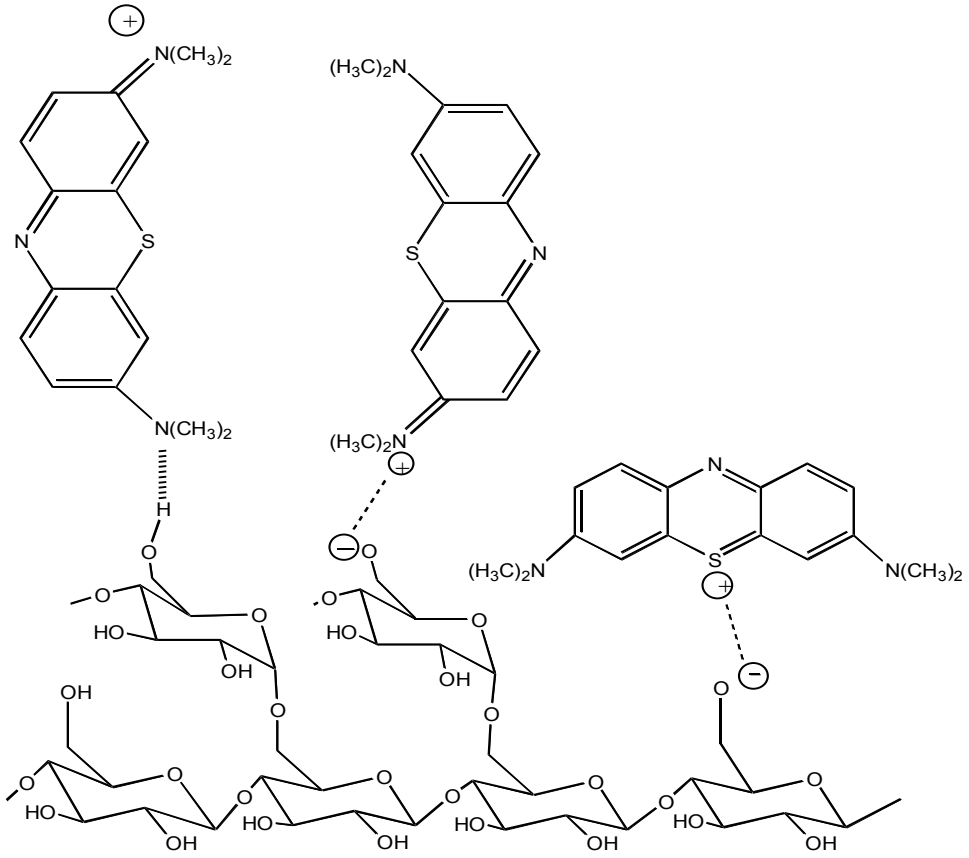

**Scheme 3.1** Main interactions between methylene blue and starch bed

Finally, a potential mechanism of the adsorption of methylene blue on starch-based biosorbents WP and TP could be proposed according to the following equations (3.15 and 3.16) [33].

$S_t\text{-OH} \rightleftharpoons S_t\text{-O-} + H^+$ (3.15)

$S_t\text{-O-} + MB^+ \rightleftharpoons S_t\text{-O-MB}$ (3.16)

The hydroxyl groups of starch dissociates as the Eq. (3.15). Then the cationic MB adsorbed on the deprotonated starch bed as the Eq. (3.16). According to this mechanism the sorption of positively charged dyes like MB is expected to increase with increasing pH. It is found to be true in the effect on pH on the adsorption of MB onto TP and WP as described in the **Section 3.5.1.1**.

In basic medium, the extent of starch dissociation increases and the deprotonated $S_t$-O- portion also increases. Therefore, sorption of MB increases with increasing pH with a rapid rise of adsorption at pH 11 as shown in **Fig. 3.12b**. This remarkable rise of adsorption could be due to the electrostatic interaction as Eq. (3.16). The other driven forces, such as hydrogen bonding and hydrophobic force, are much weak. All the possible interactions between MB and starch bed are revealed in the **Scheme 3.1**.

The adsorption mechanism of MB onto TP is slightly different from that of WP due to the presence of curcumin in TP. Curcumin is the most popular yellow natural dye and an active ingredient in turmeric (Curcuma longa L). **Scheme 3.2** shows that curcumin exists in a keto-enol tautomerism with equilibrium strongly favoring an enol form.

The enol structure enables curcumin to form additional inter- and intramolecular hydrogen bonds [50]. The hydroxyl site of curcumin attracts the cationic MB dye through electrostatic interaction as shown in the **Scheme 3.3** [51]. The adsorption of MB on the curcumin in addition to the starch content of TP is supported by the almost three times higher adsorption capacity of TP than the adsorption capacity of merely starch content of WP as shown in the **Fig. 3.12**.

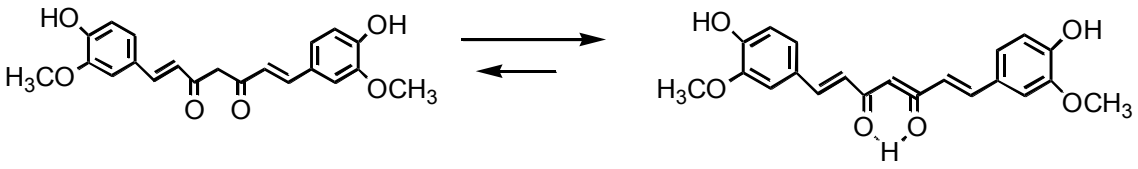


Keto form Enol form

**Scheme 3.2** Chemical structure of Curcumin

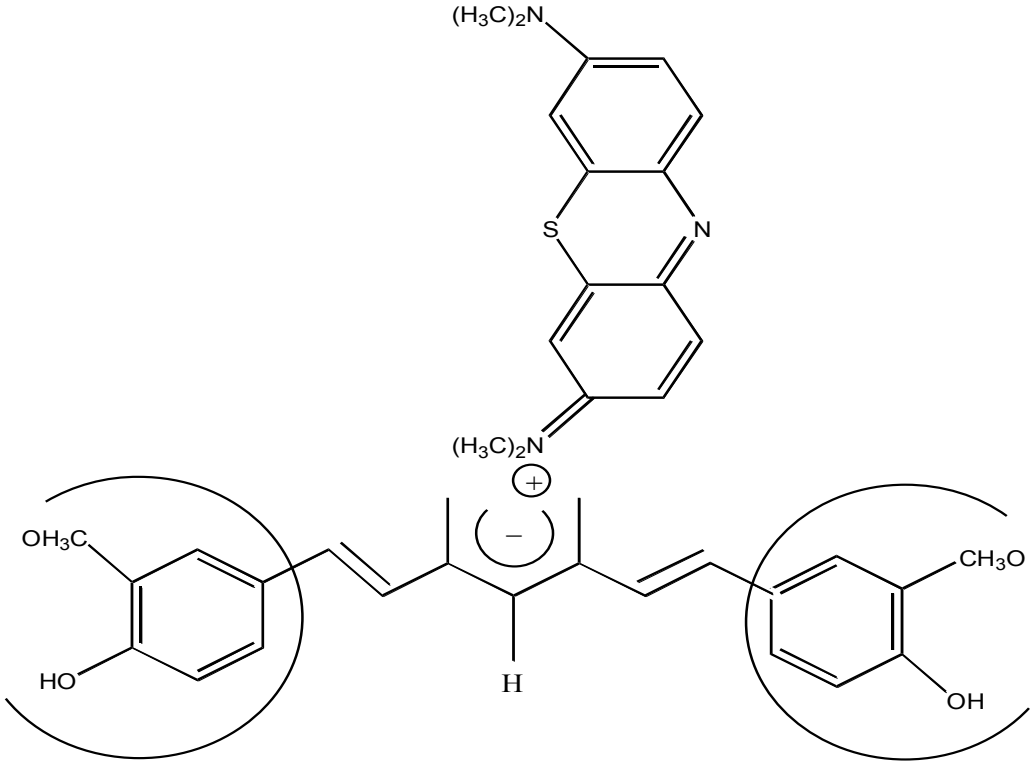


**Scheme 3.3** The probable interaction between the hydroxyl site of curcumin molecule and methylene blue. The basic diarylheptanoid groups are shown by open circle.

### 3.5.6 Role of Ferric (III) Coagulant on the MB Dye Desorption

It is very difficult to find a universal method which can be applied to a wide range of dyes due to their very different chemical structures and molecular sizes. Coagulation method still has many advantages and is still used, both on its own as well as in combination with other methods. Popic, S. et al. [52] studied the coagulation–flocculation process using an iron (III) salt for removal of reactive dye from model wastewater. They reported that there is an optimum pH that is dependent on the amount of coagulant added and the type of dye. We observed an influence of the Ferric (III) coagulant on desorption of the methylene blue dye from the dye-saturated (a) WP and (b) TP biosorbents at neutral water solution.

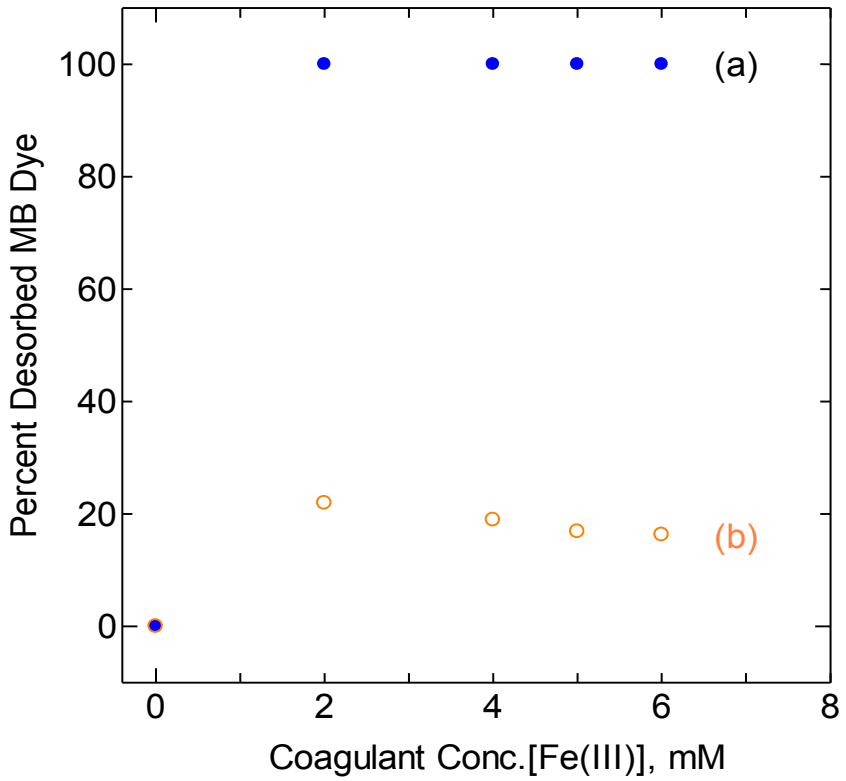


**Fig. 3.24** Effect of $FeCl_3.6H_2O$ on desorption of MB dye from MB dye-saturated (a) WP and (b) TP. [MB] = $2\times10^{-5}$ M, adsorbent dose = 1.2 g/L, pH = 6.86, agitation time = 60 min, temperature = 29 ˚C, stirring rate = 235 rpm.

**Fig. 3.24** addresses the desorption of MB dye from dye-saturated (a) WP and (b) TP employing ferric chloride hexahydrate, $FeCl_3.6H_2O$ as the coagulant. During the increasing of the [Fe (III)] from 0 to 6 mM, about 100 % dye was desorbed from the WP surface within the 2 mM of the coagulant concentration. But desorption was almost 20 % for the TP biosorbent with a maximum at [Fe (III)] = 2 mM. This influence of the coagulant on desorption facilitates the recovery of the dyes.

The role of $FeCl_3.6H_2O$ is that it forms a complex with the starch content of the biosorbents. Two models have been proposed to explain the structures of iron (III)-polysaccharide complexes. The first assumption is that iron (III) is coordinated through the saccharide moieties and forms spatially separated iron (III) centres along the backbone of polysaccharides (site binding model).

The second assumption is that iron (III) forms FeOOH precipitate which is covered by the polysaccharide (colloidal model) [53]. This positive charged iron (III)-polysaccharide complex encourage desorption of the cationic dye MB through the electrostatic repulsion with the methylthioninium cation of MB. The almost complete desorption of MB from MB-saturated WP indicate the more effective complexation of the Fe (III) ion with A-type wheat starch compared to the B-type turmeric starch whereas the desorption is much less.

### 3.6 Study of the OG Dye Adsorption onto WP and TP

#### 3.6.1 Effect of pH

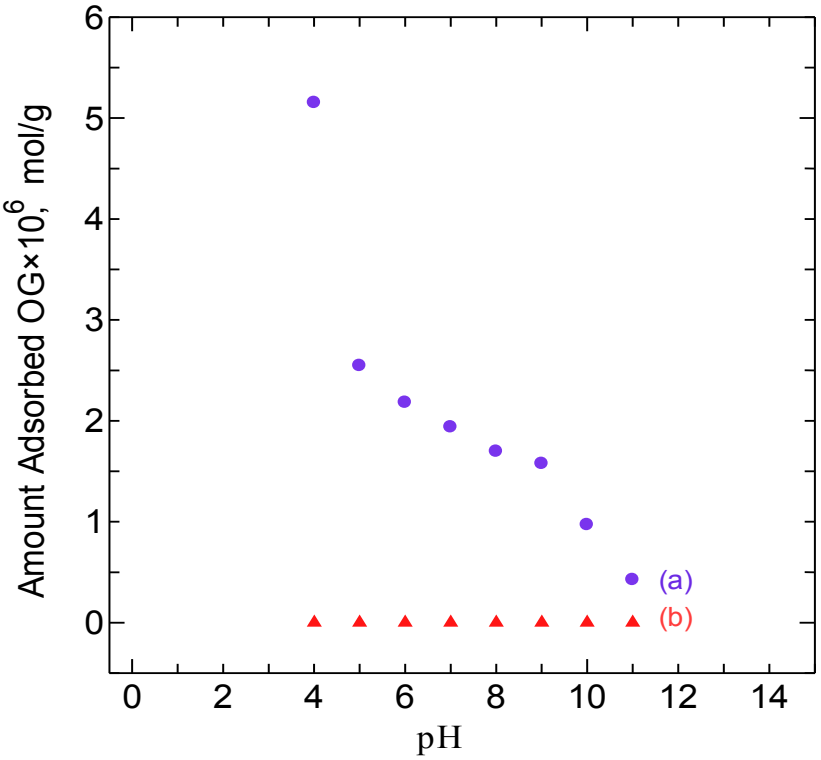


**Fig. 3.25** Effect of pH on the adsorption of OG onto (a) wheat powder (WP) and (b) turmeric powder (TP). Initial [OG] = $5\times10^{-5}$ M, adsorbent dose = 1.2 g/L and temperature = 29 ˚C.

The pH of the aqueous solution is an important controlling parameter in the dyes sorption processes. **Fig. 3.25** shows the pH effect on the adsorption of the acidic dye orange green (OG) onto (a) WP and (b) TP. The influence of pH on the adsorption capacity was observed over a pH range of 4–11. The wavelength of maximum absorbance of each dye does not shift in the pH range investigated.

As can be seen from **Fig. 3.25a**, the adsorption of OG onto WP is pH dependent and the maximum capacity achieves at pH value of 4. With the increase of pH value, the adsorption capacity for the dye decreases. Such pH-dependent trend was observed for the adsorption of acid dyes on ethylenediamine modified starch as biosorbent and in the dye removal from aqueous solutions by dithiocarbamate-modified starch [32, 39]. On contrary, OG dye was not adsorbed on the TP in this pH range shown in the **Fig. 3.25b**.

### 3.6.2 Influence of Ferric (III) Coagulant

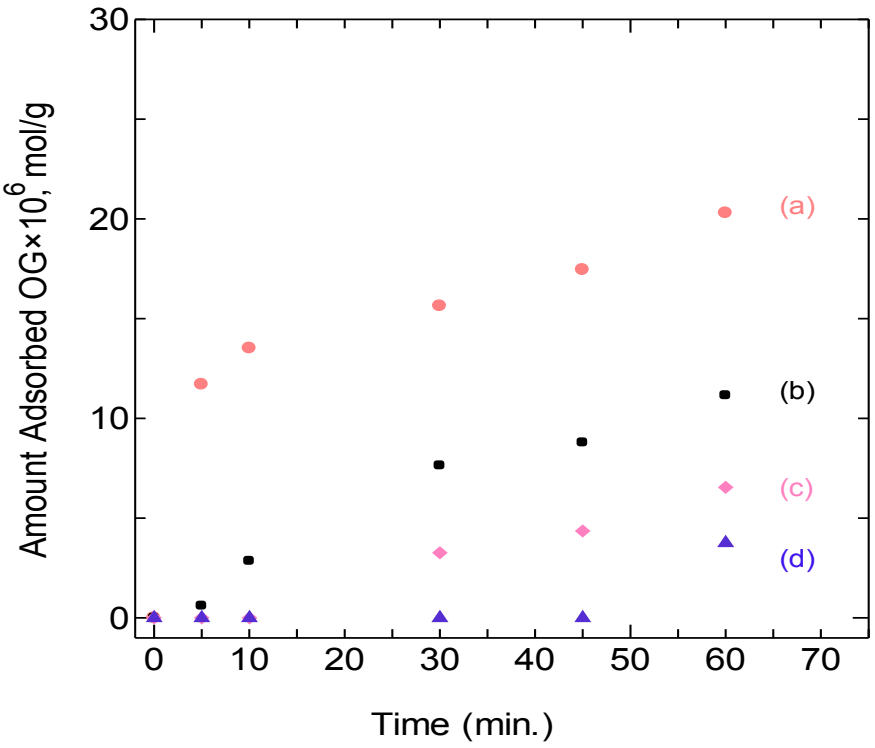


**Fig. 3.26** Influence of $FeCl_3.6H_2O$ on the adsorption of orange green (OG) onto wheat powder (WP) at (a) 2 mM, (b) 4 mM, (c) 5 mM and (d) 6 mM Fe (III) solution respectively. Initial [OG] = $5\times10^{-5}$ M, pH = 6.86, adsorbent dose = 1.2 g/L and temperature = 29 ˚C.

**Fig. 3.26** expresses the adsorption of OG dye onto WP employing ferric chloride hexahydrate, $FeCl_3.6H_2O$ as the coagulant. The coagulant concentration was varied from 2 to 6 mM. The adsorption was found highest at 2 mM [Fe (III)]. With increasing of the [Fe (III)] from 2 to 6 mM, the adsorption rate was decreased and almost exempted at 6 mM [Fe (III)]. Similarly, **Fig. 3.27** shows the influence of $FeCl_3.6H_2O$ on the adsorption of OG onto TP.

In the case of TP sorbent, the OG dye adsorbed very rapidly within first ten minutes and then reached at steady values. However, with increasing of the [Fe (III)] from 2 to 6 mM, the adsorption rate was decreased similar to the adsorption of OG onto WP.

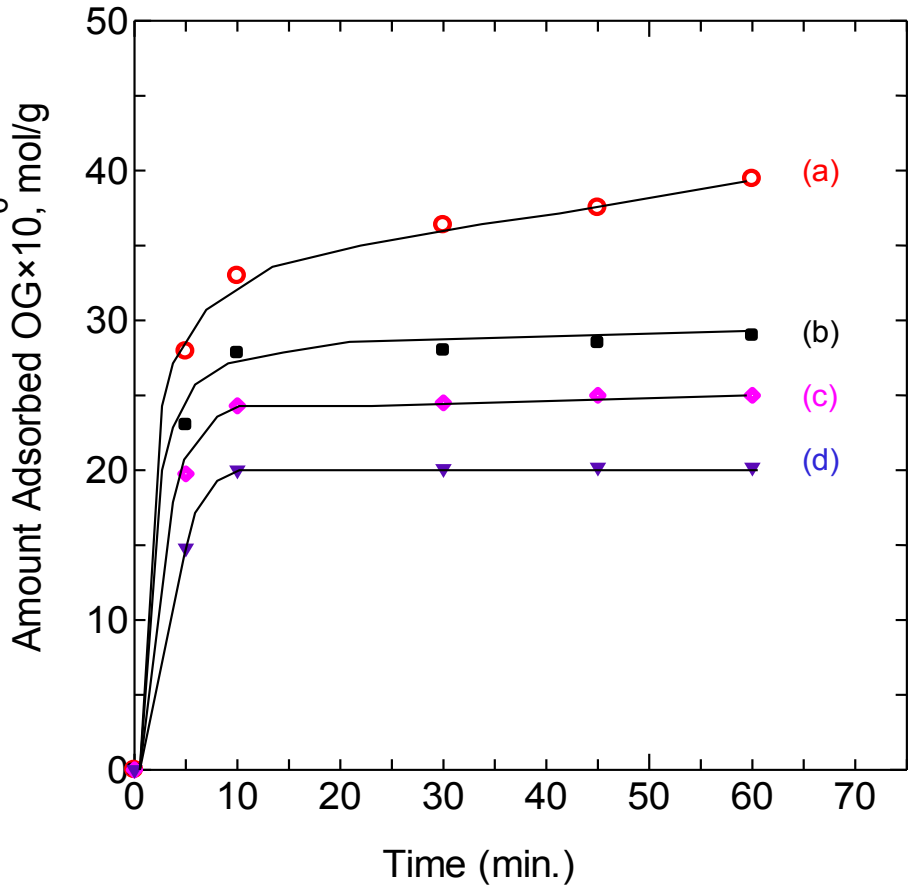


**Fig. 3.27** Influence of $FeCl_3$ electrolyte on the adsorption of orange green (OG) onto turmeric powder (TP) at (a) 2 mM, (b) 4 mM, (c) 5 mM and (d) 6 mM Fe (III) coagulant solution respectively. Initial [OG] = $5\times10^{-5}$ M, pH = 6.86, adsorbent dose = 1.2 g/L and temperature = 29 ˚C.

It is very interesting to observe that OG dye didn't undergo any adsorption onto TP (**Fig. 3.25b**) and showed a small adsorption onto WP in aqueous solution of pH 6.86. But in presence of $FeCl_3.6H_2O$, the adsorption of OG both onto WP (**Fig. 3.26**) and TP (**Fig. 3.27**) rapidly increases in the same pH. It is because the [Fe (III)] coagulant forms complex with the starch content of WP and TP as described in the **Section 3.5.6** in detail.

### 3.6.3 Adsorption Mechanism

From the knowledge of pH effect (**Section 3.6.1**) and influence of $FeCl_3.6H_2O$ (**Section 3.6.2**) on the adsorption of OG dye onto WP and TP, the mechanism of adsorption is proposed in the **Scheme 3.4**. The OG dye contains two sulfonated groups ($-SO_3Na$) and one hydroxyl (-OH) group. In acidic aqueous solutions, the functional group ($-SO_3Na$) of OG ionizes and the dye exists in anionic form as shown in the **Scheme 3.5** [54]. Thus in the presence of $H^+$, the hydroxyl groups of the starch content of WP and TP become protonated. Then the ionic interactions occur between the dye and starch bed (for example $–OH_2^+\cdots{}^-O_3S–$). This observation is strongly supported by the pH effect on the adsorption shown in the **Fig. 3.25**. These suggest that the process of the OG dye adsorption onto WP and TP is based on electrostatic attraction in addition to hydrogen bonding in acidic solution [32].

In aqueous solution of neutral pH (pH = 6.86), the orange green dye doesn't adsorb onto TP and also in WP. This is because the pKa value of OG dye (pKa = 12.8) [49] is very compatible with pKa value of starch (pKa = 13.3) [48] and both of them have similar extent of dissociation shown in **Table 3.11**. Therefore, the adsorption in aqueous solution could be due to the hydrogen bonding merely.

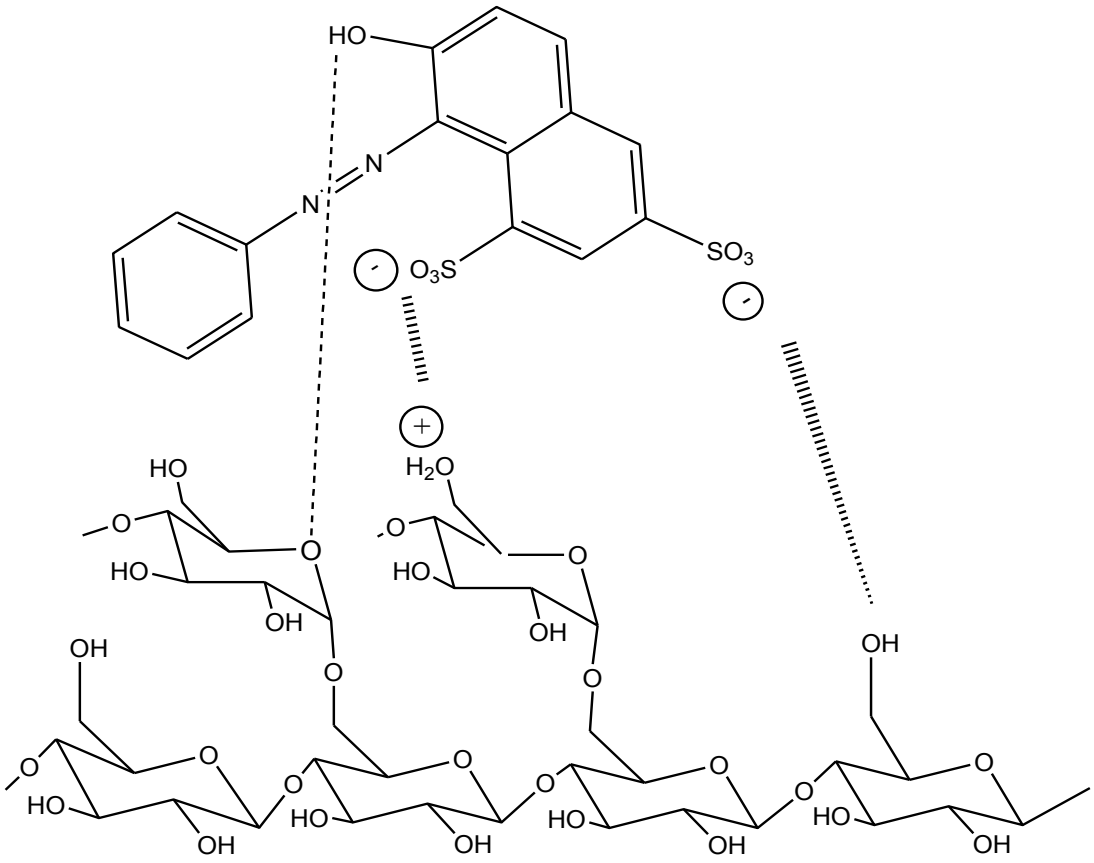


**Scheme 3.4** Possible interactions between orange green and starch

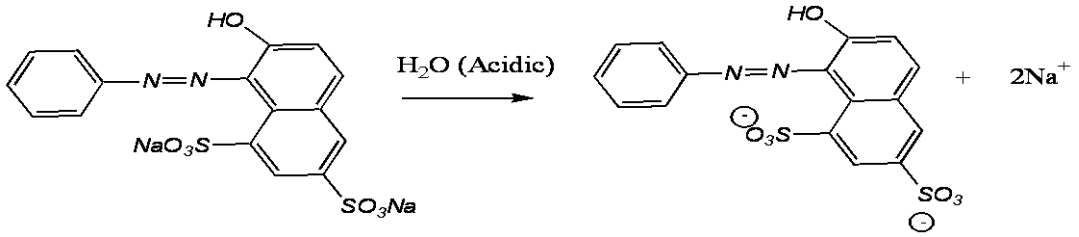


**Scheme 3.5** Dissociation of orange green dye

### 3.7 Recovery (Desorption) of MB Adsorbed onto WP

First of all, we allowed the WP to adsorb the MB dye for a period of 54 hour as shown in the **Fig. 3.28**. The adsorption was found to be increased gradually upto 0.105 mg at 24 hour then it decreased regularly to 0.087 mg at 54 hour which indicates the biodegradation of the starch bed of WP. Therefore, we optimized the maximum adsorption of MB within 24 hour.

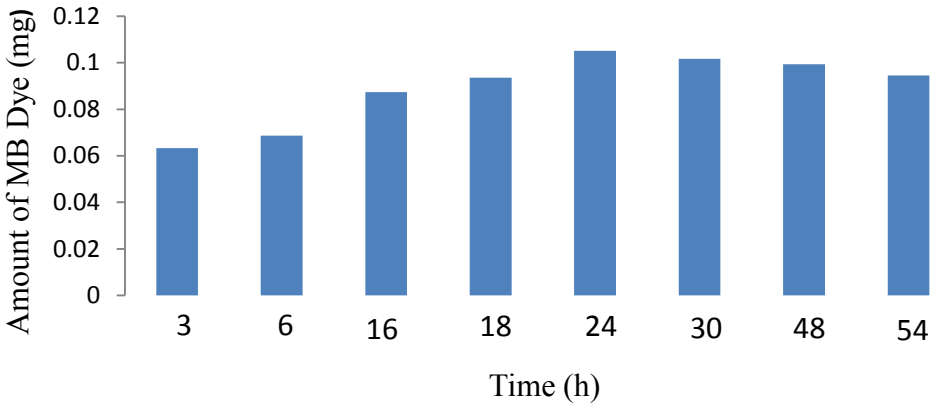


**Fig. 3.28** Optimization of MB dye adsorption onto WP. Initial [MB] = 1 $10^{-5}$ M, pH = 6.86, adsorbent dose = 25 g/L and temperature = 29 ˚C

The desorption profile of MB from the WP was conducted in a different study in the target of recycling of the dye. Firstly, the WP was permitted to adsorb the MB completely for a 24 hour period. Then the dye-saturated WP was filtered from the supernatant. Finally, the resulting dye-adsorbed residue, MB-WP, was allowed to desorb in a beaker containing fresh aqueous solution raising the volume of the beaker 50 mL at 29 ºC. A similar study was carried out at a higher temperature of 37 ºC.

It can be seen that the desorbed amount increases with time for every case. The maximum desorption at 29 ºC was found $29.34\times10^{-6}$ / (g/g) after 72 h. On the other hand, maximum desorption at 37 ºC was reported $34\times10^{-6}$ / (g/g) after the same time. In both cases, the amount and rate of desorption increased with the increase of temperature from 29 ºC to 37 ºC. The higher rate of desorption at higher temperature would be due to the increasing of thermal energy of the adsorbed species. For increasing thermal energy the adsorbed species tend to desorb from the surface of the adsorbent [55]. Percent recovery of MB was found 70 % at 29 ºC and 81 % at 37 ºC.

### 3.8 References


1. Van Soest, J. J. G.; Tournois, H.; DeWit, D.; Vliegenthart, J. F. G. Short-range Structure in (partially) Crystalline Potato Starch Determined with Attenuated Total Reflectance Fourier-transfrom IR Spectroscopy. *Carbohyd. Res*. **1995**, *279*, 201–14.
2. Ma, X.; Jian, R.; Chang, P. R.; Yu, J. Fabrication and Characterization of Citric Acid-Modified Starch Nanoparticles/Plasticized-Starch Composites. *Biomacromolecules* **2008,** *9,* 3314–3320.
3. Kuttigounder, D.; Lingamallu, J. R.; Bhattacharya, S. Turmeric Powder and Starch: Selected Physical, Physicochemical, and Microstructural Properties. *Journal of Food Science* **2011**, Vol. 00, Nr. 0.
4. Park, J. W.; Im, S. S. Biodegradable Polymer Blends of Poly (L lactic acid) and Gelatinized Starch. *Polymer Engineering and Science, December* **2000**, *40(12)*, 2539-2550.
5. Singh, S.; Singh, N.; Isono, N.; Noda, T. Relationship of Granule Size Distribution and Amylopectin Structure with Pasting, Thermal, and Retrogradation Properties in Wheat Starch. *J. Agric. Food Chem.* **2010**, *58*, 1180–1188.
6. Rubio, A. L.; Flanagan, B. M.; Gilbert, E. P.; Gidley, M. J. A Novel Approach for Calculating Starch Crystallinity amd Its Correlation with Double Helix Content: A Combined XRD and NMR Study. *Biopolymers* **2008**, *89(9)*, 761-768.
7. Whitfield, P.; Mitchell, L. X-ray Diffraction Analysis of Nanoparticles: Recent Developments, Potential Problems and Some Solutions. *International Journal of Nanoscience* **2004**, *3(6)*, 757-763.
8. Alexander, L. E. X-ray Diffraction Methods in Polymer Science. Wiley-Interscience: New York, **1969**.
9. Suryanarayana, C.; Norton, M. G. X-Ray Diffraction: A Practical Approach. *Plenum Press*, New York and London.
10. Will, G. Powder Diffraction, The Rietveld Method and the Two Stage Method. Springer, Springer-Verlag Berlin Heidelberg **2006,** Printed in Germany.

11. Bruker AXS. Leptos V7.03 User Manual **2009**, GmbH, Karlsruhe, Germany.

12. Theivasanthi, T.; Alagar, M. An Insight Analysis of Nano sized Powder of Jackfruit Seed**.** *Nano Biomed. Eng*. **2011**, *3(3)*, 163-168.

13. Corre, D. L.; Bras, J.; Dufresne, A. Starch Nanoparticles: A Review. *Biomacromolecules* **2010**, *11*, 1139-1153.

14. Saikia, J. P.; Banejee, S.; Konwar, B. K.; Kumar, A. Biocompatible Novel Starch/Polyaniline Composites: Characterization, Anti-cytotoxicity and Antioxidant Activity. *Colloids and Surfaces B: Biointerfaces* **2010**, *81*, 158-164.

15. Morita, H. Characterization of Starch and Related Polysaccharides by Differential Thermal Analysis. *Anal. Chem.* **1956**, *28(1)*, 64-67.

16. Athawale, V. D.; Lele, V. Graft Copolymerization onto Starch. II. Grafting of Acrylic Acid and Preparation of it's Hydrogels. *Carbohydrate Polymers* **1998**, *35*, 21-27.

17. Janarthanan, P.; Yunus, W. M. Z. W; Bin Ahmad, M. Thermal Behavior and Surface Morphology Studies on Polystyrene Grafted Sago Starch. *J. Appl. Polym. Sci*. **2003**, *90*, 2053-2058.

18. Lei, X.; Guo, X.; Zhang, L.; Wang, Y.; Su, Z. J. Synthesis and Properties of Novel Conducting Polyaniline Copolymers. *Applied of Polymer Science* **2007,** *103(1)*, 140-147.

19. Palaniappan ,S.; Narayana, B. H. Conducting Polyaniline Salts-Thermogravimetric and Differential Thermal Analysis. *Thermochimica Acta* **1994**, *237(1)*, 91-97.

20. Conklin, J. A.; Huang, S. C.; Huang, S. M.; Wen, T.; Kaner, R. B. Thermal Properties of Polyaniline and Poly (aniline-co-o-ethylaniline). *Macromolecules* **1995**, *28*, 6522-6527.

21. Zareh, E. N.; Moghadam, P. N.; Azariyan, E.; Sharifian, I. Conductive and Biodegradable Polyaniline/Starch Blends and Their Composites with Polystyrene. *Iranian Polymer Journal* **2011**, *20 (4)*, 319-328.

22. Jeevananda, T.; Siddaramaiah; Lee, T. S.; Lee, J. H.; Samir, O. M.; Somashekar, R. Polyaniline-Multiwalled Carbon Nanotube Composites: Characterization by WAXS and TGA. *J. Appl. Polym. Sci*. **2008**, *109*, 200-210.

23. Kim, D.; Choi, J.; Kim, J.-Y.; Han, Y.-K.; Sohn, D. Size Control of Polyaniline Nanoparticle by Polymer Surfactant. *Macromolecules* **2002,** *35,* 5314-5316.

24. Zareh, E. N; Moghadam, P. N.; Azariyan, E.; Sharifian, I. Conductive and Biodegradable Polyaniline/Starch Blends and Their Composites with Polystyrene. *Iranian Polymer Journal* **2011**, *20(4)*, 319-328.

25. Chowdhury, A. N.; Jesmeen, S. R.; Hossain, M. M. Removal of Dyes from Water by Conducting Polymeric Adsorbents. *Polym. Adv. Technol.* **2004**, *15*, 633–638.

26. Degradation of Polymers in Nature. Dow Corning Corp. **1997**.

27. Robertson, G. H. et al. Native or Raw Starch Digestion: A Key Step in Energy Efficient Biorefining of Grain. *J. Agric. Food Chem*. **2006**, *54*, 353−365.

28. Bujdak, J. et al. Clay Mineral Particles As Efficient Carriers of Methylene Blue Used for Antimicrobial Treatment. *Environ. Sci. Technol*. **2009**, *43*, 6202–6207.

29. Taghi, M.; Abbasi, T. Z.; Nasrollahzade, Z. Study of Enzymatic Degradation and Water Absorption of Nanocomposites Starch/Polyvinyl Alcohol and Sodium Montmorillonite Clay. *Journal of the Taiwan Institute of Chemical Engineers* **2012**, *43*, 120–124.

30. Chowdhury, A.-N. et al. "Influence of pH on the Specific Surface Area of Polyaniline Matrices. *Journal of Applied Polymer Science* **2008**, *109*, 1764–1771.

31. Ayad, M. M.; El-Nasr, A. A. Adsoption of Cationic Dye (Methylene Blue) from Water Using Polyaniline Nanotubes Base. *J. Phys. Chem. C* **2010**, *114*, 14377-14383.

32. Cheng, R.; Ou, S.; Li, M.; Li, Y.; Xiang, B. Ethylenediamine Modified Starch as Biosorbent for Acid Dyes. *J. Hazard. Mater.* **2009**, *172*, 1665–1670.

33. Lei, G.; Li, G.; Liu, J.; Yin, P.; Li, Q. Adsorption of Aniline on Cross-Linked Starch Sulfate from Aqueous Solution. *Ind. Eng. Chem. Res.* **2009**, *48*,10657-10663.

34. Qayoom, A.;Kazmi, S. A.;Rafiq, N. Removal of Cu(II) Ion from Aqueous Solutions by Turmeric Powder. *J. Chem. Soc. Pak*. **2009**, *31(6)*, 876.

35. Nechwatal, A.; Nicolai, M.; Mieck, K. P. Use of Absorbers Based on Starch for the Effluent Treatment of Dyeing Liquors. *Starch/Staerke* **1999**, Nr.8-9, 286-293.

36. Sar, P.; Kazy, S. K.; Asthana, R. K..; Singh, S. P. *Inter. Biodeter. Biodeg*. **1999,** *44*, 101-110.

37. Ho, Y. S.; Chiang, T. H.; Hsuesh, Y. M. Removal of Basic Dye from Aqueous Solution using Tree Fern. *Process. Biochem*. **2005**, *40*, 119-124.

38. Angellier, H.; Choisnard, L.; Boisseau, S. M.; Ozil, P.; Dufresne, A. Optimization of the Preparation of Aqueous Suspensions of Waxy Maize Starch Nanocrystals Using a Response Surface Methodology. *Biomacromolecules* **2004**, *5*, 1545-1551.

39. Cheng, R.; Xiang, B.; Li, Y.; Zhang, M. Application of Dithiocarbamate-Modified Starch for Dyes Removal from Aqueous Solutions. *J. Hazard. Mater*. **2011**, *188*, 254-260.

40. Lagergren, S. About the Theory of So-Called Adsorption of Soluble Substances. *K. SVen. Vetenskapsakad. Handl.* **1898**, *24*, 1.

41. Ho, Y. S. Adsorption of Heavy Metals from Waste Streams by Peat. Ph.D. Dissertation, University of Birmingham, Birmingham, U.K., **1995**.

42. Ho, Y. S.; Ng, J. C. Y.; McKay, G. Removal of Lead (II) from Effluents by Sorption on Peat using Second-Order Kinetics. *Sep. Sci. Technol*. **2001**, *36*, 241-261.

43. Weber, W. J.; Morris, J. C. Kinetics of Adsorption on Carbon from Solution. *J. Santi. Eng. Div.* **1963**, *ASCE 89 (SA2*), 31-59.

44. Renault, F.; Crini, N.-M.; Gimbert, F.; Badot, P. -M.; Crini, G. Cationized Starch-based Material as a New Ion-Exchanger Adsorbent for the Removal of C.I. Acid Blue 25 from Aqueous Solutions. *Bioresource Technology* **2008**, *99*, 7573–7586.

45. I. Langmuir. The Constitution and Fundamental Properties of Solids and Liquids. *J. Am. Chem. Soc*. **1916**, *38*, 2221–2295.

46. Tempkin, M. J.; Pyzhev, V. Kinetics of Ammonia Synthesis on Promoted Iron Catalysts. *Acta Physicochim*. URSS, **1940**, *12*, 217–256.

47. Gimbert, F. et al. Adsorption Isotherm Models for Dye Removal by Cationized Starch-based Material in a Single Component System: Error Analysis. *J. Hazard. Mater.* **2008**, *157*, 34–46.

48. Saric, S. P.; Schofield, R. K. Sol-Forming Polysaccharides Hydroxyl Groups in Some Insoluble and the Dissociation Constants of the Carboxyl and Sol-Forming Polysaccharides. *Proc. R. Soc. Lond. A* **1946**, *185*, 431-447.

49. Sabnis, R. W. Handbook of Biological Dyes and Stains: Synthesis and Industrial Applications. Jhon Wiley and Sons, Mar 29, **2010**.

50. El-Shishtawy, R. M.; Shokry, G. M.; Ahmed, N. S. E.; Kamel, M. M. Dyeing of Modified Acrylic Fibers with Curcumin and Madder Natural Dyes. *Fibers and Polymers* **2009**, *10(5)*, 617-624.

51. Hatamie, S. et al. Complexes of Cobalt Nanoparticles and Polyfunctional Curcumin as Antimicrobial Agents. *Materials Science and Engineering* **2012**, *C 32*, 92–97.

52. Popic, S.; Koprivanac, N.; Bozic, A. L. Removal of Reactive Dyes from Wastewater using Fe (III) Coagulant. *JSDC* **2000**, *116*, 352-358.

53. Somsook, E. et al. Interactions between Iron (III) and Sucrose, Dextran, or Starch in Complexes. *Carbohydrate Polymers* **2005**, *61*, 281–287.

54. Mahanta, D.; Madras, G.; Radhakrishnan, S.; Patil, S. Adsorption of Sulfonated Dyes by Polyaniline Emeraldine Salt and Its Kinetics. *J. Phys. Chem. B* **2008**, *112*, 10153–10157.

55. Somorjai, A.; Gabor, L. Yimin. Introduction to Surface Chemistry and Catalysis. John Wiley and Sons, Section 4.6, **2010**.

## General Conclusions

In this study, wheat powder (WP) and turmeric powder (TP) were processed mechanically and chemically to prepare their functional forms for the efficient adsorption of dyes from aqueous solution. Nanoparticles of starch (SN) and synthetic polymer, i. e., polyaniline (PANI) and two PANI/starch nanocomposites (Composite-1 and Composite-2) were prepared and characterized with infra-red spectroscopic, thermal analysis, scanning electron microscopic (SEM) and x-ray diffraction techniques.

The average size starch nanoparticles estimated from Debye-Scherrer formula is 9 nm. Besides, the average particle size of PANI/starch composites is about 18 nm which is smaller than that of PANI (20 nm). Comparison of thermal properties of the composites with the pure starch and PANI ensured the presence of both starch and PANI in the composites. A good match was found also in the IR spectrum of the materials.

We actually found a SEM image of agglomerated SN because of the lack of dispersion of the particles on the substrate. In the preparation of SN, firstly the native wheat powder was gelatinized in water and formed starch paste. The SN was formed by dropwise addition of ethanol in the resultant solution. The agglomeration of the SN may result from the inadequate stirring and reaction temperature. However, the interaction of hydrogen bond between SN and starch paste play the important role on the stability of the precipitated SN in the suspension. It is also noticeable that the samples were not pre-treated with any kind of milling which would change the shape of particles and consequently reduce the particle sizes. A similar occurrence was found in the SEM images of PANI/starch composites.

The efficiency of the prepared materials concerning the adsorption of a cationic, methylene blue (MB) and an anonic orange green (OG) dyes were investigated. At equilibrium time (48 hrs), the adsorption efficiencies of TP and PANI were found to be maximum and comparable. The efficiencies of WP, pure starch and SN were reasonably low, but the efficiency of SN was higher than that of pure starch. High adsorption efficiency of SN was revealed by XRD analysis to be due to the smaller particle size.

WP and TP are too cheaper adsorbents. Moreover these adsorbents are biodegradable. Thus, we were interested in the detail adsorption study of these low-cost, biodegradable adsorbents which could also be recycled to produce alcohol and to recover the dyes for reuse.

The adsorptions of MB on WP and TP were found to be Langmuir type and of the pseudo-second-order kinetic model. Interestingly, it was observed that the adsorption of MB on WP and TP decreased with time allowed, for example, the adsorption on WP at 120 hrs (about $3.05 \times 10^{-6}$ mol/g) is decreased by about 50 % of that observed at 72 hrs (about $1.81 \times 10^{-6}$ mol/g), indicating that the adsorbents get biodegraded and hence the MB gets desorbed.

Electrolytes inhibit the MB dye adsorption in a greater extent onto WP biosorbent than its adsorption onto TP. On the other hand, the only one electrolyte, ferric chloride influences the adsorption of OG dye onto WP and TP.

The recovery of MB adsorbed onto WP could be conducted successfully through desorption process of MB from WP in aqueous solution depending on the temperature change. In both cases, the amount and rate of desorption increased with the increase of temperature from 29 ºC to 37 ºC. Indeed, higher temperatures increase the thermal energy of the adsorbed species which ultimately enhance the rate of desorption of MB.

## 5.1 Literature Review

The cornerstone of our interest in this research was the biodegradability of the starch-based biosorbents. That's why we choice to study the adsorption of WP and TP in a more detail. It could be possible to recover the adsorbed dyes and to recycle the biosorbents through fermentation process into alcohol which would be a very cost effective and eco-friendly way of the waste water treatments.

Banerjee et al. [1] reported the direct production of alcohol from starch. They isolated a yeast from natural sources and identified it as *Saccharomyces diastaticus*. This microbe possesses both amylolytic (breaking the amylase linkages of stach) and fermentative power. It can grow well in a starch-salt-yeast extract medium containing 2 % starch. The optimum initial pH of the medium for growth of *S. diastaticus* was found 5.0 while alcohol production was maximum in the pH range of 6.0-6.5. The optimum production of alcohol took place in 72 h at 37 ˚C.

Vikman et al. [2] performed enzymatic hydrolysis of starch-based materials using excess *Bacillus licheniformis* α-amylase and *Aspergillus niger* glucoamylase at 37 ˚C and 80 ˚C. The degree of degradation was determined by measuring the dissolved carbohydrates and the weight loss of the samples. Biodegradation was also determined by incubating the samples in a compost environment and measuring the weight loss after composting. The results indicated that the enzymatic method is a rapid means of obtaining preliminary information about the biodegradability of starch-based materials because it took short time to perform the test and the large number of samples that can easily be tested. They concluded that other methods are needed to investigate more accurately the extent of biodegradability, especially in the case of complex materials in which starch is blended with other polymers.

Alonso et al. [3] evaluated the starch-degradation capacity of several amylolytic microorganisms with exocellular activity, grown on an optimized culture medium. Among sixteen amylolytic yeasts S. attinorum and two *S. cerevisiae* displayed the best behaviour during starch degradation.

Taghizadeh et al. [4] studied the a-amylase action on starch/poly(vinyl alcohol) composite film containing sodium montmorillonite nanoparticle at temperature (25± 1) ˚C. The modifications induced by the enzymatic treatment were evidenced by determination of weight loss, water absorption capacity, sugars released during biodegradation. They investigated the effect of polyvinyl alcohol (PVA) and sodium montmorillonite clay content within the thermoplastic starch (TPS) blends on the rate and extent of starch enzymatic hydrolysis using enzyme α-amylase.

The study revealed that blends with a MMT-Na content at 5 wt % exhibited a significantly reduced rate and extent of starch hydrolysis. The results suggest that this may have been attributed to interactions between starch and MMT-Na that further prevented enzymatic attack on the remaining starch phases within the blend.

In our study, biodegradation of WP and TP was carried out in aqueous medium in presence of MB dye. Although MB dye is a photodynamic antimicrobial agent, very low concentrations of MB are able to kill or inhibit the growth of microorganisms e.g., fungi, yeasts in the aqueous solution even under light conditions. On contrary microbial reduction of the phenothiazinium chromophore of MB causes decolourisation. The bactericidal activity of MB is weak due to chromophoric reduction by bacterial enzymes. Moreover, the starch content of the biosorbents has the potential to induce the growth of microorganisms. Starch secretes α-amylase isoform that also digests raw starch in a considerable extent [5, 6]. It is noticeable that there is no report regarding the antimicrobial activity of OG dye.

## 5.2 Tentative Goal

Considering the above survey, the recycling processes could be implemented by

I. Enzymatic degradation of the dye-adsorbed biosorbents namely WP and TP using the yeast *Saccharomyces diastaticus* [1]. Starch itself secretes α-amylase isoform that also digests raw starch in a considerable extent and act as a medium of the growth of the microorganisms

II. The experiment would be conducted at two different temperatures i.e., at room temperature and at 37 ˚C, the temperature for the optimal growth of the yeasts [2]

III. The enzymatic treatments might be evidenced by determination of weight loss, water absorption capacity, sugars released during biodegradation [4]

IV. The process might be monitored from the differences of SEM micrographs and DTA curves at the before and after the treatment [7]

V. Moreover, UV spectroscopy could be a perfect tool for the analysis [4]

## 5.3 References

1. Banerjee, M.; Debnath, S.; Majumdar, S. K. Production of Alcohol from Starch by Direct Fermentation. *Biotechnology and Bioengineering* **1988**, *32*, 831-834.

2. Vikman, M.; Itiivaara, M.; Poutanen, K. Measurement of the Biodegradation of Starch-Based Materials by Enzymatic Methods and Composting. *Journal of Environmental Polymer Degradation* **1995**, *3(I)*, 23-29.

3. Alonso, S.; Arevalo-Villena, M.; Ubeda, A. B. Study of Starch Degradation by Yeasts during Fermentation for Using in Animal Feed. *Appl. Biochem. Biotechnol.* **2010**, *162*, 2058-2066.

4. Taghizadeh, M. T.; Abbasi, Z.; Nasrollahzade, Z. Study of Enzymatic Degradation and Water Absorption of Nanocomposites Starch/Polyvinyl Alcohol and Sodium Montmorillonite Clay. *Journal of the Taiwan Institute of Chemical Engineers* **2012**, *43*, 120–124.

5. Robertson, G. H. et al. Native or Raw Starch Digestion: A Key Step in Energy Efficient Biorefining of Grain. *J. Agric. Food Chem*. **2006**, *54*, 353−365.

6. Bujdak, J. et al. Clay Mineral Particles As Efficient Carriers of Methylene Blue Used for Antimicrobial Treatment. *Environ. Sci. Technol*. **2009**, *43*, 6202–6207.

7. Moreno-Chulim, M. V.; Barahona-Perez, F.; Canche-Escamilla, G. Biodegradation of Starch and Acrylic-Grafted Starch by Aspergillus niger. *Journal of Applied Polymer Science* **2003**, *89*, 2764–2770.